INVESTIGATION OF THE BRAIN CONNECTIVITY DISTURBANCE IN DYSLEXIC PATIENTS

A THESIS SUBMITTED TO
THE GRADUATE SCHOOL OF NATURAL AND APPLIED SCIENCES
OF
MIDDLE EAST TECHNICAL UNIVERSITY

BY

VESAL RASOULZADEH

IN PARTIAL FULFILLMENT OF THE REQUIREMENTS
FOR
THE DEGREE OF MASTER OF SCIENCE
IN
BIOMEDICAL ENGINEERING

FEBRUARY 2016

Approval of the Thesis:

INVESTIGATION OF THE BRAIN CONNECTIVITY DISTURBANCE IN DYSLEXIC PATIENTS

submitted by **VESAL RASOULZADEH** in partial fulfillment of the requirements for the degree of **Master of Science in Biomedical Engineering Department, Middle East Technical University** by,

Prof. Dr. Gülbin Dural Ünver _____
Dean, Graduate School of **Natural and Applied Sciences**

Prof. Dr. Hakan I. Tarman _____
Head of Department, **Biomedical Engineering**

Assoc. Prof. Dr. Ilkay Ulusoy _____
Supervisor, **Electrical and Electronics Engineering, METU**

Prof. Dr. Canan Kalaycıoğlu _____
Co-Supervisor, **Physiology Dept., Faculty of Medicine, Ankara University**

Examining Committee Members:

Prof. Dr. Nevzat G. Gençer _____
Electrical and Electronics Engineering Dept., METU

Assoc. Prof. Dr. Ilkay Ulusoy _____
Electrical and Electronics Engineering, METU

Prof. Dr. Metehan Çiçek _____
Physiology Dept., Faculty of Medicine, Ankara University

Prof. Dr. Gerhard-Wilhelm Weber _____
Institute of Applied Mathematics, METU.

Assoc. Prof. Dr. Yeşim Serinağaoğlu Doğrusöz _____
Electrical and Electronics Engineering Dept., METU

Date: 05.01.2016

I hereby declare that all information in this document has been obtained and presented in accordance with academic rules and ethical conduct. I also declare that, as required by these rules and conduct, I have fully cited and referenced all material and results that are not original to this work.

Name, Lastname : Vesal Rasoulzadeh

Signature:

ABSTRACT

INVESTIGATION OF THE BRAIN CONNECTIVITY DISTURBANCE IN DYSLEXIC PATIENTS

Rasoulzadeh, Vesal

M.Sc., Department of Biomedical Engineering

Supervisor: Assoc. Prof. Dr. Ilkay Ulusoy

Co-Supervisor: Prof. Dr. Canan Kalaycıoğlu

February 2016, 99 pages

Dyslexia is a learning disability that makes reading a challenge, despite normal level of intelligence and receiving adequate instructions. The core deficit in dyslexia is attributed to phonological processing. It's been suggested that dyslexia is a disconnection syndrome. In this sense, the major sites of phonological processing in the brain are intact and the interconnection between these areas are disturbed. In this study, the disturbance in dyslectic brains based on effective connectivity models in "pre-reading" and "while reading" stages is investigated, which explains the causal interactions between different regions of the brain. Dynamic Bayesian Networks were constructed for the EEG data in theta, alpha and beta frequency bands to model the effective connectivity patterns of the brain in dyslectic and normal subjects in these bands. Analysis was performed based on the data obtained from two independent experiments, reading a word and a non-word by each subject. As the main objective of the thesis, dyslexic and normal children were classified based on the information obtained from the underlying effective connectivity models of their brains which reveal the abnormal patterns in the brain that may lead to detection and diagnosis of the condition. Dyslectic subjects were found to have a different effective connectivity patterns in "pre-reading" period, regardless of the reading task and theta frequency

band is reported to be the most informative one about the disturbance in the casual influence between two groups in this period. The classification rate of 86.21% were obtained based on “pre-reading” models. the classification rates of 86.21% in reading a word experiment and 81.03% in reading a non-word experiment were obtained in alpha band. Features used to classify two groups are the connectvity weights (obtained fron DBN models) that are significantly different between dyslectics and controls. The connection include the ones from both dorsal (which is more activated while reading a word) and ventral (which is more activated while reading a non-word) pathways. This indicates the distruption of them both in dyslectic brains.

Keywords: Dyslexia, EEG, Effective Connectivcity, DBN.

ÖZ

DYSLEXIC HASTALARDA BEYİN BAĞLANTI BOZUKLUĞUNUN İNCELENMESİ

Vesal, Rasoulzadeh
Doktora, Fizik Bölümü
Tez Yöneticisi: Doç. Dr. Ilkay Ulusoy
Ortak Tez Yöneticisi: Prof. Dr. Canan Kalaycıoğlu

February 2016, 99 sayfa

Disleksi, normal zeka seviyesi ve yeterli öğrenme düzeyine karşın okumayı zor hale getiren bir öğrenme bozukluğudur. Disleksideki temel bozukluk fonolojik işlemlerden kaynaklanmaktadır ve disleksinin bağlantısal bozukluktan kaynaklandığı öne sürülmektedir. Yani, fonolojik işlemlerin gerçekleştiği beyin bölgelerinin bağlantılı fakat arabağlantılarının bozulmuş olduğu söylenebilir. Bu çalışmada, disleksik beyinlerdeki bozukluk, beynin farklı bölgelerinin nedensel bağlantılarını açıklayan efektif bağlantısallık modellerindeki "ön-okuma" ve "okuma" aşamalarında incelenmektedir. EEG verilerindeki teta, alfa ve beta frekans bantları ile, bu bantlara göre normal ve disleksik beyinlerdeki efektif bağlantısallığı modellemek için Dinamik Bayesyen ağlar oluşturulmuştur. Analiz, kelime ve kelime olmayan sözcükleri okumadan oluşan, birbirinden bağımsız iki farklı deneyden toplanan verilerle gerçekleştirilmiştir. Tezin ana amacı olarak, disleksik ve normal çocuklarda beyindeki efektif bağlantısallık modellerinden elde edilen bilgilere dayanılarak sınıflandırma yapılmıştır. Bu sınıflandırma, bozukluğa neden olabilecek durumların tanı ve teşhisinde kullanılabilecek normal olmayan durumları ortaya çıkaracaktır. Okuma görevinin ve teta frekans bandının iki grup arasındaki nedensel etkilenmede bozukluk hakkında çok bilgi verdiği söylense de, "ön-okuma" sürecinde disleksik deneklerin daha farklı efektif bağlantısallığa sahip oldukları bulunmuştur. Sınıflandırma oranı "ön-okuma" modellerinde 86.21% olarak elde edilmiştir. Kelime

okuma deneyinde elde edilen 86.21% sınıflandırma oranı ile kelime olmayan sözcük okuma deneylerinde elde edilen 81.03% sınıflandırma oranı alfa bandından elde edilmiştir. İki grubu sınıflandırmada bağlantısallık ağırlıkları (Dinamik Bayesyan Ağları modellerinden elde edilmiştir) kullanılmıştır ve bu özellik disleksik ve kontrol grubunda büyük farklılık göstermektedir. Bağlantılar dorsal (daha çok kelime okuma sırasında etkinleşmektedir) ve ventral (daha çok kelime olmayan sözcük okuma sırasında etkinleşmektedir) yolları içermektedir. Bu, disleksik beyinlerde ikisinin de bozulduğunu göstermektedir.

Anahtar kelimeler: Dislkesi, EEG, Efektif bağlantısallık, DBN.

To My Mom and Dad

ACKNOWLEDGEMENTS

Foremost, I would like to express my deepest gratitude to my advisor, Prof. Dr. Ilkay Ulusoy, for her excellent guidance, caring, patience, and providing me with an excellent atmosphere for doing research. I also would like to thank Dr. Canan Kalaycioglu, who supports me with her knowledge during my study.

I want to thank my lab mate Ekin, and all my friends, specially Shirin, Raha, Arezoo and Nasrin for their continuous encouragement during my study.

Finally, I want to thank my parents for their unconditional support. I am so lucky to have them and cherish them with all my heart.

TABLE OF CONTENTS

APPENDICES

LIST OF TABLES

TABLES

LIST OF FIGURES

CHAPTER 1

INTRODUCTION

Dyslexia is a reading disability with neurobiological origin. It is characterized by a constant failure to gain fluent and accurate reading skills, despite the normal intellectual capacity and adequate education [1, 2, 3]. The act of reading, requires a well-established correspondence between phonemes (sounds) and graphemes (graphical symbols) in the brain. Dyslexia is the outcome of any failure in this correspondence [4]. Prevalence of dyslexia among school-aged children is reported to range from 5% to 17.5% which indicates the fairly broad range of population suffering from the condition [1, 5].

In 1996, based on the findings from PET and the neuropsychological studies, Paulesu, E., et al. suggested that dyslexia is a disconnection syndrome. Despite the intact function of major sites of phonological processing, findings suggest a connectivity problem between these areas [6]. Later on, in multiple studies neuroimaging techniques, like DTI and fMRI were used to provide evidence for disturbed connectivity patterns in dyslectic brains [7, 8, 9].

Three different forms of connectivity, namely, structural, functional and effective connectivity are introduced to study the interactions between different regions of the brain [10]. Effective connectivity, capable to extract directional influences between ROIs, is essential in the assessment of the functional integration of neuronal population and normal function of the brain [11]. There are multiple computational methods introduced in the literature to extract effective connectivity (e.g., SEM, GC, DBN) from neuroimaging data. Dynamic Bayesian network extract the dependencies in the system in a complete statistical sense and is capable of dealing with non-stationary and uncertain complex systems, which makes it suitable to model causal interactions in brain network.

Classification of normal subjects and the ones with neurological inabilities, may reveal the abnormal patterns in the brain that leads to detection and diagnosis of neurological brain disorders (e.g., dyslexia, epilepsy and attention-deficit hyperactivity disorder (ADHD)).

In this thesis, dyslexic and normal children were classified based on the information obtained from the underlying effective connectivity models of their brains. Figure 1.1 represents a schematic diagram of the employed algorithms. To our knowledge, this is the first attempt to study abnormalities in dyslexic subjects based on effective connectivity models derived from Dynamic Bayesian Networks (DBNs).

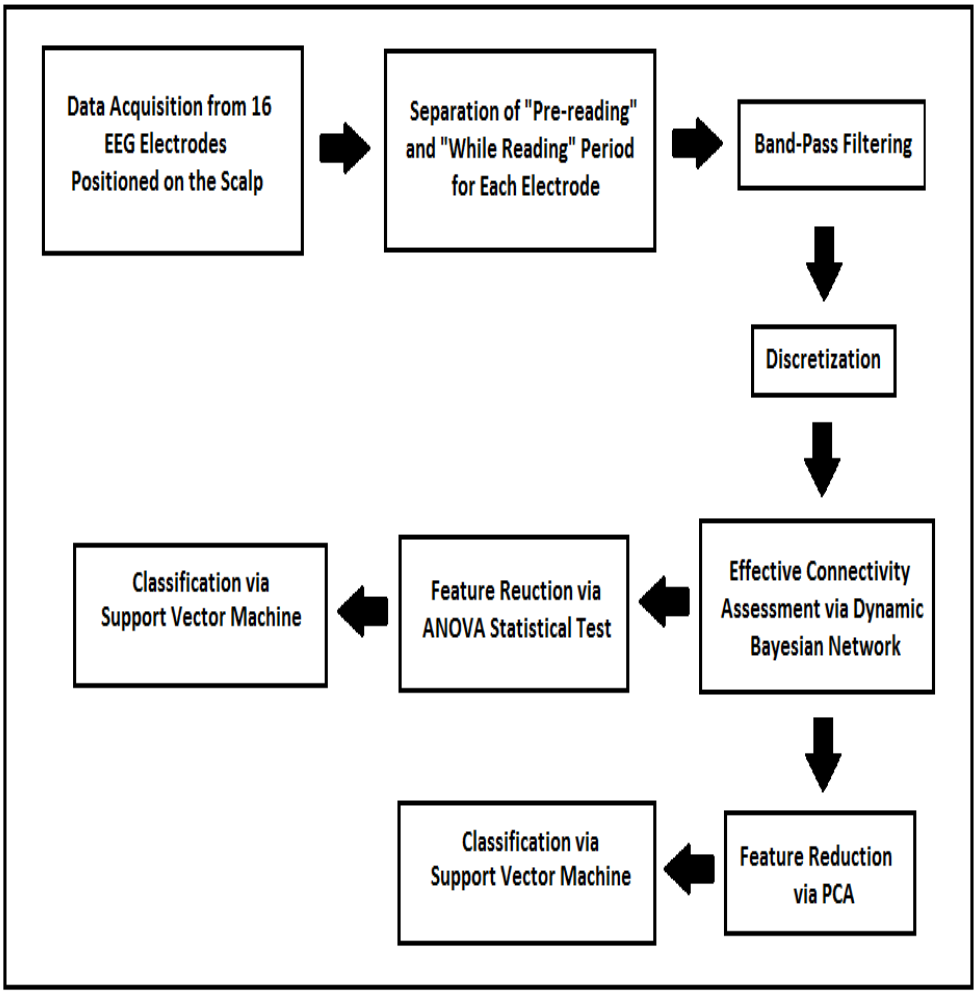

Figure 1.1. Schematic diagram of the employed algorithms to classify dyslectics from normal subjects.

1.1 Outline of the Thesis

The content of this thesis is organized as follows. In Chapter 2, preliminary knowledge that may help to a deeper understanding of the neurobiological basis of dyslexia is discussed. It starts with an explanation over the neurobiological models that have been suggested for reading in the brain. It continues by a review over the studies about dyslexia and the hypothesized impairments in dyslectic brains. Later in this chapter, effective connectivity studies of dyslexia are inspected. In Chapter 3, different computational methods for effective connectivity assessment are discussed and at the end, DBN is introduced as an efficient method for this case of study. In Chapter 4, initially, the data used in the analysis is explained. Later, the band-pass filtering and discretization methods are described, which are necessary prior to the application of DBN. Following, the DBMCMC MATLAB toolbox is explained, which is employed in this study to extract dynamic Bayesian models. At the end of the chapter, feature reduction and classification algorithms are explained. Chapter 5 contains the results and the discussion over the results. Ultimately, in Chapter 6, discussions in the Chapter 5 are summed up and multiple suggestions are made for future studies, which may improve the obtained results.

CHAPTER 2

PRELIMINARIES

Dyslexia, as the most common reading disorder, is said to have its core deficiency in phonological processing. Paulesu, E., et al. (1996) [6] and Horwitz et al. (1998) [12] suggested that dyslexia is a disconnection syndrome. This means that the inability of learning to read in dyslexics is about weak interaction between language components of the brain rather than possible deficits in related components.

This section is a review over the studies that contributed to a better understanding of the neural basis of dyslexia. It starts by describing the models proposed for functional anatomy of reading. It is continued by a review over studies that discover abnormalities in dyslexia. Following, studies that investigate effective and functional connectivity of dyslectic brains are reviewed. Finally, studies that address classification of dyslectic and normal subjects based on neuroimaging data are reviewed.

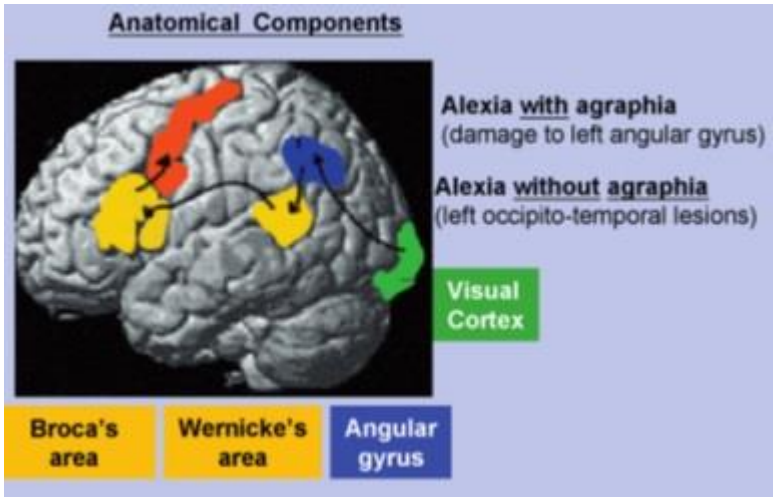

Figure 2.1. Anatomical components of 19-th century model [*13*].

2.1 Reading Models in the Brain

The early model of reading, the well-known 19-th century model, is constructed based on the results obtained from Dejerine's studies and previously found Wernicke's and Broca's areas. In 1891, Dejerine associated the problem with alexia with agraphia – a case in which the patient is unable to read or write, to a lesion in the left angular gyrus and suggested that this is the site of word form area [14]. In 1892, he reported a left occipito-temporal lesion in a patient with pure alexia- a case when the patient is able to write or speak, but reveals problems in reading task [15]. In this case, knowledge of word forms seemed to be intact, as the patient was capable to write. Therefore, the problem was reported to be in a connection between the visual processing in occipital region and word form recognition in the angular gyrus. Figure 2.1 shows the 19th-century neurological model of reading. Due to this model, reading a written word starts in occipital cortex and via the left angular gyrus, Wernicke's area and Broca's area, it ends in speech output. These areas were supposed to be respectively responsible for visual processing, visual word from images, auditory word from images, motor images and articulation. In 1885, Lichteim suggested that there exists an area, "concept centre", that has connections to and from auditory and motor cortex, and is responsible for word comprehension [16]. Figure 2.2 represents the cognitive components of the model.

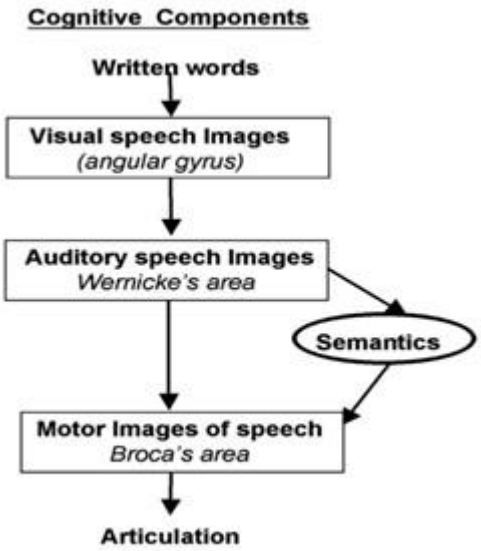

Figure 2.2. Cognitive components of 19-th century model [13].

There are multiple experiments that challenged the 19th-century model. Warrington and Shallice (1980) associated the reading problem of their cases to a word form system. Based on their explanation of word form system, there needs to be separate word form areas for reading and writing which is not explainable by the 19-th century model [17]. This model also fails to explain the "double dissociation" phenomenon between surface dyslexia and phonological dyslexia. Although phonological dyslectics are better at reading meaningful words than meaningless ones, pure dyslectics have semantics impairments. Thereafter, cognitive models start to consider more routes to meaning [18, 19].

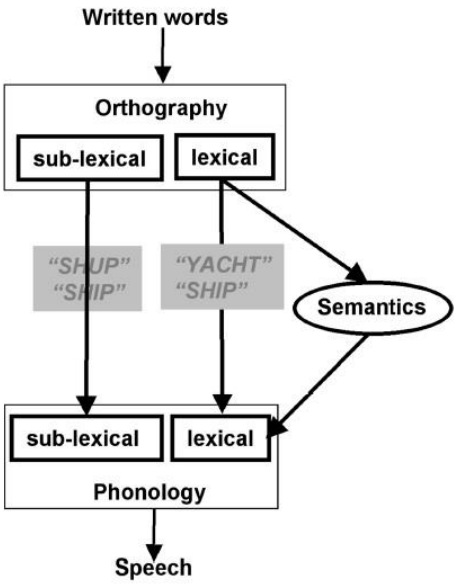

Figure 2.3. Three-route model of reading [13].

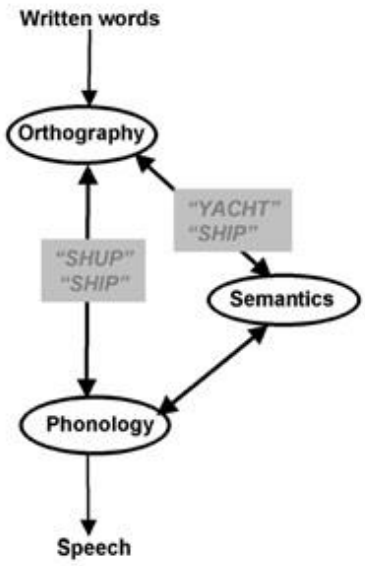

Figure 2.4. Triangular model of Reading [13]**.**

Later, popular models of reading were introduced, none of which has physiological validation. Orthography and phonology terms in the models indicate visual word form and auditory word form respectively, except the newly used terms involve both lexical and sub-lexical processes. The model illustrated in Figure 2.3 provides routes for reading unfamiliar non-words through sub-lexical path, familiar words in the absence of semantics through lexical path and semantic route which is on the basis of orthography rather than phonology. Second model illustrated in Figure 2.4 provides routes for reading meaningless non-words via orthography to phonology, meaningful words with irregular spellings via semantics and meaningful normal spelling words could be read through either routes. An interactive model of reading is represented in

Figure 2.5. According this model, visual information flow throughout orthographic-phonologic-lexical-semantic networks. In this figure, unbroken lines indicate feed forward and dashed lines indicate backward connections [20].

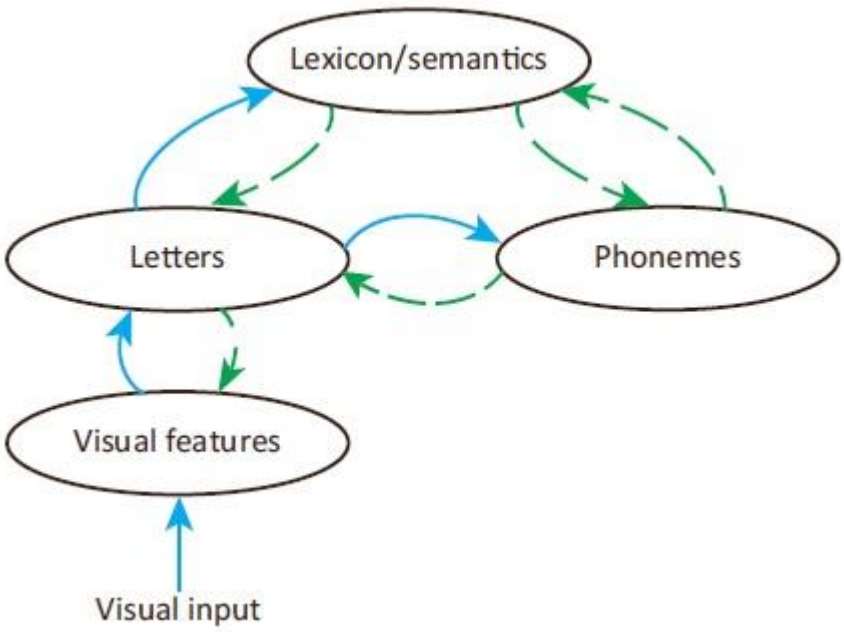

Figure 2.5. Interactive model of reading [21].

Studies from neuroimaging techniques were also used to identify the subcomponents of the neural system required for reading and make suggestions about the role of different regions of the brain. In general, findings from neuroimaging studies were not found to be in conflict with the neurological model except that a highlighted activity of left mid-fusiform area was reported from neuroimaging studies during reading, which was not specified in neurological model. It was proposed that the left mid-fusiform serves as the visual word form area and angular gyrus which was previously assumed to be visual word from area is involved in semantic processes [13].

2.1.1 Reading Circuit in the Brain

Reading, as a unique human cognitive process, requires cooperation of the signals from visual, auditory and language compartments of the brain. The reading circuitry in the brain network is studied through diffusion-weighted magnetic resonance imaging in

multiple researches. The highlighted findings are discussed here. Three large fascicles, identified to take part in reading circuit, are the arcuate fasciculus, the inferior longitudinal fasciculus and the posterior corpus callosum. Figure 2.6 represents these fascicles [22].

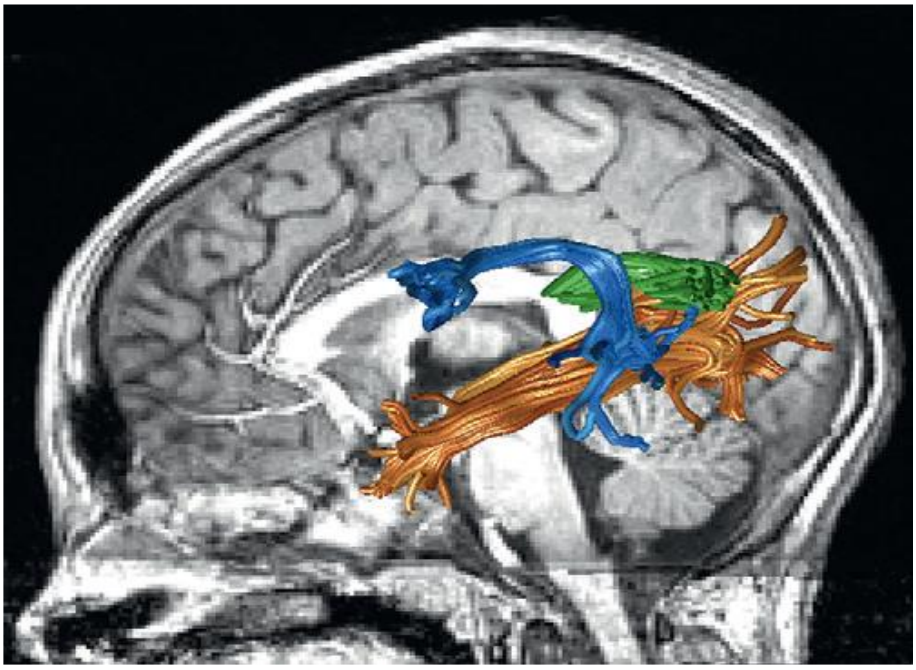

Figure 2.6. Identified fascicles in reading circuit [22].

Diffusion MRI techniques assess the diffusion process of water molecules in biological tissues and fractional anisotropy (FA) is a measure of this diffusion. Positive correlation between reading skills and FA in arcuate fascicles (shown in blue) [23, 24, 25] and inferior longitudinal fascicles (shown in orange) [26, 27] and negative correlation between reading skills and FA in posterior (temporal) callosal regions (green) were reported in multiple researches [28, 29, 30]. As a consequence, these three mentioned fascicles are considered to be as a part of reading circuitry in the network of the brain.

2.1.2 Reading a Word vs. a Non-word

Dorsal (tempo-parietal) and ventral (occipito-temporal) circuits are the two recognized reading systems in the left hemisphere (dominant hemisphere) of the brain. To perform a skilled reading task, collaboration of these two systems are reported to be necessary. At early stages of reading, the dorsal pathway is dominant. It is associated with the learning process that incorporates the orthographic features with phonological and lexical-semantic ones. Later, ventral pathway develops involving the word form system, which is responsible for the fulfillment of fluent reading. Although integrity of both circuits is reported to be necessary to perform a skilled reading task, as shown in Figure 2.7 reading words is more dependent on ventral pathway where reading non-words involve dorsal pathway [31].

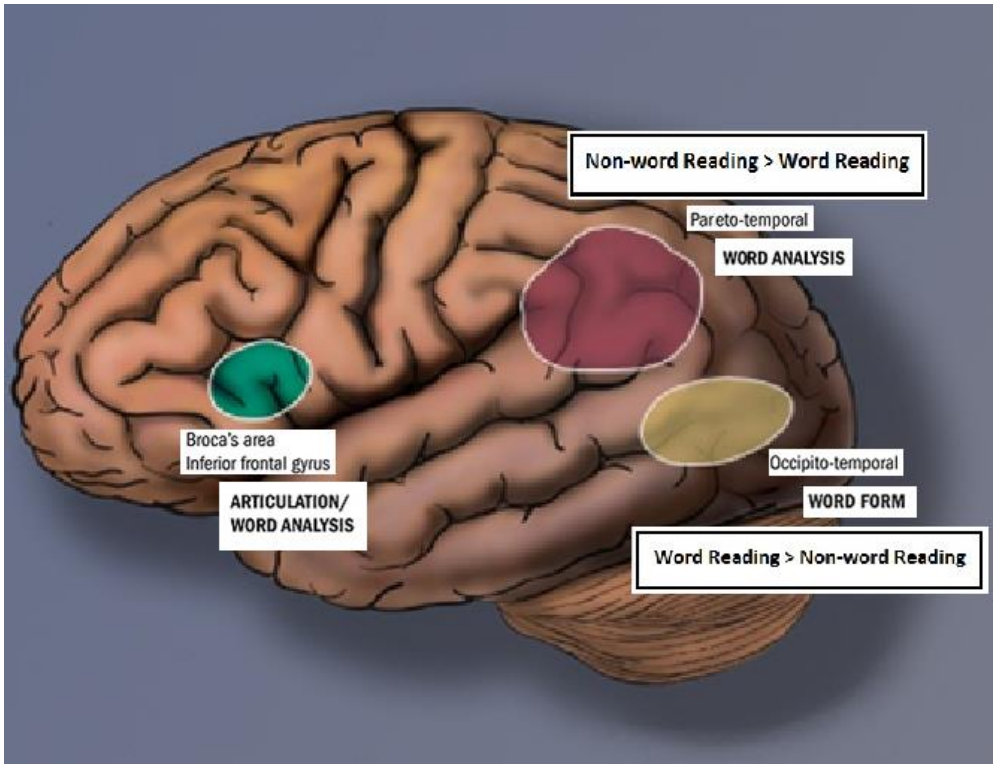

Figure 2.7. Representation of Occipito-temporal (Ventral) and Tempo-parietal (dorsal) regions [32].

2.2 Dyslexia

Developmental dyslexia is a brain disability that impairs the ability of learning to read, even with normal level of intelligence and adequate instruction. Neuroimaging techniques were widely used to investigate neural basis of dyslexia. There is a growing agreement that the focal deficit in dyslexia is associated with phonological processing. However, studies to address the neuronal impairment in dyslexia fall into three classes, studies that investigate phonological impairments, the ones that focus on visual processing and the studies that go over auditory processing abnormalities in dyslexics [33].

2.2.1 Phonological Processing and Dyslexia

There exists significant evidence for the importance of phonological information and its influence on all stages of reading, from word identification to passage comprehension [34]. From studies conducted to investigate phonological processing in dyslexia, disrupted activity patterns exist in widely distributed brain regions from occipito-temporal to posterior temporal, precentral and frontal cortical areas in dyslectic patients [35]. The most consistent areas with abnormal activation in dyslexic brains are reported to be in the left posterior inferior temporal lobe, [36, 37, 38] the angular gyrus [37, 39, 40, 41] and the left inferior frontal cortex.

There is not a consistent postulation about the function of the left posterior inferior temporal area. In some researches, it is postulated to take role in retrieving phonology from semantics [42, 43]. Nevertheless, it is suggested to serve as a word form area in some others [44, 45].

Historically, angular gyrus was reported to be a crucial component to perform reading task (Dejerine, 1891). Reduced activation in dyslexic brains was observed in many studies in this region. However, from variety of studies, activity of angular gyrus is necessary for processing semantic information across input modalities and not just for reading [46, 47, 48]. This leads to the conclusion that angular gyrus is not the center of the phonological deficit in dyslexia and the reduced activation in this area is a consequence of phonological impairment. Finally, significantly increased activation

was reported in left frontal regions in dyslexics, which was suggested to be the compensatory reflection of the brain for inadequate phonological specification.

Lately, Richlan, F., in a mini-review meta-analysis of dyslexia emphasized on the dysfunction of occipito-temporal, inferior parietal and inferior frontal areas. Figure 2.8 is representative of these areas on the left hemisphere of the brain. Occipito-temporal region involves fusiform gyrus which is suggested to be the visual word form area (VWFA) and takes role in the visual input processing before information takes its journey to the phoneme center, the Wernicke's area. As mentioned earlier, the abnormal function of frontal region is related to the compensatory pathways that the brains take to make up for the dysfunction in posterior language regions. As shown in the Figure 2.8, there is a strong evidence for the structural and functional connectivity between left occipito-temporal cortex (OT) and left inferior frontal gyrus (IFG) regions. However, the interconnection of these areas and left inferior parietal lobule (IPL) is less significant [49].

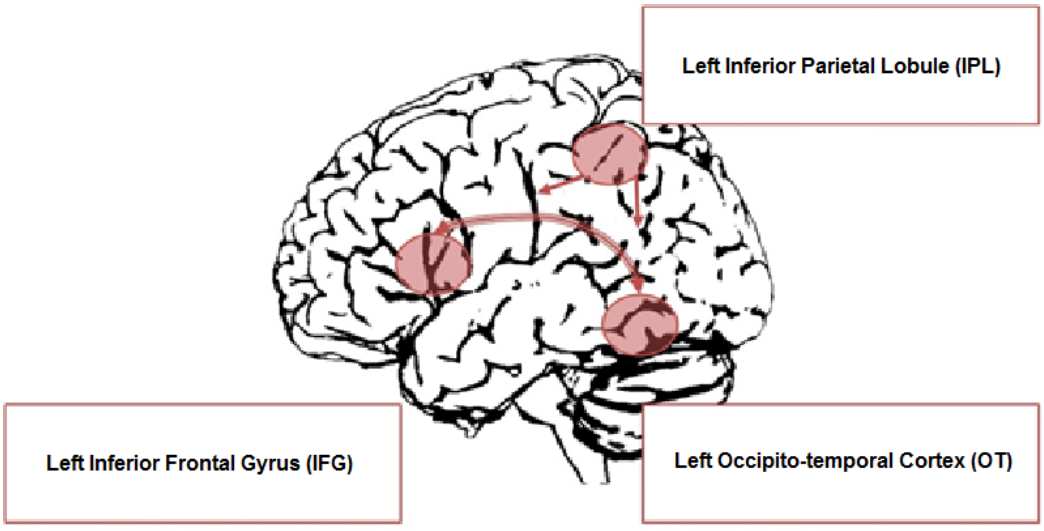

Figure 2.8. Dysfunction of a left hemisphere reading network in developmental dyslexia [49].

2.2.2 Visual and Auditory Processing Disturbance in Dyslexia

Although the focal impairment in dyslexia is associated to phonological processing, there exist variety of studies that suggest visual abnormalities in dyslexics [50]. Despite the inconsistencies in the results reported from these studies, generally,

dyslexic group appears to reveal differences in some of visual processing areas [51, 52, 53]. Other than visual processing, auditory processing is also investigated and postulated to be impaired in dyslexic brains. Studies of auditory repetition and tonal memory tasks reported right hemisphere differences in dyslexic brains [53]. However, Temple et al. reported reduced activation only in left prefrontal cortex in a study comparing rapid and slow auditory transitions between dyslexic and normal brain [54].

2.3 Brain Connectivity and Dyslexia

As mention earlier, the core deficit in dyslexia is attributed to phonological processing. In 1996, for the first time, Paulesu, E., et al. proposed that the phonological dysfunction of dyslectic brains is related to the weak connections between language areas [6]. Later in 2013, Boerts et al. found that phonetic representations are undamaged in dyslectic brains. However, the problem is associated to the accessibility of phonological information. They reported that the disturbed structural and functional connectivity patterns in temporal and frontal language-associated regions, blocks the access to the phonological knowledge [55].

2.3.1 Structural Connectivity

Diffusion tensor magnetic resonance imaging (DTI) reveals fiber pathways in the brain based on the diffusion of the water molecules in a specific direction. The diffusion coefficient or the fractional anisotropy depends on the number, orientation and the density of the axons. DTI is used in multiple studies to identify the abnormalities in structural connectivity of dyslexic brains [56]. Anomalies in tempo-parietal white matter [7, 57], arcuate fascicles [58] and shape of corpus callosum [59] are reported in dyslectic brains from these studies.

2.3.2 Functional and Effective Connectivity

Functional and effective connectivity disturbance in dyslectic patients is studied in multiple researches. These studies are classified into two main categories, resting-state and task-based ones.

Pre-stimulus and resting-state connectivity patterns are investigated in multiple studies. Table 2.1 contains a summary of these studies. In 2002, 60] Hampson, M., et al. employed two independent data sets to identify the correlations between the elements of the language system in the brain. A functional connectivity between Broca's area and Wernicke's area was reported in healthy subjects at rest based on correlation analysis of signal fluctuations of MR images [60]. In 2013, Koyama, M. S., et al. studied the intrinsic functional connectivity of control and dyslectic subjects by calculating the correlation between the time series of each region of interest (ROI) - determined based on previous studies- and every other brain voxel, based on the resting state fMRI data obtained from control subjects and three dyslectic groups (i.e., dyslectic subjects with no remediation, partial remediation and full remediation). Different intrinsic functional connectivity patterns were reported between controls and dyslectic groups. Specifically, reduced connectivity was observed between left intraparietal sulcus and left middle frontal gyrus in all dyslectic groups, which indicates the failure of the fronto-parietal (attention) network in dyslectic. Successful remediation also is characterized by changes in the intrinsic functional connectivity of the left fusiform gyrus [61]. In 2014, Schurz, M., et al. computes the temporal correlation between a given area to all other areas to analyze the functional connectivity between the regions of interest (ROIs) of left hemisphere and found a reduced connectivity between left posterior temporal areas (fusiform, inferior temporal, middle temporal and superior temporal) and left inferior frontal gyrus in dyslectic group in both resting-state and task-based conditions [62]. Lately, Zhou, W., et al. studied the functional connectivity of dyslectic subjects at rest, based on fMRI data, by computing the temporal correlation between a specific region of interest (seed) and all other voxels in the brain. They found disturbed functional connectivity from middle frontal gyrus (MFG) to two specified regions, namely, visual word form area (VWFA) and intraparietal sulcus (IPS) [63].

Task-specific investigation of functional and effective connectivity of dyslectic subjects was done in multiple researches. Table 2.2 represents a summary of these

studies. In 1998, Horwitz, B., et al. employed the positron emission tomography (PET) data obtained from dyslectic and control subjects while reading a single word to analyze the functional connectivity disturbance in dyslectic brains. In PET images neural activity of the brain is determined by the regional cerebral blood flow (rCBF) between brain regions. In Horwitz's study the correlation between the rCBF of the voxel attributed to angular gyrus [Talairach coordinates $(x, y, z) = (\pm 44, -54, +24)$] and all other voxels in the brains was calculated, as a measure of functional connectivity. Disconnection of left angular gyrus from visual areas, Wernicke's area and inferior frontal cortex in dyslectic group was reported from their study [12]. In 2000, Pugh, K. R., et al. applied multiple regression analysis on fMRI data to evaluate the correlational structure among selected regions of the brain. Data were obtained while performing 4 tasks varying in demands on orthographic, phonological, lexical-semantic processing from normal and dyslectic subjects. They reported disturbed functional connectivity between angular gyrus and left-hemisphere language-related regions, while performing tasks requiring phonological assembly in dyslectic group [23]. In 2006, Stanberry, L. I., et al. reported disturbed connectivity between left inferior frontal gyrus and frontal, occipital and cerebellar regions in the right hemisphere based on functional connectivity analysis of fMRI data obtained while reading pseudo-words. Functional connectivity patterns were extracted via clustering analysis [8]. In 2008, Richards, T. L., et al. investigate the group differences between functional connectivity of dyslectic and normal subjects before and after instructional treatment. Functional connectivity models were obtained from fMRI data based on seed-voxel correlation analysis. Disrupted functional connectivity is reported between left inferior frontal gyrus and multiple regions (right and left middle frontal gyrus, right and left supplemental motor area, left precentral gyrus, right superior frontal gyrus) [64]. In 2008, Quaglino, V., et al. applied structural equation modelling (SEM) on fMRI data obtained while performing a task including single word reading, pseudo word reading and picture-naming, to extract effective connectivity between specified regions of interest (ROIs) in a reading experiment and reported disturbed effective connectivity between supermarginal cortex and inferior frontal cortex in dyslectic group [65]. In 2008, Cao, F., et al, applied dynamic causal modelling (DCM) on fMRI data obtained during rhyming judgments to visually presented words, to study effective connectivity among specified regions of interest (ROIs) and suggested that the dyslectic subjects have problems to use left inferior parietal lobule to integrate orthography and

phonology and left inferior frontal gyrus to engage in phonological segmentation [66]. In 2010, Ligges, C., et al. applied time variant granger causality to study the effective connectivity disturbance in dyslectics and reported the right hemisphere language areas to participate in compensatory mechanism of dyslectic brains for phonological deficits [67]. In 2011, van der Mark, S., et al. based on a functional connectivity MRI study, where cross-correlation of the time series between specified ROIs and all other voxels in the brain were calculated to index functional connectivity, reported disturbed connectivity from visual word from area to frontal and parietal regions in dyslectic group [68]. In 2014, Finn, E. S., et al. analyze the functional connectivity based on fMRI data obtained from dyslectic and normal readers while performing a word- and a non-word-rhyming task from control and dyslectic subjects. They reported anomalies in the connection between visual regions and prefrontal areas, which indicates the more efficient integration of visual information in normal readers in comparison to dyslectic group. For dyslectic group an alternate phonology-based reading circuit is suggested [69].

2.4 Classification of Dyslectic and Normal Subjects

Classification of dyslectics from normal subjects with non-impaired reading disability provides the opportunity to detect future dyslectic subjects. A few researches aimed to classify two groups based on information obtained from neuroimaging techniques. In 1980, 70] Duffy, F. H., et al. classified EEG signals recorded while resting and activated testing condition based on a statistical technique and a classification of 80% to 90% was acquired [70]. In 2013, Karim, I., et al. applied kernel density estimation (KDE) to extract features from EEG signals obtained from dyslectics and controls during open and close eyes resting state and classified them by multilayer perception (MLP) method. They achieved a more than 90% accuracy in detecting the condition [71]. Table 2.3 represents a summary over these studies.

Table 2.1. Summary over studies on the resting-state functional and effective connectivity disturbance in dyslexia.

Authors	Year	Material	Method	Result
Hampson, M., et al. [60]	**2002**	**Two independent sets of resting state MR images from 11 healthy subjects aged between 23-49.**	**A hypothesis is made about connectivity between the elements of language system based on one data set and evaluation of the hypothesis based on correlation measures of the other data set. Then the roles of the data sets are changed and the procedure is repeated for other probable connections.**	**Functional connection between Broca's and Wernicke's area in healthy subjects at rest**
Koyama, M. S., et al. [61]	**2013**	**Resting-state fMR images from 33 control subjects and three dyslectic groups(i.e., no remediation, partial remediation, full remediation – total 11 subjects)**	**Correlation between brain activity from a specific region of interest (seed) to all other voxels in the brain is computed.**	**Reduced connectivity between left intraparietal sulcus and left middle frontal gyrus in all dyslectic groups. Changes in functional connectivity of the left fusiform gyrus in successfully remediated dyslectics**
Schurz, M., et al. [62]	**2014**	**Resting state and reading-based fMR images of 14 control and 15 dyslectic subjects**	**Correlation between brain activity from a specific region of interest (seed) to all other voxels in the brain is computed.**	**A consistent reduced connectivity between left posterior temporal areas (fusiform, inferior temporal, middle temporal and superior temporal) and left inferior frontal gyrus in dyslectic group**
Zhou, W., et al. [63]	**2015**	**Resting state fMR images of 26 control and 21 dyslectic subjects**	**Correlation between brain activity from a specific region of interest (seed) to all other voxels in the brain is computed.**	**Disturbed functional connectivity between IPs and MFG and also between VWFA and MFG**

Table 2.2. Summary over studies on the task-based functional and effective connectivity disturbance in dyslexia.

Authors	Year	Material	Method	Results
Pugh, K. R., et al. [23]	**2000**	**fMRI data obtained while performing 4 tasks varying in demands on orthographic, phonological, lexical-semantic processing from 31 normal and 29 dyslectic subjects**	**Multiple regression analysis is used to examine the correlational structure between angular gyrus and posterior temporal occipital sites.**	**Functional connectivity disturbance in dyslectic subjects while performing tasks requiring phonological assembly between angular gyrus and left-hemisphere language-related regions.**
Quaglino, V., et al. [65]	**2008**	**fMRI data obtained while performing a task including single word reading, pseudo word reading and picture-naming from 6 normal and 6 dyslectic subjects**	**Structural equation modelling (SEM) was applied to extract effective connectivity.**	**Disturbed effective connectivity between supermarginal cortex and inferior frontal cortex in dyslectic group**
Cao, F., et al. [66]	**2008**	**fMRI data obtained during rhyming judgments from 12 normal and 12 dyslexic subjects**	**Dynamic causal modelling (DCM) was used to extract effective connectivity models.**	**Deficits in integrating orthography and phonology utilizing left inferior parietal lobule, and in engaging phonological segmentation via the left inferior frontal gyrus by dyslectics.**
Ligges, C., et al. [67]	**2010**	**EEG and fMRI data obtained while performing a task involving basic visual, orthographic and phonological processing from 14 normal and 15 dyslexic subjects**	**Time variant granger causality was applied to study the effective connectivity.**	**Right hemisphere language areas to participate in compensatory mechanism of dyslectic brains for phonological deficits**
van der Mark, S., et al. [68]	**2011**	**fMRI data obtained during a continuous reading task requiring phonological and orthographic processing from 24 control and 18 dyslexic subjects**	**Cross-correlation of the time series between specified ROIs and all other voxels in the brain were calculated.**	**Significant disruption of functional connectivity between the VWFA and left inferior frontal and left inferior parietal language areas in dyslectic children.**

Table 2.2. Continued.

Finn, E. S., et al. [69]	**2014**	**fMRI data obtained while performing a word and non-word-rhyming task from 32 control and 43 dyslectic subjects**	**Pairwise correlation coefficient between the time courses of each possible pair of nodes was calculated to estimate functional connectivity**	**Anomalies in the connection between visual regions and prefrontal areas**
Stanberry, L. I., et al. [8]	**2006**	**fMRI data obtained while reading pseudo-words (continuous phoneme-mapping task) from 10 control and 13 dyslexic subjects**	**Clustering method is applied to extract regions with similar temporal behavior**	**Disturbed connectivity between left inferior frontal gyrus and frontal, occipital and cerebellar regions in the right hemisphere in dyslectic subjects**
Richards, T. L., et al. [64]	**2008**	**fMRI data obtained from 21 normal and 18 dyslectic subjects while performing a phoneme mapping task before and after receiving treatment by dyslectic group**	**Seed voxel correlation analysis was used to extract functional connectivity**	**Disrupted connectivity between left inferior frontal gyrus and multiple regions (right and left middle frontal gyrus, right and left supplemental motor area, left precentral gyrus, right superior frontal gyrus) before treatment and no difference were reported between two groups after treatment**
Horwitz, B., et al. [12]	**1998**	**PET images obtained while reading a single word from 14 control and 17 dyslexic subjects**	**Correlation between brain activity from a specific region of interest (seed) to all other voxels in the brain is computed**	**Disconnection of left angular gyrus from visual areas, from Wernicke's area and from inferior frontal cortex in dyslectic brains.**

Table 2.3. Summary over studies that challenge the classification of dyslexics from normal subjects.

Author	year	Material	Method	Result
Duffy, F. H., et al. [70]	**1980**	**EEG and evoked potentials gathered from 18 normal and 11 dyslectic subjects, during 13 experiments varying from no instruction to complex discrimination task (A total 183 features were extracted from the measurements).**	**After feature reduction, classic discriminant analysis was applied to demonstrate statistically significant differences between two groups**	**classification rate of 80 to 90%**
Karim, I., et al. [71]	**2013**	**EEG signals recorded during resting state from 3 control and 3 dyslectic children aged between 4-7.**	**Feature extraction via Kernel Density Estimation (KDE) and classification by multilayer perception (MLP) was applied on data**	**classification rate of more than 90%**

CHAPTER 3

CONNECTIVITY ANALYSIS OF HUMAN BRAIN

In the human brain, there exist multiple individual elements. These elements interact with each other to combine their individual actions. The integrated response of specific interacting elements gives rise to specific human brain function. As so, for a normal brain function, a well-established connectivity is necessary between multiple brain regions. Studying interconnections among neuronal components could shed light on the basics of neurological disorders like dyslexia [72, 73].

Three different but related forms of connectivity, namely, structural, functional and effective are introduced to analyze interactions between neuronal components of the brain [10]. Structural connectivity is about understanding the anatomical links that exist in the brain and is commonly determined by fiber tracking from Diffusion tensor MR images [74]. Plausibility of the estimated functional and effective connectivity can be verified by the findings from structural connectivity analysis [75]. Functional connectivity is expressed as temporal dependencies between remote neuronal units. Correlation, coherence and such statistical measures in either time or frequency domain is been broadly applied on neurophysiological data to evaluate functional connectivity, as a fundamentally statistical concept [76, 77, 78, 79]. Effective connectivity is a measure of "the influence one neural system exerts on another" [10]. It captures the causal relationships between neuronal populations and determines the directionality of the information flow between brain networks [80, 81, 82].

3.1 Effective Connectivity

Investigating effective connectivity is been reported to be essential in the assessment of the functional integration of neuronal population and normal function of the brain [11, 76]. The connectivity patterns of the brain are usually restricted by structural connectivity and the related anatomical links. Still, it is not possible to infer effective connectivity, which is a dynamic model and changes with the context of the experiments, from structural connectivity [74]. Furthermore, since more than one arrangement of neurons may result in the same final behavior, information from structural connectivity cannot give rise to a unique effective connectivity model [83]. Functional connectivity, as a measure of statistical dependencies, is a function of probability distributions over observations (an information theoretic measure) and involves no inference about the coupling between two brain regions [78]. Conversely, effective brain connectivity corresponds to the parameters of a model that explains the dependencies between brain regions and correlates with the notion of coupling and directed causal influence [78]. In general, effective connectivity is becoming increasingly popular in the analysis of functional integration of the brain since its underlying model indicates the mechanism of neuronal coupling and provides information about directionality of the information flow between brain regions [74].

3.2 Methods to Model Effective Connectivity

Although statistical measurements like covariance and correlation are mostly used to find functional connectivity, various mathematical methods are used to model effective connectivity. Here is a brief review over these methods.

3.2.1 Transfer Entropy (TE)

In 2000, transfer entropy was introduced as a measure of causal influences in a coupled complex network by Schreiber. This method is able to quantify the statistical coherence between the elements of linear or non-linear networks. Detecting the information exchange between elements in the system is a challenging task. Transfer entropy derives directional interaction properly by ignoring the common input and

common history of the elements in the computations [84, 85]. Sabesan, S., et al. applied TE on EEG data obtained from epileptic patients and the foci specified by the method was in total agreement with the clinically assessed centers in the brain [85]. However, the execution of this method depends on the estimation of transition probabilities requiring selection of the memory of the variables [79]. Mathematical basics of transfer entropy (TE) is explained below [85].

Probability of a specific state of a k-th order Markov process depends only on the *k* past states of the system, as expressed in Equation (3.1), where *P* defines the conditional probability of a random process *X* taking the value x_{n+1} at time *n* + 1:

$$P(x_{n+1}|x_n, x_{n-1}, \dots, x_{n-k+1}) = P(x_{n+1}|x_n, x_{n-1}, \dots, x_{n-k}). \quad (3.1)$$

Past *k* states of the random process *X*, [$x_n, x_{n-1}, \dots, x_{n-k+1}$], is specified by $x_n^{(k)}$. An extension of Equation (3.1), is the Markov interdependence of two random processes *X* and *Y*, as expressed in Equation (3.2), where $y_n^{(l)}$ defines the past *l* state of random process *Y*:

$$P(x_{n+1}|x_n^{(k)}) = P(x_{n+1}|x_n^{(k)}, y_n^{(l)}). \quad (3.2)$$

This implies that the probability of the random process *X* happens to be at state x_{n+1} at time *n* + 1, is independent of past *l* states of process *Y* and it only depends on the past *k* states on process *X*. However, if the past states of both processes (*X* and *Y*) influences the state of process *X* at time *n* + 1, Kullback–Leibler measure determines the divergence between the hypothesized transition probability, $P(x_{n+1}|x_n^{(k)})$, and the true transition probability, $P(x_{n+1}|x_n^{(k)}, y_n^{(l)})$. This measure quantifies the influence of random process *Y* on random process *X* and is expressed in Equation (3.3), where *N* indicates the number of points of the processes in the system and *k* and *l* are the orders of the Markov process for *X* and and *Y*, respectively:

$$TE(Y \rightarrow X) = \sum_{n=1}^{N} P(x_{n+1}|x_n^{(k)}, y_n^{(l)}) \; log_2 \frac{P(x_{n+1}|x_n^{(k)}, y_n^{(l)})}{P(x_{n+1}|x_n^{(k)})}. \quad (3.3)$$

Transfer entropy (TE) can be also expressed in terms of conditional entropies, as in Equation (3.4), where $H(x_{n+1}|x_n^{(k)})$ is the information obtained about x_{n+1} based on the information of $x_n^{(k)}$ and $H(x_{n+1}|x_n^{(k)}, y_n^{(l)})$ is the information obtained about x_{n+1}

based on the information of $x_n^{(k)}$ and $y_n^{(l)}$. So, $TE(Y \rightarrow X)$ is the extra information that the past *l* point of *Y* provides about the future state of *X*:

$$TE(\mathrm{Y} \rightarrow \mathrm{X}) = H(x_{n+1}|x_n^{(k)}) - H(x_{n+1}|x_n^{(k)}, y_n^{(l)}). \quad (3.4)$$

3.2.2 Multivariate Autoregressive Model (MVAR)

The linear multivariate autoregressive is considered to be a simple approach to model the interactions of a multivariate time series. The basic assumption of the method is that the current state of the series can be estimated by a linear combination of its last N points. The coefficients of the model are determined such that the relative linear combination of the past values gives the best possible prediction for the current value (evaluated in the least square sense). The coefficients of the model can be interpreted as the influence of one time series upon the other one [86]. MVAR is a linear measure and imposes problem when dealing with clearly nonlinear networks like brain [75], [87]. Following is an explanation over the mathematical basics of multivariate autoregressive model (MVAR) [86]. Considering a univariate time series, current value of the variable is modelled by a weighted linear summation over its previous values. Number of previous data points used in the modelling process is the order of the model and the weights are the parameters of the model. An extension of this approach to multivariate time series gives rise to multivariate autoregressive model (MVAR). In a MVAR a vector of current values of all variables is represented as a linear weighted sum over previous values of the variables in the system. Consider a d-dimensional multivariate system modelled by a MVAR of order p. The value of the multivariate d-dimensional system is predicted by the weighted linear summation over previous p vectors, as shown in Equation (3.5), where

$y_n = [y_n(1), y_n(2), \dots, y_n(d)]$, is the *n*-th sample of the time series, A(i) is a d-by-d matrix containing the weights and *e(n)* is the error vector which is considered to be a Gaussian noise with zero mean:

$$y_n = \sum_{i=}^{p} y_{n-i} A(i) + e(n). \quad (3.5)$$

Parameters of the model determines the influence of a random variable on other variables. In other words, weights are a measure of linear dependency between variables and a zero weight indicate the independency between pair of variables in the system.

3.2.3 Directed Information Theory (DIT)

Directed information is a method that recently attract attentions for quantifying causal relationship from neurophysiological data [79]. This method involves measures such as transfer entropy which explains it in an information theoretic sense and make it suitable to be used in neuroscience problems [88]. However, it is incapable to distinguish between totally dependent and independent processes [79]. Hinrichs, H., et al. provide evidence that directed information theory (DIT) can be used as an efficient method to extract directional information flow among cortical regions of the brain based on EEG/MEG data obtained during a visual spatial attention task [89]. Mathematical essentials of DIT is discussed here. Considering two random variables *X* and *Y*, mutual information of them is defined as the amount of information that *Y* provides about *X*, as illustrated in Equation (3.6):

$$I(X;Y) = H(X) - H(X \mid Y). \tag{3.6}$$

An extension of the mutual information to random vectors ($X^N = (X_1, X_2, \dots, X_N)$ and $Y^N = (Y_1, Y_2, \dots, Y_N)$), mutual information is expressed as Equation (3.7):

$$I(X^N;Y^N) = H(X^N) - H(X^N \mid Y^N). \tag{3.7}$$

Mutual information is incapable of revealing any causal or directional influences in the system. This problem is addressed by introducing the concept of directed information, formulized as shown in Equation (3.8), where $H(Y^N \mid |X^N)$ is the entropy of Y^N causally conditioned on X^N and its value is calculated by Equation (3.9):

$$\mathrm{DI}(X^N \to Y^N) = H(Y^N) - H(Y^N \mid | X^N). \tag{3.8}$$

$$H(Y^N \mid |X^N) = \sum_{n=1}^{N} H(Y^N \mid Y^{N-1} X^N). \tag{3.9}$$

3.2.4 Granger Causality (GC)

In 1956, Weiner proposed that causal influence between two series can be identified, if statistical information of one of them, augments the prediction of the other one. Later in 1969, the popular operational definition of causality, the so-called, "Granger Causality" was introduced by Granger. It indicates that if a time series *X* provides predictive information about the future of time series *Y* better than past values of *Y*, *X* is said to Granger-cause *Y*. Although Granger causality is usually estimated with multivariate autoregressive (MVAR) methods, there exist other methods like mutual information which might be used to investigate Granger causality (GC) [75, 90]. Following a mathematical explanation for the case GC is estimated based on MVAR model. Suppose that *X* and *Y* are two elements of a multi-variate system. Equations (3.10) and (3.11) represent the univariate autoregressive models of *X* and *Y* and Equations (3.12) and (3.13) illustrate the bivariate autoregressive models of them:

$$x(n) = \sum_{k=1}^{p} a_{1k} x(n-k) + u_1(n). \quad (3.10)$$

$$y(n) = \sum_{k=1}^{p} b_{1k} y(n-k) + v_1(n). \quad (3.11)$$

In univariate autoregressive models, the prediction of the signal depends only on the past value of the signal, where in bivariate autoregressive models, the past values of the own signal and also the other signal both influence the predicted value of the signal:

$$x(n) = \sum_{k=1}^{p} a_{2k} x(n-k) + \sum_{k=1}^{p} c_{2k} y(n-k) + u_2(n). \quad (3.12)$$

$$y(n) = \sum_{k=1}^{p} b_{2k} x(n-k) + \sum_{k=1}^{p} d_{2k} y(n-k) + v_2(n). \quad (3.13)$$

The accuracy of prediction is measured by the variance of the prediction errors in univariate and bivariate autoregressive models, as represented in Equations (3.14) to (3.17):

$$\sum_{X \mid X^-} = var\,(u1). \quad (3.14)$$

$$\sum_{Y \mid Y^-} = var\,(v1). \quad (3.15)$$

$$\sum_{X \mid X^-, Y^-} = var\,(u2). \quad (3.16)$$

$$\sum_{Y \mid Y^-, X^-} = var\,(v2). \quad (3.17)$$

If considering the past values of signal *Y*, improves the prediction of the signal *X* (The variance of prediction error decreases), it is said that signal *Y* causes signal *X*. Granger Causality of *Y* to *X* is expressed in Equation (3.18):

$$F_{Y \to X} = \frac{\Sigma_{X \mid X^-}}{\Sigma_{X \mid X^-, Y^-}}. \tag{3.18}$$

And in a similar way, the granger causality of X to Y is defined as shown in Equation (3.19):

$$F_{X \to Y} = \frac{\Sigma_{Y \mid Y^-}}{\Sigma_{Y \mid Y^-, X^-}}. \tag{3.19}$$

The maximum of the terms represented in Equations (3.18) and (3.19), indicates the strength of direction (or in some cases bi-directional) causal interconnection between signals.

3.2.5 Directed Transfer Function (DTF)

Directed transfer function (DTF) is a spectral measure to extract casual relationships between brain regions by detecting directional influences between each pair of multivariate data. This method basically relies on Granger causality concept and requires a MVAR model to fit the whole set of data [73, 91, 92]. DTF distinguishes between the forward and backward information flow and serves as a method to detect directionality. Furthermore, since it is not responsive to volume conduction, it is considered a good measure for EEG data analysis [73]. Mathematical fundamentals of this method is explained here [73]. A *p*-ordered multivariate autoregressive model of a *M*-dimensional multivariate signal *X* is described such that the signal at time *n*, is expressed as Equation (3.20), where A_k is the coefficient matrix containing the weights of the model which determine the influence of each past signals at time instant n-k on current signal and *E(n*) is the noise term assumed to be zero-mean normally distributed:

$$X(n) = \sum_{k=1}^{p} A_k \, X(n-k) + E(n). \tag{3.20}$$

After transformation into z domain and substitution of z^{-1} with $e^{-i2\pi f/f_s}$, Equation (3.20) takes the form represented in Equation (3.21), where *E(f)*, *X(f)*, and *A(f)* are the

E(n), *X(n)* and $\acute{A}$ in the frequency domain, A_0 is the identity metrix and $\acute{A}_k = -A_k$, when k tkes the values from 1 to *p*:

$$X(f) = E(f)\ (\sum_{k=0}^{p} \acute{A}_k e^{-i2\pi f/f_s})^{-1} = E(f)A^{-1}(f) = E(F)H(f). \quad (3.21)$$

H(f) is called the transfer matrix and DTF is measured as shown in Equation (3.22). It is a value between zero and one, where zero value indicates the two variables, *i* and *j*, are completely uncorrelated:

$$DTF_{ij}(f) = \frac{|H_{ij}(f)|}{\sqrt{\sum_{j=1}^{d} |H_{ij}(f)|^2}}. \quad (3.22)$$

3.2.6 Partial Directed Coherence (PDC)

Partial directed coherence proposed by Baccalá, L. A., et al, in 2001 is another approach to describe relationships between multivariate time series. This method provides a frequency-domain representation for Granger causality. In comparison to DTF, PDC gives rise to a more statistically and numerically reliable results [93]. Bjorn Schelter, B., et al. applied PDC to detect directed relationships on EEG data obtained from a patient suffering from essential tremor [94]. Here is a brief explanation over mathematical background of partial directed coherence [94]. Consider a p-ordered multivariate autoregressive model of a *n*-dimensional multivariate signal **x** which is modelled by a multivariate autoregressive (MVAR) model as represented in Equation (3.23):

$$x(t) = \sum_{r=1}^{p} a(r)x(t-r) + \varepsilon(t). \quad (3.23)$$

Consider $A(w) = I - \sum_{r=1}^{p} a(r)e^{-iwr}$, indicates the difference between the identity matrix and the Fourier transform of parameters of MVAR model. The partial directed coherence described in Equation (3.24) provides a measure of directed linear influence of x_j on x_i at frequency *w*:

$$\left|\pi_{i\leftarrow j}(w)\right| = \frac{|A_{ij}(w)|}{\sqrt{\sum_k |A_{kj}(w)|^2}}. \quad (3.24)$$

3.2.7 Structural Equation Modeling (SEM)

Structural equation model is reported to be the most widely used method in analyzing effective connectivity [91, 95]. This technique uses both available priori information about brain anatomy and the inter-regional co-variances between observed variables to extract the causal relationships in the brain network. It consists of a set of linear structural equations made up of observed variables and parameters of the model. These parameters define causal relationships between the variables and are estimated by minimizing the difference between the functional interaction and the knowledge of physical connections from priori information [95], where functional interaction is estimated by decomposing interregional co-variance among brain regions [96]. Mathematical background of the structural equation modelling is discussed here [91]. Consider a system having multiple variables with *n* observations. The structural equation model over the variables is illustrated in Equation (3.25), where y is a (*m*×1) vector of dependent variables, *x* is a (*n*×1) vector of independent variables, ζ is a (*m* ×1) vector of equation errors, *B* is a (*m*×*m*) coefficient matrix of dependent variables, Γ is a (*m*×*n*) coefficient matrix of independent variables. ζ is assumed to be uncorrelated to the independent variables and the diagonal elements of *B* are zero since independent variables should not influence themselves:

$$y = By + \Gamma x + \zeta. \quad (3.25)$$

In this model $\Phi = E[xx^T]$ and $\Psi = E[\zeta\zeta^T]$ are considered as the covariances of the model, which are covariance matrix of the independent variables and covariance matrix of the errors, respectively. If *Z* is a vector containing all the variables in the network, in the order shown in Equation (3.26), the observed covariance will be described as in Equation (3.27), where Z is the *n*×*p* matrix of *p* variable in the network for each *n* observation. The covariance matrix from the model is calculated from Equation (3.28):

$$z^T = [x_1 \dots x_n y_1 \dots y_n]. \quad (3.26)$$

$$\sum_{obs} = \left(\frac{1}{N-1}\right).\ Z\ .\ Z^{T}. \tag{3.27}$$

$$\sum_{mod} = \begin{bmatrix} \Phi & (I-B)^{-1}\Phi \\ ((I-B)^{-1}\Phi)^{T} & (I-B)^{-1}(\Gamma\Phi\Gamma+\Psi)((I-B)^{-1})^{T} \end{bmatrix}. \tag{3.28}$$

To minimize the difference between the $\sum_{mod}$ and $\sum_{obs}$, since the number of unknowns (the number of elements of B, Ψ, Γ and Φ) are more than the number of equations, $(n+m+1)(n+m)/2$, SEM required a priori formulation of an anatomical model. This model point the existence of a few casual relationships among variables of the system. Parameters of the arcs that are not present in the hypothetical model are called free parameters. Number of free parameters (t) should be less than $(n+m+1)(n+m)/2$. These parameters are determined by minimizing a function of implied and observed covariance matrices. Most of the SEM applications use the maximum likelihood function as illustrated in Equation (3.29), where *tr(.)* implies the trace of the argument matrix:

$$F_{ML} = log\,|\sum_{mod}| + tr(\sum_{obs}) - \log|\sum_{obs}| - p\ . \tag{3.29}$$

3.2.8 Dynamic Causal Modeling (DCM)

Dynamic causal modeling (DCM), which was designed specifically for neuroimaging data, is a powerful method in investigating effective connectivity [72]. DCM initially estimates the underlying neuronal sources from the measured data. Thereafter, it models the effective connectivity based on estimated neuronal activities rather than the measured data. This may cause the results obtained from DCM to be more realistic [11]. DCM derives the dynamic interactions among different regions of the brain by first estimating intrinsic connections between sources and then changes the connections of the model considering the influence of external perturbation. Effective connections are evaluated by a Bayesian estimation procedure to find the best model [72, 97]. Alike SEM, DCM needs a prior model which usually serves as an anatomical constraint [96]. This method assumes deterministic relationships between different brain regions and do not take into account the noisy interactions [98]. The basic idea of DCM is explained here. Dynamic models are constructed based on a general bilinear state equation represented in Equation (3.30), where x indicates the state of the system,

ẋ indicates the changes in the state, u is the external input of the experimental manipulations, C is the parameters of the input which shows the direct effect of input on specific areas, A matrix represent the coupling between different areas in the absence of external manipulation and B matrix contains the changes that occurs to the couplings in presence of external manipulation:

$$\dot{x} = (A + \sum_{j=1}^{m} u_j B^j) x + Cu. \quad (3.30)$$

DCMs are generated multiple layouts of forward and backward self-connections and their modulations. These models are later analyzed via Bayesian model comparison to select the best model that fits the data [99].

3.2.9 Bayesian Network (BN)

Typical medical problems are associated with dozens or even hundreds of explanatory features. It is confusing and in some cases impractical to determine the joint distribution over all features and characterize the condition in complex networks based on all the data. Probabilistic graphical models provide a compact structure to describe the distributions over the intricate systems [100].

A Bayesian Network is a graphical model that represents conditional independencies between the variables of the network under investigation [101]. It involves concepts from probability, statistics and graph theory [76]. BN is able to detect the optimal connectivity structure without any structural knowledge. It learns the overall effective connectivity pattern rather than the pairwise connections between the variables of the system [102]. Bayesian network, involving concepts from statistics and machine learning, is reported to be a powerful tool to extract dependencies among the variables of the system under investigation [103]. As mentioned earlier, neurons in the brain interact with each other via the neuronal links and this interaction is modeled in a structurally similar way using BN. The flexibility of BN, which makes it possible to employ different statistical measures to explain the dependency relationships between random variables, makes it a very efficient method to address effective connectivity in the brain [11]. However, BN cannot capture the temporal characteristics, since it gives a single snapshot of the connectivity which is dominant over the whole data [104].

A Bayesian network (BN) is a graphical representation over a joint probability distribution. The structure of a Bayesian network provides the opportunity to extract the conditional independence assumption or the local independencies in the network. Each Bayesian network has two units, one qualitative and one quantitative unit.

The qualitative part is a directed acyclic graph (DAG) which is the structure of Bayesian network. The nodes in the structure of BN are representative of random variables in the system and the edges between the nodes indicate the direct statistical dependencies between corresponding random variables. If there exists an edge from one node, called the parent node, to another one, called the child node, the value that the child node takes depends of the value of the parent node. The descendants of each node are all the nodes that are reachable from that node by tracking the direction of the edges. The rest of the nods in the system are called the non-descendants [103]. The quantitative part of a BN is the conditional probability distribution (CPD) specified for each node, given its parents [105]. For the variable that take discrete values, these CPDs are usually illustrated in a table. The probability of each possible value for the child node is represented for all feasible combination of values of its parents in a tabular form. Succinctly, a Bayesian network is characterized by its structure and associated parameters that are the existed conditional probabilities in the structure [105, 106]. Following is an explanation over the mathematical basics of Bayesian networks.

3.2.9.1 Conditional Probability Distribution of Bayesian Network

Consider there exists n random variables in the network denoted by $X_1,\ldots, X_n$, G is the Bayesian network structure over the random variables and $Pa_{X_i}^{G}$ indicates the parent of X_i.

Based on the chain rule, the joint probability distribution over the random variables is measured from the Equation (3.31):

$$P(X_1,\ldots, X_n) = P(X_2 \mid X_1)P(X_3 \mid X_1, X_2) \ldots P(X_n \mid X_1, X_2, \ldots, X_{n-1}). \quad (3.31)$$

From the Bayesian network semantics, X_i is independent of its nondescendants given its parents:

For each variable X_i : $(X_i \perp NonDescendants_{X_i} \mid Pa_{X_i}^G)$.

This property is utilized to measure the joint probability distribution over the random variables in the network with the involvement of reduced number of parameters. Based on the Bayesian chain rule, the joint probability distribution over the random variables is measured from the following equation which is calculated based on local probabilistic quantities termed as $P(X_i \mid Pa_{X_i}^G)$:

$$P(X_1,\ldots,X_n) = \prod_{i=1}^{n} P(X_i \mid Pa_{X_i}^G) . \quad (3.32)$$

The parameters of the dynamic Bayesian network are $P(X_i \mid Pa_{X_i}^G)$ for all the variables i=1,..,n in the system. $P(X_i \mid Pa_{X_i}^G)$ is specified by $\theta_{X_i \mid Pa_{X_i}^G}$ in Equation (3.33). The parameters of the Bayesian network are the ones that maximize the log-likelihood function represented in Equation (3.33), where n(x_i, x_{pa_i}) indicates the number of observed instances with a particular setting of the variable and its parents:

$$l(D; \theta, G) = log\ (P|D)$$

$$= \sum_{i=1}^{n} \sum_{x_i, x_{pa_i}} n(x_i, x_{pa_i}) \log \theta_{x_i|x_{pa_i}} . \quad (3.33)$$

Parameters that maximize the log-likelihood function ($\hat{\theta}_{x_i|x_{pa_i}}$) is calculated via Equation (3.34), where r_i is the number of different values that the variable x_i takes [107]:

$$\hat{\theta}_{x_i|x_{pa_i}} = \frac{n(x_i, x_{pa_i})}{\sum_{\acute{x}_i=1}^{r_i} (\acute{x}_i, x_{pa_i})} . \quad (3.34)$$

3.2.9.1 Structure of Bayesian Network

The problem of learning a Bayesian network is about finding a network that best matches the training data set [108]. Multiple methods such as, K2 algorithm, Markov Chain Conte Carlo (MCMC), Bayesian Network Power Constructor (BNPC) and Greedy Search in Markov Equivalent Space, are proposed to learn the structure of a Bayesian network from a data set [109].

The methods that have been introduced to address the problem of learning a Bayesian network are classified into three groups, constraint-based structure learning, score-based structure learning and Bayesian model averaging technique.

In constraint-based structure learning, initially the aim is to extract the dependencies and independencies in the network and then to find a network which best explains these dependencies and independencies. The drawback of this method is its sensitivity to individual independence tests employed to extract dependencies and independencies in the network. Even one wrong answer may lead to a mistaken structure learning procedure [110].

In Bayesian model averaging technique, it is attempted to produce a set of possible structures based on Bayesian reasoning and then average over all possible structures.

In score-based structure learning, initially a space of potential models are defined and then a score function is used to evaluate how well the models fit the data. Score-based structure learning algorithms are less sensitive to individual independence tests, since they evaluate the whole structure all at once. The number of structures in the space of potential models is 2 to the power of $O(n^2)$, where n indicates the number of random variables. It is obvious that scoring all the possible models is impractical and finding the one optimal network is a NP-hard problem. Thus, heuristic search techniques are applied to select a hypothesis space of possible models. Multiple methods like greedy hill climbing, Markov Chain Monte Carlo (MCMC), K2 and exhaustive search has been introduced to select the possible structures [111].

Scoring functions for learning Bayesian networks, are classified into two main groups, Bayesian scores and information-theoretic scores [105]. Information-theoretic scores determined how well a structure fits to data, based on the concepts from information theory and codification [112]. LL, AIC, BIC/minimum description length (MDL), Normalized Minimum Likelihood (NML) and mutual information tests (MIT) are all examples of information-theoretic scoring functions. The basic idea of Bayesian scoring methods (e.g. K2, BD, BDe, BDeu) is that a prior probability over the possible networks is assumed and then the posterior probability of the networks is calculated conditioned on the data. The best structure is the one with the highest posterior probability [105].

3.2.9.1.1 Structure Learning Algorithm

As mentioned earlier, since the number of all possible networks is exponential to the number of nodes in the network and evaluating all the structures is impractical, score-based structure learning algorithms require heuristic search techniques to select a hypothesis space of possible structures. In this study, Markov Chain Monte Carlo (MCMC) technique was used to select possible networks from the space of potential structures. MCMC simulation was started with an initial graph structure. Posterior probability of the initial graph was calculated. Considering the initial network, a new graph is generated by adding or removing an edge. The posterior probability of the new graph structure is calculated. Then the acceptance of the new graph is determined by the Metropolis-Hastings acceptance criterion (MHAC) shown in Equation (3.35), where posterior probabilities are calculates by Bayesian score (BDeu). The term $\frac{Q(G_{old}|G_{new})}{Q(G_{new}|G_{old})}$ is the hasting ratio, which involves the proposal probabilities (Q):

$$P_{M\,H} = min\left\{ 1 , \frac{P(G_{new}|D)}{P(G_{old}|D)} \; x \; \frac{Q(G_{old}|G_{new})}{Q(G_{new}|G_{old})} \right\}. \tag{3.35}$$

If $P_{M\,H}$ is bigger than one, this indicates that the proposal move, augment the fitness of the graph structure to the data and the new structure will be accepted. Otherwise, the proposal move gives rise to a graph structure which is less preferable than the old graph. In this case the newly generated graph is rejected, the old graph structure is kept and the rest of the simulation will continue with generating new structures based on the old graph.

The steps of MCMC simulation are repeated for several times and eventually there will be an averaging task over all the kept graphs. The obtained value for each edge will be representative of its posterior probability. The algorithm includes a burn-in step that includes the initial sampled graphs. Since these initial networks are no stable and reliable, they are not considered in the final averaging task [103].

The initial graph to start the MCMC simulation is a graph with one edge, which is selected randomly. MCMC is simulated multiple times initiating from different one-edge randomly selected graph structures. The final step of the algorithm is averaging over the posterior probabilities of edges obtained as the results of all the simulations which finally gives us an adjacency matrix which assign a weigh to each possible edge.

3.2.9.1.2 BDeu Scoring Function [105]

The posterior probabilities in the structure learning algorithm are calculated via a Bayesian-based scoring function, called BDeu scoring function. As mentioned earlier, to calculate the score of a network, Bayesian-based scoring algorithms consider a prior probability over the structure of the network and then a score is assigned to the structure based on the computed posterior probability conditioned on the data.
In 1995, Heckerman et al. proposed the Bayesian Dirichlet (BD) score considering 4 assumptions about *P(B,D),* where *B* is the Bayesian network and *D* is the data.

Notations:

$\boldsymbol{\Theta_G} = \{\boldsymbol{\Theta_i}\}_{\boldsymbol{i=1,\ldots,n}}$

Encodes parameters of a BN, B with underlying DAG G, where n is the number of nodes in the network.

$\boldsymbol{\Theta_i} = \{\boldsymbol{\Theta_{ij}}\}_{\boldsymbol{i=1,\ldots,q_i}}$

Encodes parameters concerning only the variable X_i *of* $\boldsymbol{X}$ *in B, where* q_i *is the number of configuration for the parents of node* X_i.

$\boldsymbol{\Theta_{ij}} = \{\Theta_{\boldsymbol{ijk}}\}_{\boldsymbol{i=1,\ldots,r_i}}$

Encodes parameters for variable X_i *of* $\boldsymbol{X}$ *in B given that its parents take their j-th configuration, where* r_i *is the number of states of node* X_i *in the data.*

Assumption 1. Multinomial sample

The multinomial sample assumption indicates that the probability assigned to the *t*-th instance of data is conditionally independent of the previous observations.

Assumption 2. Dirichlet

Given a directed acyclic graph *G* such that *P(G)* > 0 then Θ_{ij} is Dirichlet for all Θ_{ij}in Θ_G. Under the dirichlet assumption, the probability distribution function for Θ_{ij} is obtained from Equation (3.36):

$$\rho\ (\boldsymbol{\Theta}_{ij} |\ G) = \prod_{k=1}^{r_i} \rho\ (\ \boldsymbol{\Theta}_{ijk}^{N'_{ijk}-1}\ )\ . \qquad (3.36)$$

where $N'_{ijk} > 0$, where $\{N'_{ijk}\}_{k=1,\ldots,r_i}$ are the hyperparameters (exponents) of the Dirichlet distribution.

Assumption 3. Parameter independence

Given a directed acyclic graph G such that P(G) > 0 then

1) $\rho\ (\boldsymbol{\Theta}_G|G) = \prod_{i=1}^{n} \rho\ (\boldsymbol{\Theta}_i|\ G)$ (Global Parameter Independence)

This indicates that associated parameters with each variable is independent of the parameters of other variables.

2) $\rho\ (\boldsymbol{\Theta}_i|G) = \prod_{j=1}^{q_i} \rho\ (\boldsymbol{\Theta_{ij}}|\ G)$ for i=1,…,n. (Local Parameter Independence)

This indicates that the parameters associated with each configuration of the parents of a variable are independent.

Assumption 4. Parameter Modularity

Given two directed acyclic graphs, G and G', such that P(G) > 0 and P(G') > 0, if X_i has the same parents in G and G', then:

$$\rho\ (\boldsymbol{\Theta}_{ij}|G) = \rho\ (\boldsymbol{\Theta}_{ij}\ |\ G') \qquad \text{for all } j = 1, \ldots, q_i. \tag{3.37}$$

Based on the four mentioned assumptions, the Bayesian Dirichlet score is defined as shown in Equation (3.38), where Γ is the Gamma function and $P(B)$ represents the prior probability of the network B:

$$BD(B,D) = log(P(B)) + \sum_{i=1}^{n} \sum_{j=1}^{q_n} \left(log\left(\frac{\Gamma(N'_{ij})}{\Gamma(N_{ij} + N'_{ij})}\right) + \sum_{k=1}^{r_i} log\left(\frac{\Gamma(N_{ij} + N'_{ij})}{\Gamma(N'_{ij})}\right)\right). \tag{3.38}$$

Determining all the hyperparameters or exponents of the Dirichlet function (N'_{ijk}) is a challenging task. Heckerman et al. (1995) address the problem of specifications of the hyperparameters by considering two more assumptions:

Assumption 5. Likelihood Equivalence

Based on this assumption, if two possible directed acyclic graphs (G and G') are equivalent, then:

$$\rho\ (\boldsymbol{\Theta_D}|G) = \rho(\boldsymbol{\Theta_D}|\ G'))\ . \tag{3.39}$$

where

$$\boldsymbol{\Theta}_D = \{\boldsymbol{\Theta}_{x_1,\ldots,x_n}\}_{x_i=1,\ldots,r_i\ ,i\in 1,\ldots,n} \quad \text{and} \quad \boldsymbol{\Theta}_{x_1,\ldots,x_n} = \prod_{i=1}^{n} \boldsymbol{\Theta}_{x_i\,|\,Pa(x_i)}.$$

Assumption 6. Structure Possibility

The probability of any complete directed acyclic graph is bigger than zero. Based on all 6 assumptions, Heckerman et al introduced BDe scoring function defined as follows:
If $\rho(\Theta_D|G)$ is Dirichlet with equivalent sample size N′ for some complete directed acyclic graph *G* in *D*, then:

$$P(B,D)= P(B) \times \prod_{i=1}^{n} \prod_{j=1}^{q_n} \left(\frac{\Gamma(N'_{ij})}{\Gamma(N_{ij} + N'_{ij})} \times \prod_{k=1}^{r_i} \left(\frac{\Gamma(N_{ijk} + N'_{ijk})}{\Gamma(N'_{ijk})} \right) \right). \quad (3.40)$$

Where $N'_{ijk} = N' \times P(X_i = x_{ik}, pa(X_i) = w_{ij} \mid G)$ and $N' = \sum_{x_1,\ldots,x_n \in D} N'_{x_1,\ldots,x_n}$.
Calculation of BDe score is not so popular in practical, since it requires knowing $P(X_i = x_{ik}, pa(X_i) = w_{ij} \mid G)$ for all *i, j* and *k.*
BDeu is a special case of BDe, which was originally suggested by Buntine (1991). In this method a uniform probability is assigned to each configuration of a node and its parents.

$$P(X_i = x_{ik}, pa(X_i) = w_{ij} \mid G) = \frac{1}{r_i q_i}. \quad (3.41)$$

The resultant score is calculated by Equation (3.42).

$$BDeu(B,D) = log(P(B)) + \sum_{i=1}^{n} \sum_{j=1}^{q_i} \left(log\left(\frac{\Gamma(\frac{N'}{q_i})}{\Gamma(N_{ij} + \frac{N'}{q_i})} \right) + \sum_{k=1}^{r_i} log\left(\frac{\Gamma(N_{ijk} + \frac{N'}{r_i q_i})}{\Gamma(\frac{N'}{r_i q_i})} \right) \right). \quad (3.42)$$

3.2.10 Dynamic Bayesian Network (DBN)

Dynamic Bayesian network is a modelling approach which is extended from BN to describe temporal processes [113]. It is reported to give rise to more precise and informative results in comparison to previously introduced methods. Temporal characteristics of the time series are considered in the modeling process which can be explained in a complete statistical sense [97, 104]. DBN is capable of modeling the temporal behavior of the system being studied. These networks provide a model that demonstrate the probabilistic transition from the state at time *t* to the state at time *t*+1 for variables in the system [114]. DBN captures the non-linear dependencies in the network which makes it suitable to model non-linear systems like brain [115] . Studies based on application of DBN on fMRI data can be found in [104, 116, 117] and Anne

Smith et al. provided the proof for efficiency of the algorithm to infer effective connectivity from EEG data in her study [118]. Other promising results obtained by applying DBN in the analysis of time series could be found in [104, 119].

Briefly, among all the methods that have been introduced to extract causal relationships and effective connectivity from neurophysiological data, DBN is the most preferable one. The reason lies in its solid base in statistics, potential in dealing with incomplete data and uncertainty [114], capability to capture temporal characteristic, flexibility to employ various algorithms to find dependencies, ability to dealing with non-linear and non-deterministic complex networks and eventually the graphical representation of the model which can represent the ROIs with nodes and the information flow between them by the edges.

The basics of the Dynamic Bayesian network are not different than the Bayesian network except that the DBN includes the temporal characteristics of the time series. To keep away from the model complexity, in this study the temporal changes in the system is assumed to be stationary and first-order Markovian, which means the transition probabilities shown in the following equation hold for all the instances t=1, 2, …T, as shown in Equation (3.43):

$$P(x(t+1) \mid x(t),\ldots,x(1)) = P(x(t+1) \mid x(t)). \quad (3.43)$$

The network structure of a dynamic Bayesian network illustrate the connectivity pattern between two consecutive scans of the system [104].

CHAPTER 4

MATERIAL AND METHODS

During the past decades, investigation of disorders associated to central nervous system becomes feasible in vivo due to the fast development of non-invasive functional imaging techniques, like electroencephalogram (EEG), magneto encephalogram (MEG), and functional magnetic resonance imaging (fMRI) [73]. EEG is a measure of the brain activity derived from an ensemble of neuronal oscillating generators. After any cognitive, motory or sensory stimulation, generators that were randomly active, synchronize and this results in an alteration in EEG rhythm. It's been introduced as an appropriate modality to study the dynamics of the brain due to its high temporal resolution and relatively low cost of acquisition [120].

4.1 Data

Co-occurrence of dyslexia and Attention Deficit and Hyperactivity Disorder is reported from multiple studies. In this study, children using ADHD medicine were asked to stop taking the medicine 24 hours before recording EEG. (Recording was done during the school period. The period to stop taking the drug was not asked to be more than 24 hours to avoid any negative influence on the life of subjects)
EEG was recorded by a 16 channel BrainAmp DC system in a continuous way. Electrodes, F3/F4, F7/F8, C3/C4, T7/T8, P3/P4, P7/P8, O1/O2, were positioned based on a subset of 10-20 system shown in Figure 4.1. Reference electrodes were placed on the earlobes and earth electrode was placed on the left eye. Eye artifacts are determined by the electrode positioned on the right eye and the ones placed around it. Sampling frequency is 1000(Hz) and the impedance of all the electrodes is lower than 20 KOhm. Data was recorded in an isolated area from sound and electromagnetic signals, with a low-light environment. Children were sited 114(cm) from the screen.

4.1.1 Reading Stimulus

To assess the reading ability of the subjects, a stimulus set compromising of 100 words was prepared. During the preliminary study, the errors of reading and writing in the recorded data were examined by the researchers in the project team from Ankara University, Faculty of Language and History, Department of Linguistics. 50 meaningful words and 50 non-meaningful words (non-word- ex. abrık, loskum, hitmi) were set, based on Turkish synthetic operation principles, such that they include all Turkish sounds. The stimulus set was created under the leadership of lecturers from Middle East Technical University, Faculty of Electric and Electronics. Meaningful words in the stimulus set include original-based words (ex. Güzel), words derived from other words (ex. güçlü), and compound words. These 100 words were sequenced in a mixed way to construct the stimulus set. In the experiment, two different stimulus set were employed with the same words and different sequencing.

Words were represented in the middle of a screen in a shuffled way. Subjects were asked to read the words silently. In each block of the experiment 3-4 breaks were given, when children were asked the last word they read to control if he/she is taking the test. The period that each word stays on the screen is set such that each child can read the word easily. EEG recording is started as the words appear on the screen. The period between the two stimuli is between 1000-1500(ms). EEG signals were recorded from 27 control and 31 dyslectic subjects.

4.1.2 Data Analysis

Recorded data was filtered between 0.5-100Hz and 50Hz notch filter was also applied. Independent Component Analysis (ICA) was applied to eliminate the eye movement artifacts. After artifact removal, the recording was sliced to pieces consisting 1000(ms) before stimulus and 1000(ms) after stimulus for each presentation. For each piece, baseline-correction was done based on the first 100(ms). For groups of words and non-words the average was calculated over 50 pieces. To perform the averaging task, following latencies and amplitudes are taken into consideration.

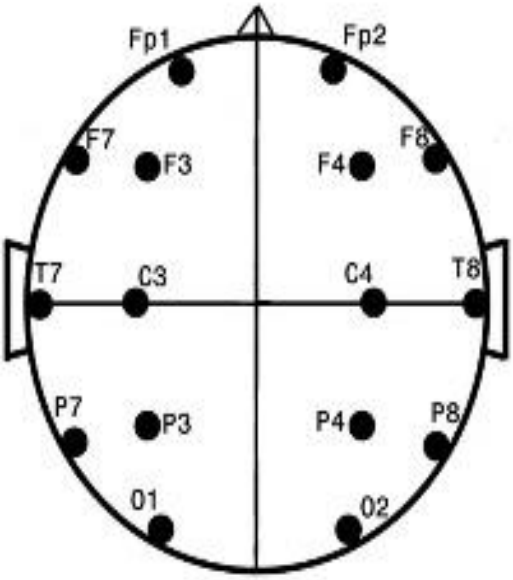

Figure 4.1. Position of the electrodes on the scalp.

To analyze the dynamics of the brain in the pre-reading stage, the time interval between 50 milliseconds and 450 milliseconds before starting to read and to analyze the dynamics of the brain in the reading stage the time interval between 50 milliseconds and 750 milliseconds after starting to read is considered. Figure 4.2 and Figure 4.3 represent the left and right hemisphere EEG signals obtained from a control subject (non-word reading experiment), where the pre-reading and while reading intervals are identified by red and green colors, respectively.

4.2 Method

In this study, Dynamic Bayesian networks (DBNs) were used to describe the dynamic behavior of the brain in pre-reading, while reading a single word and while reading a single non-word stages, for each individual, separately. To be able to use the information lie in EEG data in frequency domain, EEG data was band-pass filtered, before the structure learning algorithms are applied to learn DBN. After frequency band separation, EEG data was discretized, since discrete time Bayesian networks are more efficient than continuous time Bayesian networks to model nonlinear interactions in the system under investigation. After the structure of the DBNs were identified, the associated parameters of the networks are used to classify dyslectics and normal

subjects. In this section, all the applied algorithms and their applications on EEG data are discussed in detail.

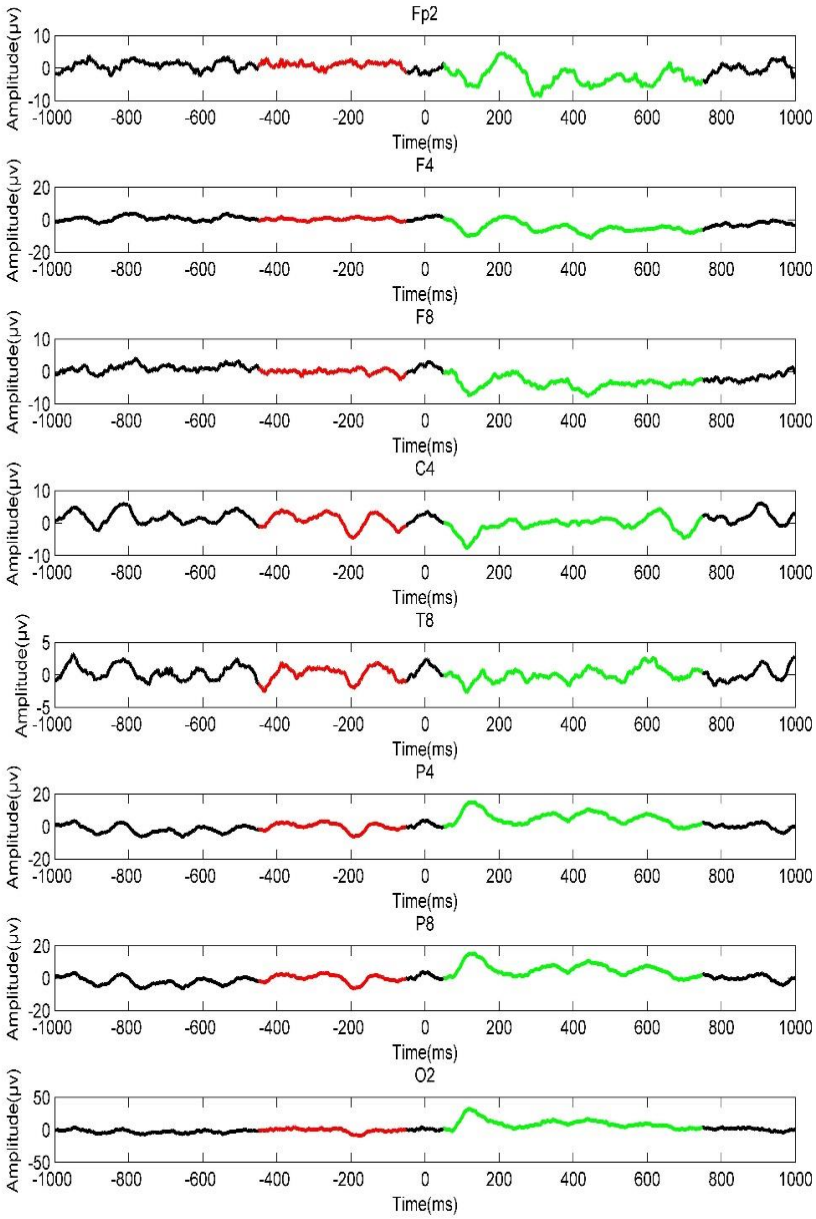

Figure 4.2. EEG signals obtained from right hemisphere electrodes from a control subject. The interval marked by red color is used to model pre-reading stage and the interval marked by green is used to model while reading period.

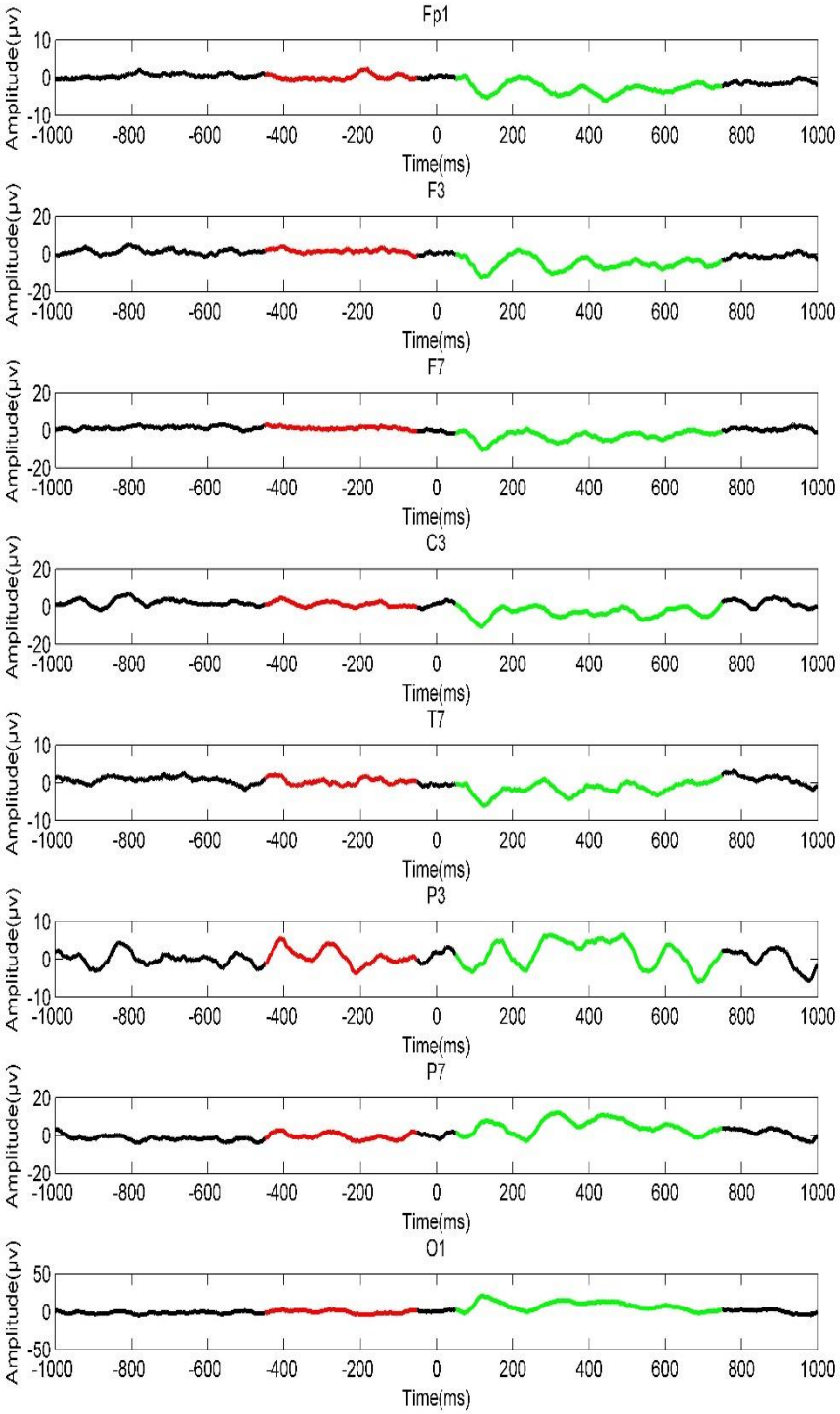

Figure 4.3. EEG signals obtained from left hemisphere electrodes from a control subject. The interval marked by red color is used to model pre-reading stage and the interval marked by green is used to model while reading period.

4.2.1 Band-pass Filtering

In EEG data, remarkable information can be derived from frequency domain rather than the time domain [91]. Hence, three specific frequency bands, namely theta, alpha and beta, which were earlier proved to be essential in investigation of neurological disorders, shown in Table 4.1 were used to investigate the causal interaction between the regions of interest.

Table 4.1. Specification of frequency bands.

Frequency band	Range
Theta	3Hz-7.5Hz
Alpha	8Hz-13.5Hz
Beta	14Hz-30Hz

Butterworth filters were used to extract the data in each frequency band. These filters are referred to as maximally flat magnitude filter which means frequency response of unity in pass-band and zero response in stop-band. They are characterized by their smooth, monotonically decreasing frequency response, which makes them a desirable filter to derive the frequency components of the data. Figure 4.4 represents the specification of the filters. The filters were design such that the stop-band attenuation and band-pass ripple was considered 20dB and 3dB, respectively. The length of the transition band in each filter is calculated as shown in Equation (4.1), where L indicates the length of the transition band, P1 is the first pass band edge frequency, P2 is the second pass band edge frequency and ceil function gives the smallest integer not less than its argument.

$$L = (\text{Ceil}\ (P2–P1))/4. \quad (4.1)$$

Figure 4.5 represents the shape of the beta band pass filter as an example of Butterworth filter. Butterworth filter is an example of Infinite Impulse Response (IIR) filter. Unlike Finite Impulse Response (FIR) filters, IIR filters contain a recursive part

which results in a more accurate frequency response. However, their phase characteristics are not linear. Thus, in digital signal processing applications, where the phase of the signal is of importance, IIR filters are not recommended. Albeit the phase of the butter worth filter is nonlinear, in this study, the band pass filtering was done within MATLAB software, where the entire sequence was available before filtering initiation. This eliminates the nonlinear phase distortions and makes zero-phase filtering possible (by applying filtfilt function).

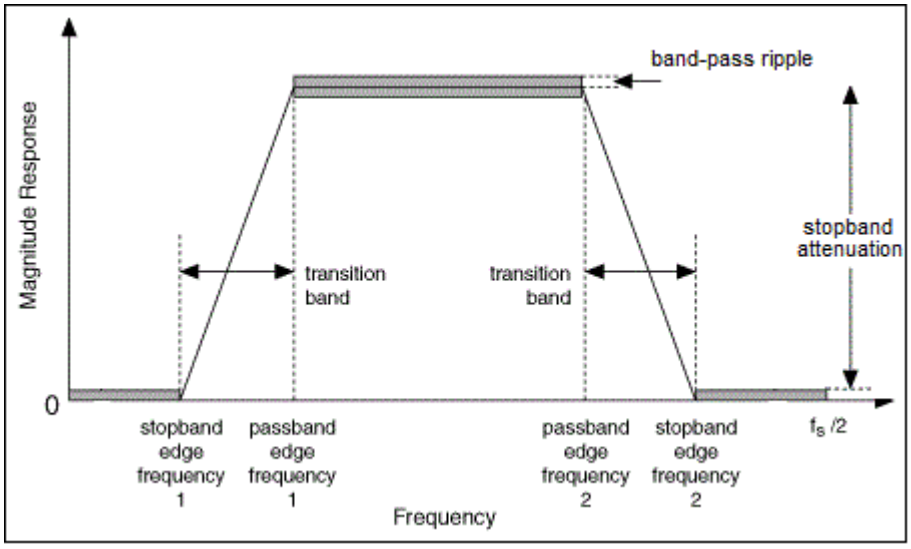

Figure 4.4. Specification of filters

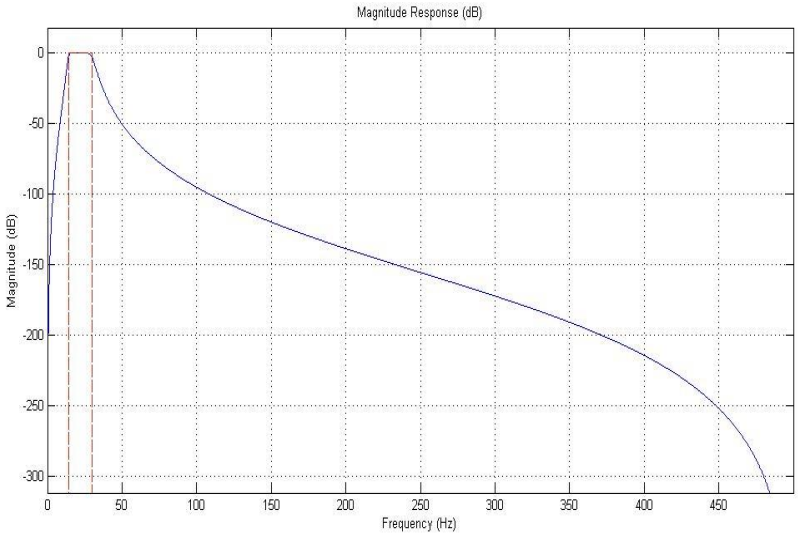

Figure 4.5. Shape of beta band pass filter.

4.2.2 Discretization

Bayesian networks may deal with systems with discrete variables, continuous variables or both of them (in hybrid models). For continuous Bayesian networks, when variables in the system take real values, there is no presentation that can capture all conditional densities. Gaussian distributions is a common choice for multivariate continuous distributions [121]. The interaction between variables of a system modeled by Gaussian Bayesian networks is considered a linear relationship with Gaussian noise. Due to Pearl 1988, continuous variables are problematic in Bayesian networks of non-linear systems [122]. Discrete Bayesian networks, on the other hand, are able to model non-linear relationships within non-linear systems [119]. When variables in the system take discrete values, conditional probabilities in the system can be represented as a table that specifies the probability of values for each variable, per each configuration of its parents [121]. However, training these networks require discrete data and since biological data are typically continuous, data is required to be discretized [123]. Determination of the number of classes and the boarders that separate the classes is challenging.

Information loss may occur as a consequence of discretization when important variations are not considered in discretization process. Then again, discretization may also give rise to a more robust data by getting rid of uninformative random noise. To control computational load for learning Discrete Bayesian network, the number of states of the data should be as small as possible. Here, to compromise between the computational load and information loss, each band pass filtered signal is discretized into ternary form to implement Discrete Dynamic Bayesian Network, based on a discretization formula applied earlier on both fMRI [113] and EEG [115] data, in effective connectivity studies:

$$d_i(\mathrm{t}) = \begin{cases} 1, & if\ x_i(\mathrm{t}) \geq \overline{x_i} + \frac{x_{i,max} - \overline{x_i}}{3}, \\ -1, & if\ x_i(\mathrm{t}) \leq \overline{x_i} - \frac{\overline{x_i} - x_{i,min}}{3}, \\ 0, & otherwise\ . \end{cases} \tag{4.2}$$

where $\overline{x_i}$, $x_{i,min}$ and $x_{i,max}$ are the mean, minimum and maximum values of the data.

To visualize the discretization process and the efficiency of the algorithm, the proposed discretization method is applied on a sample signal and the result is shown in Figure 4.6. Figure 4.6.a represents the shape of the original signal. Figure 4.6.b shows the alpha band pass filtered signal and Figure 4.6.c represents the discretization result.

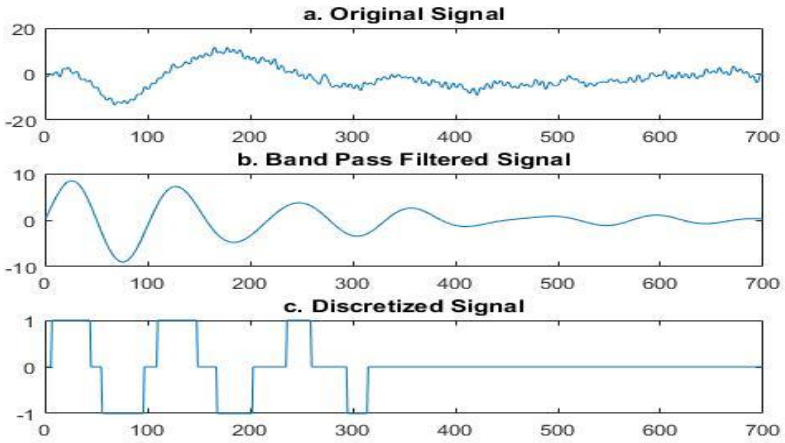

Figure 4.6. Using proposed method to discretize data:
a) original signal, b) filtered signal, c) discretized signal.

4.2.3 DBN via DBMCMC TOOLBOX

In this study, DBMCMC (dynamic Bayesian Markov Chain Monte Carlo) Toolbox written by Dirk Husmeier in MATLAB is employed to obtain dynamic Bayesian network using Markov Chain Monte Carlo algorithm. This toolbox call commands from Bayesian Network Toolbox written by Kevin Murphy. Both toolboxes are available online [124].

The parameters inserted as input to train the structure of the DBN are as follows:

1) Burn-in phase :

   As explained earlier, initial sampled graphs are not involved in the averaging process that gives rise to the posterior probabilities of edges. The number of steps to take before drawing samples was suggested to be 5 times the number of nodes which in our case of study will be 140.

2）Sampling phase:

The least number of samples to draw from the chain after burn-in step is suggested to be 100 times the number of nodes which in our case of study will be 2800. We draw 3000 samples from the Markov chain in our experiment for each MCMC simulation.

3) Number of simulations:

In our experiment, data from 14 electrodes was used to investigate effective connectivity pattern of the brain. Thus, number of possible edges in the structure is 196. As explained, the initial graph to start each MCMC simulation is a graph with one edge which is selected randomly. If we assume that the probability of selecting all the edges is equal for initial graph generation, 200 times simulation will probably give the chance to start the simulation with all possible one-edge initial graphs.

4.2.3.1 Implementation on Real EEG Data

To visualize the final output of DBMCMC toolbox, a sample of learned DBN is shown in Figure 4.8. Figure 4.7 illustrates the final adjacency matrix that contains the assigned weight for each edge of the DBN (Figure 4.8) obtained for the green segments of the data in Figures 4.2 and 4.3. To avoid confusion, in Figure 4.7, in the structure of the graph, only the edges with the weights higher that 0.1 is shown.

	F3	F4	F7	F8	P3	P4	P7	P8	O1	O2	T7	T8	C3	C4
F3	0,97	0,91	0,25	0,05	0,04	0,14	0,02	0,24	0,04	0,06	0,02	0,02	0,03	0,02
F4	0,07	0,78	0,72	0,05	0,03	0,32	0,04	0,40	0,13	0,05	0,01	0,03	0,02	0,02
F7	0,02	0,12	0,96	0,01	0,02	0,01	0,01	0,03	0,40	0,65	0,02	0,03	0,02	0,03
F8	0,04	0,22	0,01	0,97	0,02	0,01	0,04	0,01	0,04	0,02	0,05	0,04	0,06	0,03
P3	0,02	0,03	0,02	0,02	0,97	0,01	0,05	0,01	0,02	0,01	0,79	0,04	0,92	0,04
P4	0,01	0,01	0,02	0,03	0,03	0,81	0,02	0,95	0,04	0,02	0,02	0,02	0,01	0,01
P7	0,01	0,03	0,02	0,05	0,05	0,04	0,98	0,04	0,02	0,01	0,02	0,01	0,02	0,01
P8	0,01	0,01	0,01	0,02	0,02	0,22	0,02	0,09	0,04	0,04	0,01	0,01	0,01	0,01
O1	0,01	0,01	0,04	0,04	0,02	0,18	0,01	0,04	0,96	0,04	0,02	0,03	0,01	0,01
O2	0,02	0,07	0,02	0,03	0,01	0,06	0,01	0,24	0,13	0,97	0,08	0,02	0,02	0,04
T7	0,10	0,01	0,02	0,06	0,06	0,03	0,02	0,06	0,02	0,02	0,96	0,03	0,03	0,01
T8	0,04	0,03	0,38	0,05	0,02	0,16	0,01	0,02	0,25	0,23	0,03	0,98	0,01	0,01
C3	0,04	0,02	0,07	0,02	0,07	0,01	0,01	0,01	0,01	0,02	0,18	0,46	0,96	0,86
C4	0,26	0,08	0,20	0,02	0,02	0,01	0,02	0,01	0,01	0,04	0,02	0,43	0,08	0,98

Figure 4.7. A sample adjacency matrix that represents causal influence between electrodes.

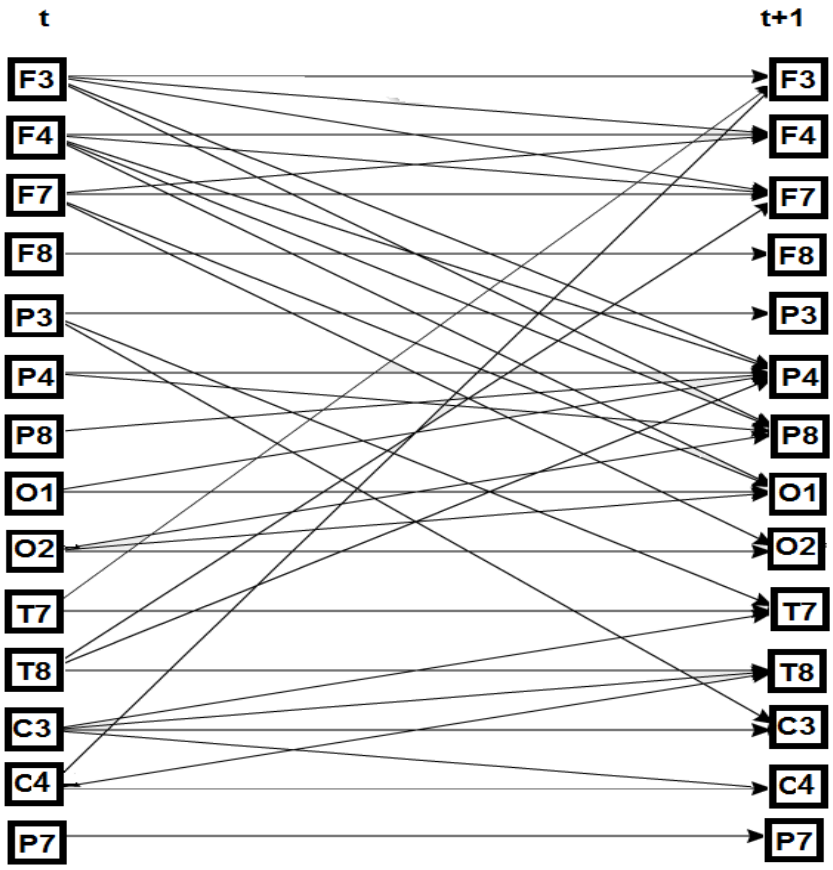

Figure 4.8. DBN Representation of a sample.

4.2.4 Support Vector Machine (SVM)

DBN models trained for all the subjects separately for pre-reading and while reading periods. Each model contains 196 (14 x 14) weights indicating causal relationships between electrode pairs. These weights are used as features to train SVM classifier.

Support vector machine is a classification algorithm introduced by Boser, Guyon and Vapnik in 1992. The origins of this method lie in statistical learning theory which was mainly developed by Vapnik and Chervonenkis in 1960s. Support vector machine is been reported to be a promising classification algorithm in multiple real-world problems. Strong theoretical basics and rich experimental success are attributed characteristics of SVM classifiers [125]. Its capability of dealing with large number of features and small number of training set, makes it a preferable classification method in multiple problems [126]. The basic idea of SVM is explained in appendix.

In this study, MATLAB built-in function (fitcsvm) was employed to train linear SVM classifiers from the data.

4.2.4.1 Leave One Out

In machine learning problems, assessing the efficiency of the algorithm is an important issue [130]. To determine how well the SVM classification works, other than the train data set, we need a test set to evaluate the performance of the classifier. The total data samples used in this study was 58 (31 dyslectic and 27 control subjects). To acquire a more precise result, it is preferable to train the SVM classifier with higher number of data samples. Leave-One-Out method was used to fulfill the best possible classification. In this method, the classifier is trained for several times such that in each training tour, all the samples in the data set is used except one specific sample and the classification algorithm is evaluated based on that specific sample. Finally, after SVM was trained 58 times, each time missing one sample, the overall efficiency of the algorithm was calculated based on how well the classifier predicted the class of the missing specific samples in all 58 tours of classification.

4.2.5 Feature Reduction Algorithms

Although SVM classifiers are capable of dealing with large number of features, still feature reduction algorithms are suggested to improve the generalization performances and avoid any probable over fitting error, since in the orientation of the learned hyper plane found by SVM classifiers is sensitive to the noisy features. In this study, Principle Component analysis (PCA) and Statistical *t*-test are applied to reduce the dimension of features. The basic concepts of these methods are described in appendix.

CHAPTER 5

EXPERIMENTS AND RESULTS

DBN models were found for each subject (dyslectic or control) in pre-reading stage (50ms to 450ms before starting to read) and while reading stage (50ms to 750ms after starting to read) separately for each of the frequency bands (theta, alpha and beta bands), introduced earlier in chapter four. Thus, a total of six models were obtained for each subject, for each of the two experiments (reading a single word and reading a single non-word). Figures 5.1 and 5.2 represent the adjacency matrices obtained for the first control subject in theta frequency band, based on the data obtained from "reading a non-word" experiment in pre-reading stage and while reading stage, respectively. The matrices illustrate the weights each of which is a measure of the causal influence that one electrode (name of the corresponding row of the matrix) has on another electrode (name of the corresponding column of the matrix). To visualize the effective connectivity patterns in the brain between electrode pairs, figures 5.3 and 5.4 are illustrated which represent the DBNs associated to the matrices in figure 5. 1 and 5.2, respectively. To avoid confusion, in these figures, only the edges with the weights higher that 0.1 are shown in the structure of the graph. The edges illustrated in the structure are colored based on the value of their weights. Weight of the edges colored in blue is between 0.7 and 1, where the edges with weights between 0.4 and 0.7 are shown in red and green color implies that the weight of the corresponding edge is between 0.1 and 0.4. It is clearly shown in these figures that, to perform the reading task, the connectivity patterns in brain modify themselves, such that multiple connections become stronger, where some other connections become weaker.

	F3	F4	F7	F8	P3	P4	P7	P8	O1	O2	T7	T8	C3	C4
F3	0,93	0,80	0,05	0,02	0,04	0,14	0,04	0,15	0,02	0,87	0,03	0,02	0,01	0,18
F4	0,04	0,96	0,03	0,05	0,05	0,24	0,02	0,29	0,07	0,04	0,03	0,03	0,01	0,23
F7	0,02	0,01	0,97	0,03	0,26	0,01	0,31	0,01	0,02	0,01	0,10	0,03	0,05	0,01
F8	0,05	0,06	0,07	0,97	0,03	0,02	0,55	0,02	0,68	0,03	0,06	0,01	0,35	0,03
P3	0,09	0,03	0,02	0,03	0,69	0,16	0,03	0,13	0,86	0,06	0,02	0,03	0,06	0,17
P4	0,02	0,01	0,02	0,01	0,04	0,52	0,01	0,49	0,01	0,03	0,03	0,40	0,01	0,04
P7	0,03	0,02	0,65	0,45	0,67	0,03	0,96	0,02	0,29	0,01	0,04	0,01	0,58	0,05
P8	0,02	0,01	0,02	0,02	0,05	0,47	0,01	0,50	0,01	0,03	0,02	0,38	0,01	0,05
O1	0,97	0,19	0,02	0,17	0,11	0,09	0,04	0,10	0,36	0,07	0,02	0,01	0,01	0,13
O2	0,01	0,08	0,01	0,01	0,02	0,29	0,01	0,26	0,01	0,97	0,75	0,03	0,01	0,17
T7	0,01	0,02	0,06	0,06	0,02	0,01	0,04	0,01	0,01	0,06	0,96	0,05	0,01	0,01
T8	0,01	0,01	0,05	0,03	0,06	0,02	0,02	0,03	0,01	0,04	0,16	0,97	0,01	0,01
C3	0,03	0,02	0,06	0,01	0,97	0,05	0,02	0,03	0,13	0,03	0,10	0,01	0,97	0,06
C4	0,01	0,02	0,01	0,01	0,06	0,18	0,01	0,17	0,01	0,02	0,03	0,15	0,01	0,97

Figure 5.1. Adjacency matrix of the 1st control subject in theta frequency band in "pre-reading" stage based on the data obtained from "a single non-word reading" experiment.

	F3	F4	F7	F8	P3	P4	P7	P8	O1	O2	T7	T8	C3	C4
F3	0,975	0,219	0,105	0,131	0,019	0,025	0,012	0,239	0,018	0,361	0,037	0,021	0,032	0,032
F4	0,639	0,856	0,805	0,435	0,016	0,035	0,007	0,105	0,058	0,155	0,048	0,016	0,027	0,049
F7	0,029	0,136	0,677	0,084	0,007	0,159	0,013	0,034	0,23	0,015	0,029	0,009	0,006	0,013
F8	0,02	0,011	0,958	0,944	0,03	0,07	0,023	0,03	0,345	0,122	0,009	0,015	0,01	0,014
P3	0,016	0,032	0,008	0,013	0,965	0,04	0,051	0,011	0,061	0,025	0,029	0,033	0,739	0,089
P4	0,011	0,091	0,02	0,407	0,016	0,074	0,034	0,265	0,061	0,045	0,02	0,012	0,017	0,019
P7	0,013	0,013	0,006	0,012	0,373	0,02	0,972	0,021	0,064	0,026	0,026	0,037	0,034	0,019
P8	0,017	0,094	0,01	0,062	0,008	0,967	0,027	0,743	0,062	0,824	0,03	0,008	0,016	0,015
O1	0,01	0,025	0,047	0,061	0,025	0,03	0,048	0,386	0,964	0,015	0,008	0,014	0,015	0,015
O2	0,014	0,013	0,021	0,067	0,016	0,046	0,017	0,087	0,289	0,952	0,043	0,026	0,007	0,024
T7	0,009	0,092	0,026	0,009	0,03	0,394	0,052	0,671	0,011	0,066	0,967	0,054	0,04	0,338
T8	0,03	0,576	0,006	0,035	0,028	0,011	0,037	0,007	0,035	0,047	0,057	0,97	0,047	0,074
C3	0,069	0,351	0,006	0,014	0,068	0,184	0,024	0,017	0,015	0,021	0,834	0,203	0,971	0,737
C4	0,288	0,214	0,01	0,009	0,018	0,015	0,024	0,008	0,015	0,083	0,019	0,365	0,049	0,967

Figure 5.2. Adjacency matrix of the 1st control subject in theta frequency band in "while reading" stage based on the data obtained from "a single non-word reading" experiment.

As illustrated in Figures 5.1 and 5.2, each model contains 196 (14×14) weights determining the effective connectivity of the brain. These weights are used as features

to train SVM classifier. Principle Component analysis (PCA) and Statistical *t*-test are applied to reduce the dimension of features. Results indicate that in comparison to PCA, applying *t*-test to reduce features, gives rise to a more efficient classification.

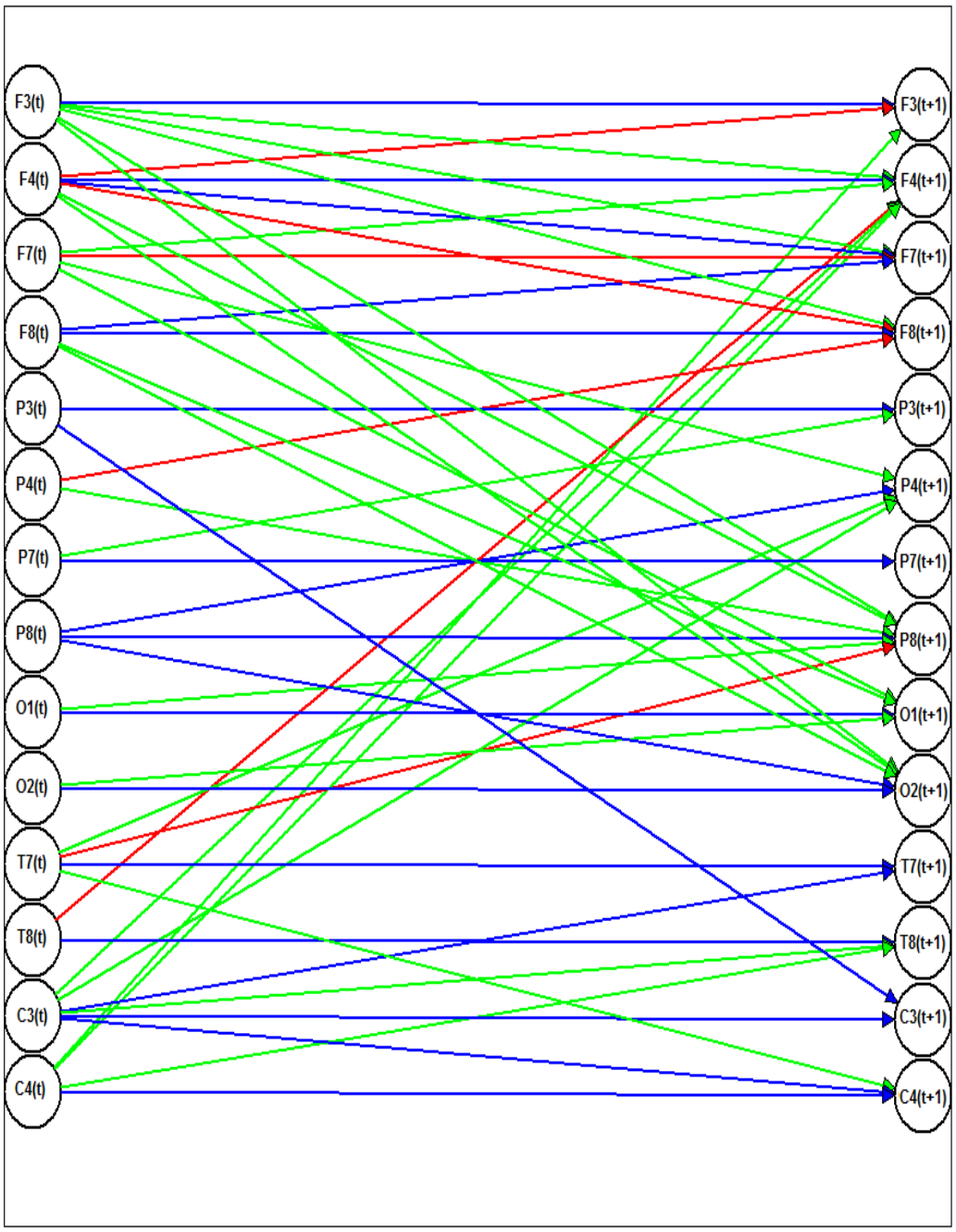

Figure 5.3. DBN of the 1st control subject in theta frequency band in "pre-reading" stage based on the data obtained from "a single non-word reading" experiment.

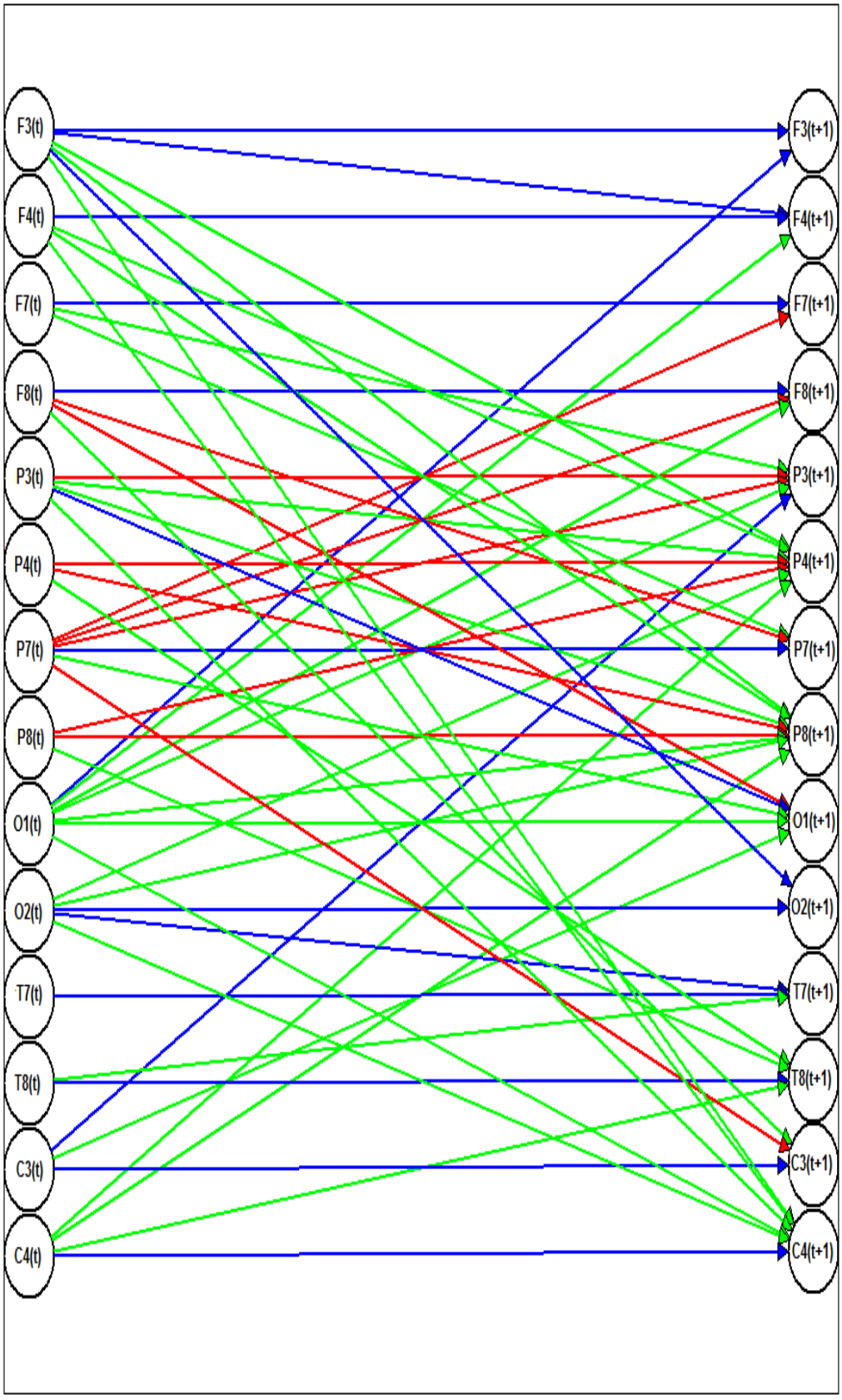

Figure 5.4. DBN of the 1st control subject in theta frequency band in "while reading" stage based on the data obtained from "a single non-word reading" experiment.

In each frequency band, dyslectics and controls are classified in three separate cases. In the first case, two groups are classified according to the weights obtained from models of pre-reading stage. It was aimed to check if two groups behave differently before the initiation of reading process in the brain. In the second case, we classified them based on the weights obtained from while reading stage. In the third case, we made the classification based on the weights obtained from both pre-reading stage and while reading stage. Each weight in the pre-reading stage is subtracted from its counterpart in adjacency matrix obtained for while reading stage. This gives us a measure of the required variation in each connection to fulfill the reading task. Since parameters (weights) of the learned DBN are basically influenced by the background thoughts in each subject's mind (each individual may have something different in her/his mind unconsciously or consciously), the subtraction task, eliminate the influence of the background effect and gives a measure of the effort (in terms of changes in the effective connectivity pattern) the brain takes to perform the reading task. In other words, in the third case, classification is done based on how different the brains of the two groups modify their connections to execute the act of reading.

Classification rates reveal how well the group that each subject (control or dyslectic) belongs to, is identified. For each classification case, sensitivity and specificity were determined which are statistical measures of a binary classification performance. Specificity (or true negative rate) measures the proportion of normal subjects that are correctly identified. Sensitivity (or true positive rate) measures the proportion of dyslectic patients that are correctly identified. An efficient classification algorithm is characterized by not only high classification rate, but also high measures of specificity and sensitivity, which indicates identification of both groups by an acceptable rate.

5.1 Classification Rates

Tables 5.1 and 5.2 represent the classification rates for reading a word and a non-word experiments, respectively. These rates are obtained by applying SVM to classify two groups from each other, using all the weights obtained from DBN models as features. Tables 5.3 and 5.4 represent the SVM classification results, where the feature dimension was reduced by applying PCA algorithm in experiments that subjects were asked to read a word and a non-word, respectively. Classification rate is calculated for

all possible number of components and the obtained maximum classification rate is accepted and introduced in the table. Tables 5.5 and 5.6 represent the SVM classification results, where the features of the classifier were selected based on the results obtained from statistical *t*-test, when subjects were asked to read a word and a non-word, respectively.

In each case, for all the frequency bands, classification rate (proportion of all subjects identified correctly by the classification algorithm), sensitivity (proportion of dyslectic subjects identified correctly by the classification algorithm), and specificity (proportion of normal subjects identified correctly by the classification algorithm), are identified. Classification rates were calculated based on the parameters of DBN obtained for individual subjects in separate experiments. If we wanted to classify the two groups based on the combined information from both experiments, the number of features that were supposed to be involved in classification task, even after applying statistical *t*-test to select the significantly different connections between two groups, would be more than the number of subjects in the study, which would result in the malfunction of the SVM classification algorithm and consequently misleading values.

Table 5.1. SVM Classification rates in word reading experiment – No feature reduction algorithm was applied.

	Reading a word			
Theta	Case I: Pre-reading	51.72%	Specificity	44.44%
			Sensitivity	58.06%
	Case II: While reading	60.34%	Specificity	59.26%
			Sensitivity	61.29%
	Case III: Variation between pre-reading and while reading	48.28%	Specificity	48.15%
			Sensitivity	48.39%
Alpha	Case I: Pre-reading	50.00%	Specificity	48.15%
			Sensitivity	51.61%
	Case II: While reading	60.34%	Specificity	59.26%
			Sensitivity	61.29%
	Case III: Variation between pre-reading and while reading	62.07%	Specificity	51.85%
			Sensitivity	70.97%
Beta	Case I: Pre-reading	46.55%	Specificity	48.15%
			Sensitivity	45.16%
	Case II: While reading	43.10%	Specificity	40.74%
			Sensitivity	45.16%
	Case III: Variation between pre-reading and while reading	41.38%	Specificity	48.15%
			Sensitivity	35.48%

Table 5.2. SVM Classification rates in non-word reading experiment – No feature reduction algorithm was applied.

	Reading a non-word			
Theta	Case I: Pre-reading	50.00%	Specificity	44.44%
			Sensitivity	54.84%
	Case II: While reading	39.66%	Specificity	33.33%
			Sensitivity	45.16%
	Case III: Variation between pre-reading and while reading	53.45%	Specificity	44.44%
			Sensitivity	61.29%
Alpha	Case I: Pre-reading	36.21%	Specificity	29.63%
			Sensitivity	41.94%
	Case II: While reading	58.62%	Specificity	55.56%
			Sensitivity	61.29%
	Case III: Variation between pre-reading and while reading	46.55%	Specificity	40.74%
			Sensitivity	51.61%
Beta	Case I: Pre-reading	48.28%	Specificity	44.44%
			Sensitivity	51.61%
	Case II: While reading	43.10%	Specificity	40.74%
			Sensitivity	45.16%
	Case III: Variation between pre-reading and while reading	48.28%	Specificity	37.04%
			Sensitivity	58.06%

Table 5.3. SVM Classification rates in word reading experiment - PCA was used for feature reduction.

	Reading a word			
Theta	Case I: Pre-reading	79.31%	Specificity	77.78%
			Sensitivity	80.65%
	Case II: While reading	75.86%	Specificity	68.52%
			Sensitivity	82.26%
	Case III: Variation between pre-reading and while reading	63.79%	Specificity	62.96%
			Sensitivity	64.52%
Alpha	Case I: pre-reading	65.52%	Specificity	59.26%
			Sensitivity	70.97%
	Case II: While reading	72.41%	Specificity	66.67%
			Sensitivity	77.42%
	Case III: Variation between pre-reading and while reading	68.97%	Specificity	62.96%
			Sensitivity	74.19%
Beta	Case I: Pre-reading	68.97%	Specificity	44.44%
			Sensitivity	90.32%
	Case II: While reading	65.52%	Specificity	80.65%
			Sensitivity	48.15%
	Case III: Variation between pre-reading and while reading	65.52%	Specificity	55.56%
			Sensitivity	74.19%

Table 5.4. SVM Classification rates in non-word reading experiment - PCA was used for feature reduction.

	Reading a non-word			
Theta	Case I: Pre-reading	67.24%	Specificity	62.96%
			Sensitivity	70.97%
	Case II: While reading	67.24%	Specificity	70.37%
			Sensitivity	64.52%
	Case III: Variation between pre-reading and while reading	63.79%	Specificity	62.96%
			Sensitivity	64.52%
Alpha	Case I: pre-reading	62.07%	Specificity	62.96%
			Sensitivity	61.29%
	Case II: While reading	63.79%	Specificity	62.96%
			Sensitivity	64.51%
	Case III: Variation between pre-reading and while reading	70.69%	Specificity	70.37%
			Sensitivity	70.97%
Beta	Case I: Pre-reading	67.24%	Specificity	59.26%
			Sensitivity	74.19%
	Case II: While reading	68.97%	Specificity	55.56%
			Sensitivity	80.65%
	Case III: Variation between pre-reading and while reading	65.52%	Specificity	53.10%
			Sensitivity	76.34%

Table 5.5. SVM Classification rates in word reading experiment – statistical *t*-test was used for feature reduction.

	Reading a word			
Theta	Case I: Pre-reading	86.21%	Specificity	92.59%
			Sensitivity	80.65%
	Case II: While reading	74.14%	Specificity	59.26%
			Sensitivity	87.10%
	Case III: Variation between pre-reading and while reading	84.48%	Specificity	81.48%
			Sensitivity	87.10%
Alpha	Case I: pre-reading	70.69%	Specificity	44.44%
			Sensitivity	93.55%
	Case II: While reading	75.86%	Specificity	55.56%
			Sensitivity	93.55%
	Case III: Variation between pre-reading and while reading	86.21%	Specificity	81.48%
			Sensitivity	90.32%
Beta	Case I: Pre-reading	75.86%	Specificity	62.96%
			Sensitivity	87.10%
	Case II: While reading	68.97%	Specificity	40.74%
			Sensitivity	93.55%
	Case III: Variation between pre-reading and while reading	67.24%	Specificity	55.56%
			Sensitivity	77.42%

Table 5.6. SVM Classification rates in non-word reading experiment – statistical *t*-test was used for feature reduction.

	Reading a non-word			
Theta	Case I: Pre-reading	86.21%	Specificity	81.48%
			Sensitivity	90.32%
	Case II: While reading	51.72%	Specificity	70.37%
			Sensitivity	35.48%
	Case III: Variation between pre-reading and while reading	72.41%	Specificity	62.96%
			Sensitivity	80.65%
Alpha	Case I: Pre-reading	65.52%	Specificity	55.56%
			Sensitivity	74.19%
	Case II: While reading	77.59%	Specificity	92.59%
			Sensitivity	64.52%
	Case III: Variation between pre-reading and while reading	81.03%	Specificity	85.19%
			Sensitivity	77.42%
Beta	Case I: Pre-reading	79.31%	Specificity	62.96%
			Sensitivity	93.55%
	Case II: While reading	51.72%	Specificity	29.63%
			Sensitivity	70.97%
	Case III: Variation between pre-reading and while reading	62.07%	Specificity	51.85%
			Sensitivity	70.97%

5.2 Feature Reduction Increases Classification Rates

Figures 5.5 and 5.6 represents the classification rate obtained by applying SVM without feature reduction (blue), applying SVM accompanying PCA, as the feature reduction algorithm (orange) and applying SVM accompanying *t*-test to select features (gray). All the results obtained for all the cases, in all the frequency bands are illustrated in these figures. In all cases and all frequency bands, SVM accompanying each of feature reduction algorithms, result in a better classification job. Thus, feature reduction is an important step in classifying two groups. Between the two applied methods, to reduce the dimension of the data, namely, PCA and *t*-test, although in some cases PCA separates the data more efficiently, in most of them, *t*-test is a better choice to lower the dimension of the data.

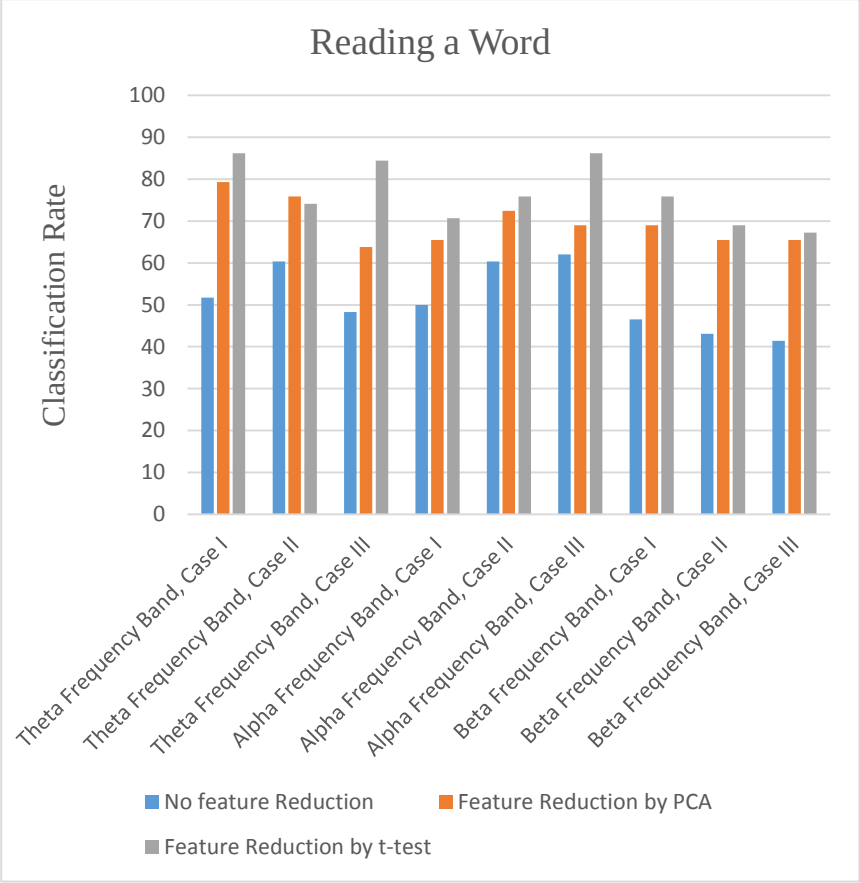

Figure 5.5. Comparison of the feature reduction methods in word reading experiment.

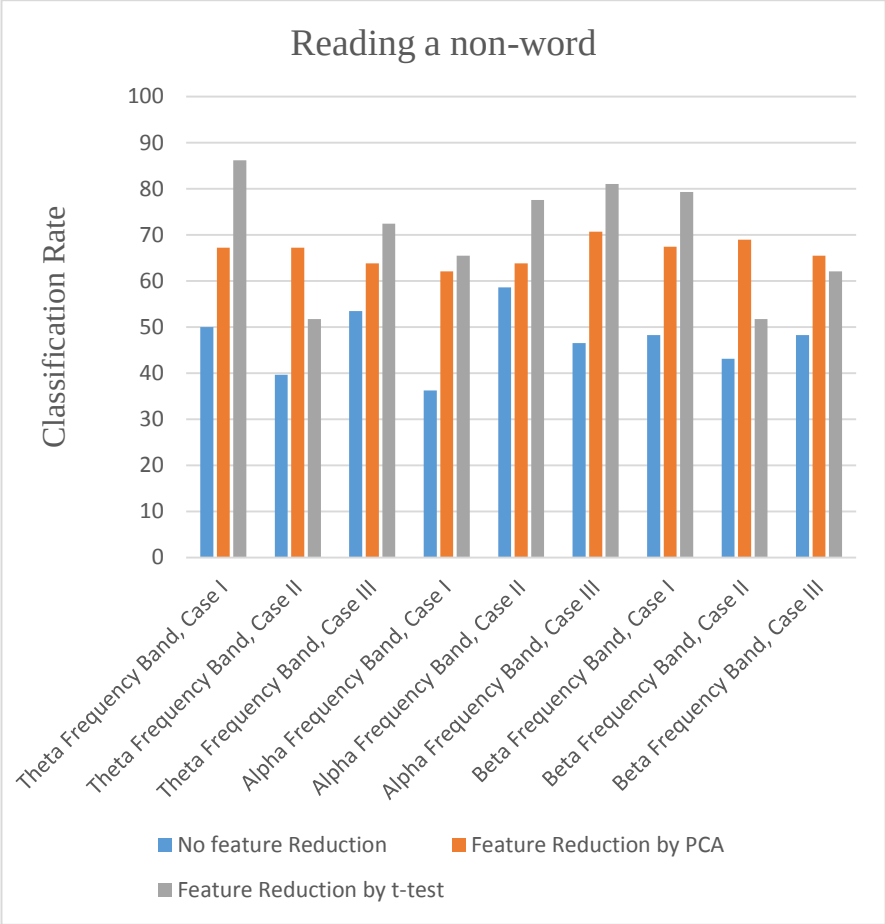

Figure 5.6. Comparison of the feature reduction methods in non-word reading experiment.

5.3 Classification Results after Feature Reduction by Statistical *t*-test

Now that we have introduced statistical *t*-test feature reduction as the more reliable feature reduction method, in this section we will discuss obtained results based on this method in more details.

5.3.1 Discussion over Pre-reading Classification Rates

Figures 5.7 and 5.8 visualize the classification rates obtained from three different cases in different frequency bands represented in Tables 5.5 and 5.6, for word and non-word experiments, respectively. Case I, represented in blue, is the classification based on parameters from the models of "pre-reading" stage. As illustrated, in this case,

classification rate is higher in theta band in comparison to alpha and beta bands in both experiments. Thus, differences in the casual interactions in the networks of the two groups before reading initiation are more distinguishable in theta band. In other words, theta band is the most informative frequency band to study the disturbance in the dyslectic brains before starting to read.

In 2012, Babiloni, C., et al. suggested that dyslexia may be characterized by some cortical neuronal synchronization involved in the resting state condition [124]. In a recent study, Schiavone, G., et al. reported abnormalities in open-eyes resting state EEG of dyslexics in 6-8 Hz frequency band. Here, theta band (3-7.5Hz) is suggested to reveal the abnormalities in dyslexic subjects before reading initiation [134]. Although before starting to read period of our experiment and the open-eyes resting state of Schiavone's are not the same, this is the closest condition to our case. Both claim the common 6-7.5 Hz frequency band range to be abnormal in dyslectics in the absence of any stimulation.

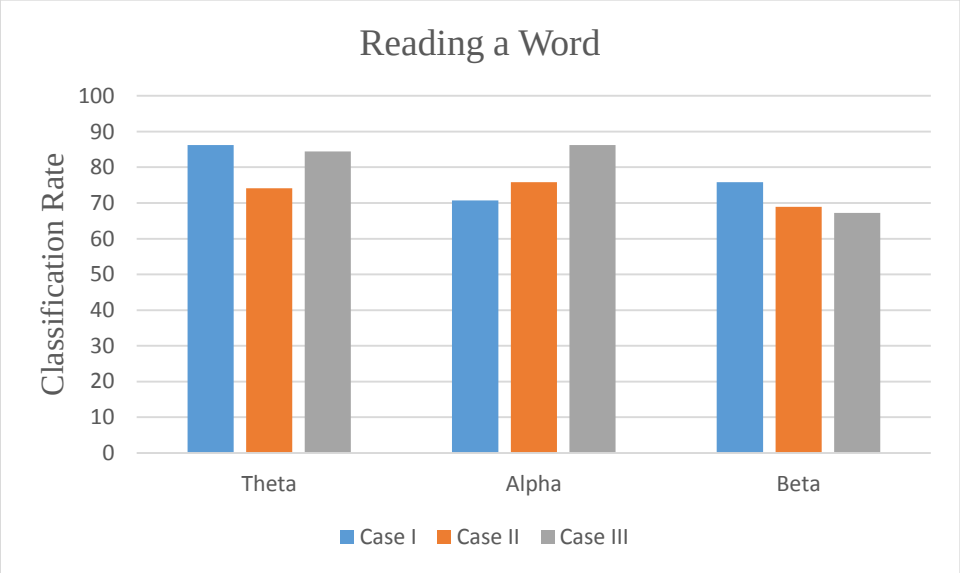

Figure 5.7. Classification rates of different cases in different frequency bands in word reading experiment.

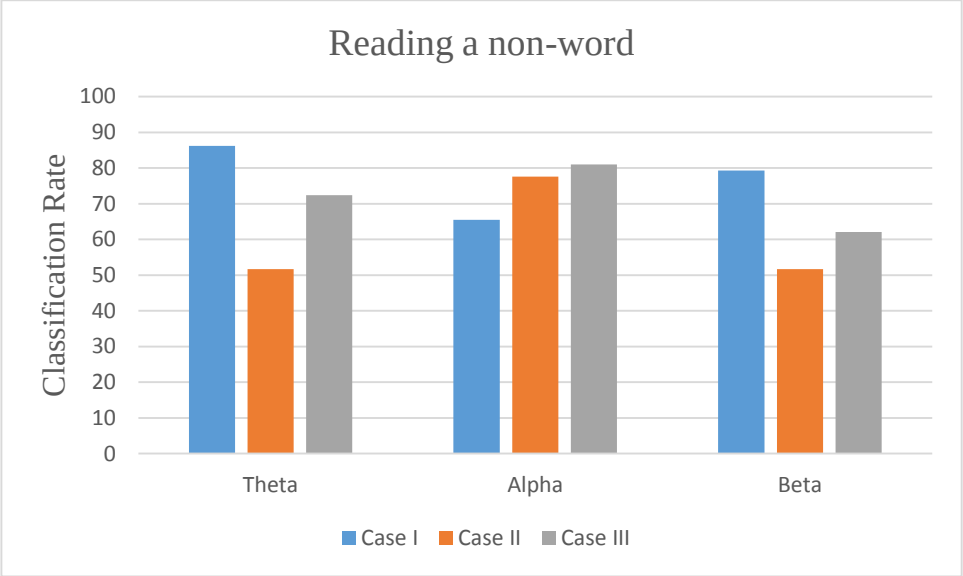

Figure 5.8. Classification rates of different cases in different frequency bands in non-word reading experiment.

5.3.2 Differences in the Reading Mechanism of the Two Groups

Once a visual stimulus (word or non-word) appears, pre-stimulus network modifies to make an appropriate response. Pre-stimulus differences between two groups, discussed in the previous section, interfere with subsequent required activation and deactivation of related sub-networks to fulfill the reading task. As a result, to study the underlying differences in the reading mechanism of two groups, we used a combination of the obtained weights for "pre-reading" models and "while reading" models (Case III). For each subject, changes of the weights before and while reading were calculated. Such that, the weight assigned to each connection from "before reading" model is subtracted from "while reading" model. The resultant values are the established changes in causal influences between ROIs to perform the reading task for each subject. These values were used as features of case III classification.

While performing the reading task (a word or a non-word), Case II and Case III classification rates, are higher in alpha frequency band. Thus, alpha frequency waves are the most disrupted ones in dyslectics while reading.

Making a comparison between the classification rates of case II and III, which involve the task of reading, for word and non-word experiments, in alpha and beta bands,

reveals that the classification rates are higher for reading a word than reading a non-word.

The best classification rate based on the parameters of "pre-reading" stage (Case I) is 86.21% in theta band. (It was common for both of the experiments). The best classification rate involving parameters of "while reading" stage is 81.03% for reading a non-word and 86.21% for reading a word experiments, both of which were obtained from alpha band parameters. Accordingly, theta and alpha bands are introduce as the most informative frequency bands about the connectivity disturbance in dyslectic brain in "pre-reading" and " while reading" stages, respectively.

5.4 Effective Connectivity Differences between the Two Groups

As mentioned, in the transition procedure from "pre-reading" state to "while-reading" state, weights of the connections in the brain network alter. In this section, the connections that alter significantly different between two groups to perform reading task is discussed in neurobiological sense. Initially, the significantly different connections in each frequency band are reported, which were used in the Case III classification. Then, the anatomical projections of EEG electrodes are identified on the left hemisphere of the brain, which is the dominant hemisphere for language related tasks. Finally, the compatibility of the obtained results is checked with previously findings based on fMR studies.

5.4.1 Significantly Different Connections between Two Groups

Significantly different connections between dyslectics and normal readers are identified and used as features for Case III classification, in each frequency band, in each experiment. Table 5.7 and 5.8 contain these connections in each frequency band, for "reading a single word" and "reading a single non-word" experiments, respectively.

Table 5.7. Significantly different connections between two groups - word reading eaxperiment

Theta Band	(F4➔F3), (F4➔F8), (T7➔F4), (P7➔F7), (O1➔O1), (O1➔C4)
Alpha Band	(F4➔C4), (C4➔F8), (O2➔F3), (F7➔O1), (F3➔F7), (C3➔F7), (F7➔F3), (C3➔F3)
Beta Band	(F4➔F3), (P7➔F3), (F4➔O1), (P4➔P8), (P8➔T8), (P8➔P8), (O1➔O1), (F7➔O1), (C3➔O1)

Table 5.8. Significantly different connections between two groups - non-word reading eaxperiment.

Theta Band	(F3➔P4), (F3➔T7), (F4➔F7), (F4➔C4), (C3➔F3), (C3➔P8), (P3➔F4), (T8➔T7), (O2➔O1)
Alpha Band	(F3➔F8), (F4➔C4), (F8➔P8), (C3➔F4), (P3➔P8), (O2➔O1), (T7➔F3), (T8➔F3)
Beta Band	(P7➔F3), (T7➔C3), (C3➔F7), (C4➔T7), (P8➔T7), (T7➔O2), (T8➔F7), (P8➔F7), (F4➔F8), (P8➔T8), (O2➔F7), (P3➔F4)

5.4.2 Electrode Mapping

EEG signal was recorded via 16 electrodes positioned on the scalp based on a subset of 10-20 system, earlier shown in Figure 4.1. Recorded signal from Fp1 and Fp2 is the electrical activity associated with eye movement which were not incorporated in our model. Figure 5.9 represents the positions of the electrodes on the left sagittal plane.

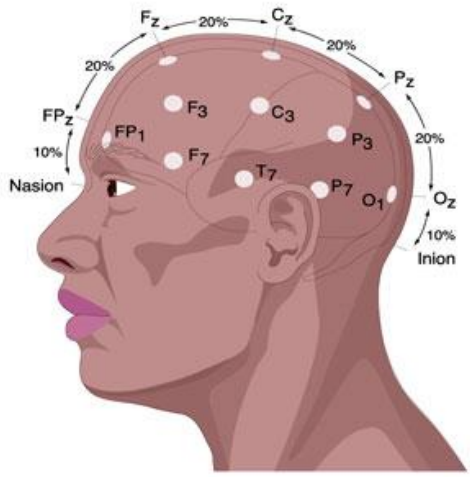

Figure 5.9. position of the electrodes on the left sagittal plane [135].

In 2010, Richlan, F., et al., in a meta-analysis over the previous studies from neuroimaging data, identified the brain regions with consistent under- or over activation in dyslectics. These regions are considered as regions of interest (ROIs) in our study. These areas, all located in left hemisphere, are inferior parietal regions, fusiform area, inferior frontal region, primary motor cortex and temporal cortex (superior, middle and inferior) [51,136]. Figure 5.10 represents the anatomical position of Broddman areas on the left hemisphere. Table 5.9 represents the ROIs, their related cytoarchitectonic areas and the closest EEG electrodes to each ROI. This provides us with the opportunity to check the compatibility of our results with previously reported abnormalities in dyslectic brains.

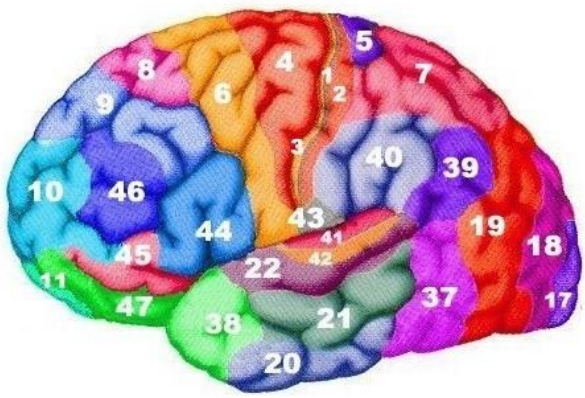

Figure 5.10. Anatomical position of Broddman areas on left hemisphere of the scalp [137].

The electrical activity of each ROI is approximated by the recorded signal from a specific electrode. The term approximation is used due to three reasons. Firstly, the recorded signal by each electrode is representative of a summation over all the activities in the nearby areas. Besides, the experiment was not provided with a high density EEG equipment which leads to a less accurate source localization. Finally, the electrical fields transmit through biological tissue (volume conduction phenomenon) and this makes confusion in regional measurements.

Table 5.9. ROIs and the correspondent electrodes on the scalp.

ROI	Related Broddman area	Correspondent electrodes	Role
Inferior parietal region	39,40	P3,C3	Encompass super marginal gyrus and angular gyrus, language processing areas
Fusiform area	37	P7	Visual word form area
Inferior frontal region	44,45,47	F3,F7	Encompass Broca's area, responsible for motor images
Primary motor cortex	4	C3	Responsible for articulation
Temporal cortex	20,21,22	T7	Encompass Wernicke's area, phonology center, information about sounds of speech component

Inferior parietal region (BA 39 and 40) is considered to include supermarginal gyrus and angular gyrus, which takes role as a conductor which makes the communication between the orthography (visual word form area) and phonology (Wernicke's area),

possible. Fusiform area, also known as occipito-temporal gyrus, (BA 37) is the hypothetical word form area and inferior frontal region (BA 44, 45 and 47) encompasses the Broca's area, which contains the information for motor images. Inferior and middle temporal regions (BA 20 and 21) are considered to provide access for semantic-lexical presentations [136]. Superior temporal region (BA 22) involve Wernicke's area which serves as phonological processing unit. Primary motor cortex (BA 4) is expected to be involved in articulation procedure. Figure 5.11 represents these functional units of the brain that are involved in language processing task.

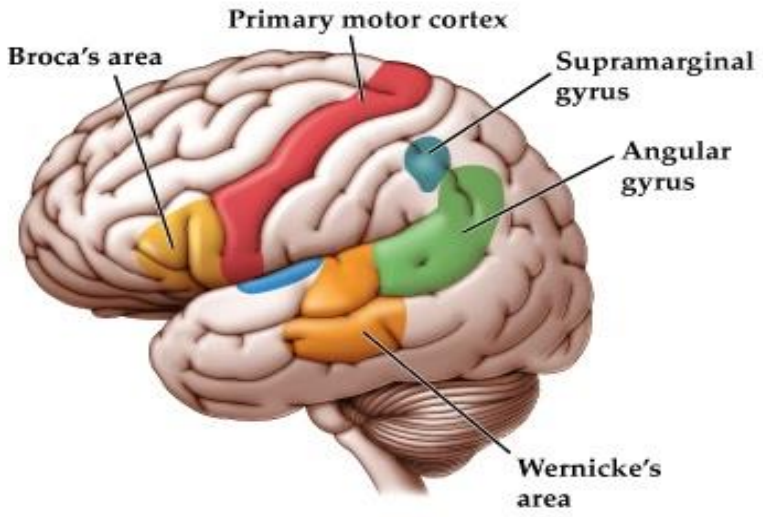

Figure 5.11. Language specific areas of the brain [138].

5.4.3 Different Connections between Dyslectics and Controls

Significantly different connections between two groups obtained from our study, are reported in Tables 5.7 and 5.8. The compatibility of these findings with previously reported abnormal connectivity patterns in dyslectic brains were checked. Figures 5.12 and 5.13 illustrate the findings from our study and the connections in red, are the ones that has been attenuated by previous studies. Table 5.10 contains previous study and shows which connections are attenuated by which study.

Table 5.10. Comparison of the found abnormalities with previous studies.

Authors	***Results***	***Compare the results with the findings from our study***
Pugh, K. R., et al. [23]	Functional connectivity disturbance is revealed in dyslectic subjects while performing tasks requiring phonological assembly between angular gyrus and left-hemisphere language-related regions.	(Not Detected)
Quaglino, V., et al. [65]	disturbed effective connectivity between supermarginal cortex and inferior frontal cortex in dyslectic group	-The activity of "Inferior frontal cortex" is measured by electrodes "F3 and F7". -The activity of "Supermarginal cortex" is measured by electrodes "C3 and P3". - In word reading experiment, connections (C3➔F3- in alpha band) (C3➔F7- in alpha band) are found to be siginifcantly different between dyslectics and controls, which are compatible with the findings of this study. -In non-word redaing experiment, connection (C3➔F7-theta, beta) is found to be siginifcantly different between dyslectics and controls, which is compatible with the findings of this study.
Cao, F., et al. [66]	Dyslectics have deficits in integrating orthography and phonology utilizing left inferior parietal lobule, and in engaging phonological segmentation via the left inferior frontal gyrus.	-The activity of "Left inferior parietal" regior measured by electrodes "C3 and P3". -The activity of "Left Inferior Frontal" region is measured by electrides "F3 and F7". - In word reading experiment, connections (C3➔F3-alpha) (C3➔F7-alpha) are found to be siginifcantly different between dyslectics and controls, which are compatible with the findings of this study. -In non-word redaing experiment, connection (C3➔F7-theta, beta) is found to be siginifcantly different between dyslectics and controls, which is compatible with the findings of this study.
Ligges, C., et al. [67]	right hemisphere language areas to participate in compensatory mechanism of dyslectic brains for phonological deficits	Disruption in connections between right hemisphere regions is observed. - In word reading experiment, connections (P4➔P8 - beta) (P8➔T8 - beta) (T8➔P8- alpha) are found to be siginifcantly different between dyslectics and controls. - In non-word redaing experiment, connection (P8➔T8- beta) is found to be siginifcantly different between dyslectics and controls.

Table 5.11. Continued.

Finn, E. S., et al. [69]	anomalies in the connection between visual regions and prefrontal areas	- The activity of "Visual regions" is measured by electrodes "O1 and O2". -The activity of "Pre-frontal areas" is measured by electrodes "F3 and F7". - In word reading experiment, connections (O2➔F3-alpha) (F7➔O1- alpha, beta) are found to be siginifcantly different between dyslectics and controls, which is compatible with the findings of this study. -In non-word redaing experiment, connection (O2➔F7-beta) is found to be siginifcantly different between dyslectics and controls, which is compatible with the findings of this study.
Stanberry, L. I., et al. [8]	Disturbed connectivity between left inferior frontal gyrus and frontal, occipital and cerebellar regions in the right hemisphere in dyslectic subjects	-The activity of "Left Inferior Frontal" region measured by electrodes "F3 and F7". -The activity of "Right Frontal" region is measured by electrodes "F4 and F8". -The activity of "Right Occipital" region is measured by electrode "O2". - In word reading experiment, connections (F4➔f3, theta, beta) (O2➔F3-alpha) are found to be siginifcantly different between dyslectics and controls, which is compatible with the findings of this study. -In non-word redaing experiment, connections (F3➔F8.alpha) (F4➔F7-theta) (O2➔F7-beta) are found to be siginifcantly different between dyslectics and controls, which is compatible with the findings of this study.
Richards, T. L., et al. [64]	Disrupted connectivity between left inferior frontal gyrus and multiple regions (right and left middle frontal gyrus, right and left supplemental motor area, left precentral gyrus, right superior frontal gyrus) before treatment and no difference were reported between two groups after treatment	-The activity of "Left Inferior Frontal" region is me electrodes "F3 and F7". -the activity of "Right and left middle frontal gyrus" is measured by electrodes "F3 and F4". -The activity of "Right and left motor area" is measured by electrodes "C3 and C4". - In word reading experiment, connections (F4➔F3, theta, beta) (C3➔F3-alpha) (F3➔F7-alpha) (C3➔F7-alpha) are found to be siginifcantly different between dyslectics and controls, which is compatible with the findings of this study. -In non-word redaing experiment, connections (F4➔F7-theta) (C3➔F7-theta, beta) are found to be siginifcantly different between dyslectics and controls, which is compatible with the findings of this study.
Horwitz, B., et al. [12]	Disconnection of left angular gyrus from visual areas, from Wernicke's area and from inferior frontal cortex in dyslectic brains.	(Partially Detected) -The activity of "Angular gyrus" is measured by electrode "P3". - The activity of "Inferior frontal cortex" is measured by electrodes "F3, F4, F7 and F8". -In non-word reading experiment, connection (P3➔F4, theta, beta) is found to be siginifcantly different between dyslectics and controls, which is compatible with the findings of this study.

Table 5.12. Continued.

van der Mark, S., et al. [68]	Significant disruption of functional connectivity between the VWFA and left inferior frontal and left inferior parietal language areas in dyslectic children.	-The activity of "Visual Word From Area" is by electrodes "P7". -The activity of "Left Inferior Frontal" region is measured by electrides "F3 and F7". -The activity of "Left inferior parietal" measured by electrodes "C3 and P3". - In word reading experiment, connections (P7➔T7-theta) (P7➔F3-beta) are found to be siginifcantly different between dyslectics and controls, which are compatible with the findings of this study. -In non-word redaing experiment, connection (P7➔F3-beta) is found to be siginifcantly different between dyslectics and controls, which is compatible with the findings of this study.

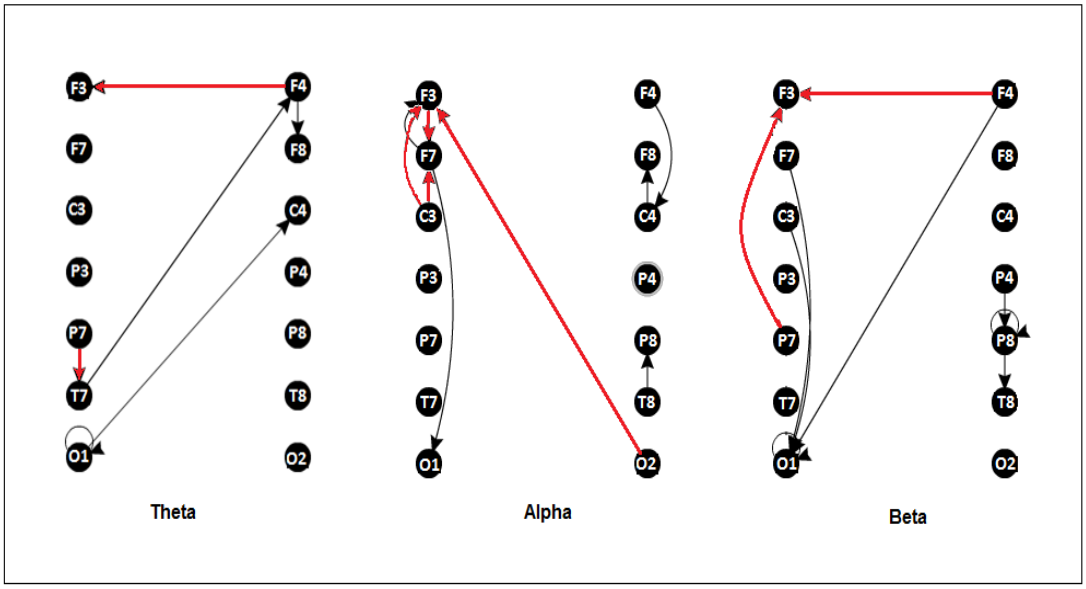

Figure 5.12. Presentation of significantly different connections between two groups – word reading experiment.

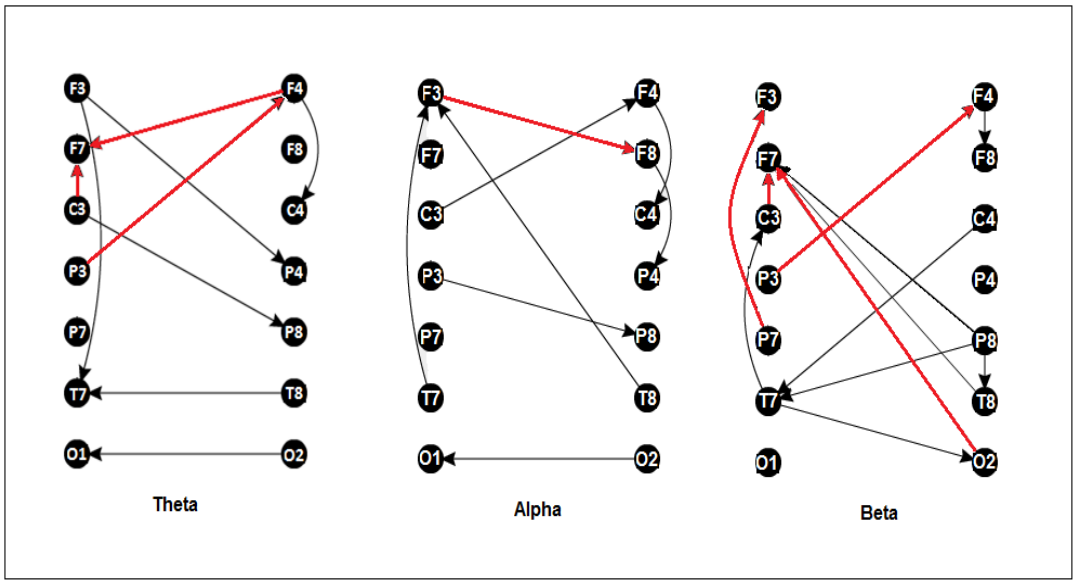

Figure 5.13. Presentation of significantly different connections between two groups – non-word reading experiment.

Increased activity in frontal areas (associated to F3 and F7 electrodes) and also in right hemisphere is reported in dyslectic brains which is associated to take role in compensatory mechanism for poor phonological processing [9]. Disturbed connections not reported directly from previous studies are supposed to participate in

the compensatory mechanism of dyslectic brains involving mostly electrodes measuring the activity of frontal areas and right hemisphere regions.

Based on the interactive reading model of the brain, represented in figure 2.5, subjects take use two pathways in the brain to acquire the phonological knowledge of the word. To read a non-word, the route from letters to phonemes (ventral pathway) is more activated. However, to read a word, the lexicon/semantic route (dorsal pathway) is more activated to transfer the information from graphemes to phonemes. There are multiple connections found to be disrupted in dyslectic brains which are part of each of these pathways. The ventral pathway transfer the visual information percepted in occipital region and visual word form area to frontal region. The dorsal pathway, information is transferred initially to angular gyrus and supermarginal regions (P3,C3) and then goes to Wernicke's area (T7) and Broca's area (F3,F7). Table 5.11 represent these connections.

Table 5.13. Disrupted connections in dyslectics which take role in dorsal or ventral pathways.

	Ventral Pathway	Dorsal Pathway
Word reading Experiment	(O2➔F3-alpha) (F7➔O1-alpha f beta)	(P7➔T7-theta)
Non-word Reading Experiment	(O2➔F7-beta), (P7➔F3-beta)	(T7➔C3-beta) (T7➔F3-beta) (F3➔T7-beta)

As seen in Table 5.11, in both experiments, the disrupted connections include the ones from both dorsal and ventral pathways.

CHAPTER 6

CONCLUSION

The main objective of this study is to classify dyslexic and normal readers based on the differences in causal interactions that exist in the network of their brains. Effective connectivity model, as a measure of causal interactions, was extracted by Dynamic Bayesian Network. Then, the 196 weights of the DBN structure, representing the causal influence between all possible pairs of electrodes, was used as features in the SVM classifier.

Since the number of cases in the training set was limited (57 subjects) in comparison to number of features, to avoid over fitting, feature reduction was proposed to increase the efficiency of the classification. Principle component analysis and statistical *t*-test were used to reduce the dimension of the features. Application of the both feature reduction algorithms result in a more efficient classification than no feature reduction case. From the comparison of the methods, applying statistical *t*-test gives rise to a better classification results.

Theta frequency band is found to be the most informative band about the disturbance of the casual interactions in dyslectic brains in the "pre-reading" stage. From the parameters of this period in theta band, we classified two groups by 86.21% in both experiments (reading a non-word and reading a word). This provides evidence for the perturbed effective connectivity in the networks of dyslectic brains regardless of the reading task.

In case III, the parameters from "pre-reading" period and "while reading" period were combined. New parameters are a measure of established changes in causal influences in the network to perform the reading task. The best classification rate based on the new parameters was obtained 86.21% for word reading experiment in alpha band and 81.03% in the same band for non-word reading experiment.

The significantly different connections between two groups, which were used as input features to train SVM classifiers, involve connections from both ventral (takes significant role in non-word reading) and dorsal (takes significant role in word reading) pathway.

The significantly different connections between two groups suggest a mainly disturbed network among brain regions. Most of these connections were previously reported form other studies. The remaining perturbed connections are the ones involving frontal and right hemisphere regions which are suggested to take role in compensatory pathways that dyslectic brains take.

Finally, Dynamic Bayesian network is used to reveal the effective connectivity and the causal interactions in the brain network. Successful classification based on the parameters of model indicates the efficiency of the DBN to reveal the differences of the interconnections in the networks of the two groups.

6.1 Future Work

Following are multiple methods proposed that may be applied to improve our results. Although EEG signals have high temporal resolution, which makes them suitable to study the temporal characteristics of the underlying system, their spatial resolution of these signals is low. One reason lies on the fact that EEG electrodes record the ongoing electrical activity in the brain from the scalp. Besides, events like volume conduction, defined as the transmission of electric fields from an electric primary current source through biological tissue, make EEG recordings less reliable in terms of the location of the signal. There are multiple algorithms (e.g. ICA) that can be applied to localize the source of the EEG data. EEG source localization make up for the low spatial resolution of EEG and may result in a more accurate model.

One other method to improve our results is to incorporate hidden nodes in the structure of our dynamic Bayesian network. These hidden nodes may be representative of the ROIs placed in the deeper regions of the brain which EEG electrodes are not capable to record. The value of these nodes, that their activities are not recorded by EEG electrode, are estimated by expectation maximization algorithms.

In this study, the temporal characteristics of the network were studied based on a 1 millisecond time unit. Effective connectivity analysis with different time units (e.g.,

2ms) may result in DBN models that are more informative in terms of the differences between dyslectics and controls. Le Song et al, introduced a time-varying DBN for modeling the structurally varying directed dependency structures underlying non-stationary neural time series. Time Varying Dynamic Bayesian Network (TV-DBN) is capable of determining the time-evolving network structures underlying non-stationary biological signals. Though, it probably is an efficient algorithm to model a multi-stage process like reading [139].

REFERENCES

[1] Démonet, J. F., Taylor, M. J., and Chaix, Y. (2004). Developmental dyslexia.*The Lancet*, *363*(9419), 1451-1460.

[2] Andreadis, I. I., Giannakakis, G. A., Papageorgiou, C., and Nikita, K. S. (2009, September). Detecting complexity abnormalities in dyslexia measuring approximate entropy of electroencephalographic signals. In *Engineering in Medicine and Biology Society, 2009. EMBC 2009. Annual International Conference of the IEEE* (pp. 6292-6295). IEEE.

[3] Lyon, G. R., Shaywitz, S. E., and Shaywitz, B. A. (2003). A definition of dyslexia. *Annals of dyslexia*, *53*(1), 1-14.

[4] Arduini, R. G., Capellini, S. A., and Ciasca, S. M. (2006). Comparative study of the neuropsychological and neuroimaging evaluations in children with dyslexia. *Arquivos de Neuro-psiquiatria*, *64*(2B), 369-375.

[5] Ferrer, E., Shaywitz, B. A., Holahan, J. M., Marchione, K., and Shaywitz, S. E. (2010). Uncoupling of reading and IQ over time empirical evidence for a definition of dyslexia. *Psychological science*, *21*(1), 93-101.

[6] Paulesu, E., Frith, U., Snowling, M., Gallagher, A., Morton, J., Frackowiak, R. S., and Frith, C. D. (1996). Is developmental dyslexia a disconnection syndrome?. *Brain*, *119*(1), 143-157.

[7] Beaulieu, C., Plewes, C., Paulson, L. A., Roy, D., Snook, L., Concha, L., and Phillips, L. (2005). Imaging brain connectivity in children with diverse reading ability. *Neuroimage*, *25*(4), 1266-1271.

[8] Stanberry, L. I., Richards, T. L., Berninger, V. W., Nandy, R. R., Aylward, E. H., Maravilla, K. R., Stock, P.S. and Cordes, D. (2006). Low-frequency signal changes reflect differences in functional connectivity between good readers and dyslexics during continuous phoneme mapping. *Magnetic resonance imaging*, *24*(3), 217-229.

[9] Liederman, J., Wu, M. H., Frye, R. E., and Fisher, J. M. (2010). Greater pre-stimulus effective connectivity from the left inferior frontal area to other areas is associated with better phonological decoding in dyslexic readers.

[10] Friston, K. J. (1994). Functional and effective connectivity in neuroimaging: a synthesis. *Human brain mapping*, *2*(1-2), 56-78.

[11] Li, J. (2007). Dynamic Bayesian networks: modelling and analysis of neural

signals.

[12] Horwitz, B., Rumsey, J. M., and Donohue, B. C. (1998). Functional connectivity of the angular gyrus in normal reading and dyslexia.*Proceedings of the National Academy of Sciences*, *95*(15), 8939-8944.

[13] Frackowiak, R. S., Friston, K. J., Frith, C. D., Dolan, R. J., and Mazziotta, J. C. (2004). Human brain function. *San Diego, CA:*

[14] Dejerine, J. (1891). Sur un cas de cécité verbale avec agraphie, suivi d'autopsie. *CR Société du Biologie*, *43*, 197-201.

[15] Dejerine, J. J. (1892). Contribution à l'étude anatomo-pathologique et clinique des différentes variétés de cécité verbale.

[16] Lichteim, L. (1885). On aphasia. *Brain*, *7*(4), 433-484.

[17] Warrington, E. K., and Shallice, T. I. M. (1980). Word-form dyslexia. *Brain: a journal of neurology*, *103*(1), 99-112.

[18] Coltheart, M., Curtis, B., Atkins, P., and Haller, M. (1993). Models of reading aloud: Dual-route and parallel-distributed-processing approaches.*Psychological review*, *100*(4), 589.

[19] Marshall, J. C., and Newcombe, F. (1973). Patterns of paralexia: A psycholinguistic approach. *Journal of psycholinguistic research*, *2*(3), 175-199.

[20] McClelland, J. L., and Rumelhart, D. E. (1981). An interactive activation model of context effects in letter perception: I. An account of basic findings.*Psychological review*, *88*(5), 375.

[21] Carreiras, M., Armstrong, B. C., Perea, M., and Frost, R. (2014). The what, when, where, and how of visual word recognition. *Trends in Cognitive Sciences*, *18*(2), 90-98.

[22] Wandell, B. A., and Yeatman, J. D. (2013). Biological development of reading circuits. *Current opinion in neurobiology*, *23*(2), 261-268.

[23] Pugh, K. R., Mencl, W. E., Shaywitz, B. A., Shaywitz, S. E., Fulbright, R. K., Constable, R. T., Skudlarski, P., Marchione, K.E., Jenner, A.R., Fletcher, J.M. and Liberman, A.M., (2000). The angular gyrus in developmental dyslexia: task-specific differences in functional connectivity within posterior cortex. *Psychological science*, *11*(1), 51-56.

[24] Jones, D. K. (2008). Studying connections in the living human brain with diffusion MRI. *Cortex*, *44*(8), 936-952.

[25] Rolheiser, T., Stamatakis, E. A., and Tyler, L. K. (2011). Dynamic processing in the human language system: synergy between the arcuate fascicle and extreme capsule. *The Journal of Neuroscience*, *31*(47), 16949-16957.

[26] Steinbrink, C., Vogt, K., Kastrup, A., Müller, H. P., Juengling, F. D., Kassubek, J., and Riecker, A. (2008). The contribution of white and gray matter differences to developmental dyslexia: insights from DTI and VBM at 3.0 T. *Neuropsychologia*, *46*(13), 3170-3178.

[27] Yeatman, J. D., Dougherty, R. F., Ben-Shachar, M., and Wandell, B. A. (2012). Development of white matter and reading skills. *Proceedings of the National Academy of Sciences*, *109*(44), E3045-E3053.

[28] Dougherty, R. F., Ben-Shachar, M., Deutsch, G. K., Hernandez, A., Fox, G. R., and Wandell, B. A. (2007). Temporal-callosal pathway diffusivity predicts phonological skills in children. *Proceedings of the National Academy of Sciences*, *104*(20), 8556-8561.

[29] Frye, R. E., Hasan, K., Xue, L., Strickland, D., Malmberg, B., Liederman, J., and Papanicolaou, A. (2008). Splenium microstructure is related to two dimensions of reading skill. *Neuroreport*, *19*(16), 1627.

[30] Odegard, T. N., Farris, E. A., Ring, J., McColl, R., and Black, J. (2009). Brain connectivity in non-reading impaired children and children diagnosed with developmental dyslexia. *Neuropsychologia*, *47*(8), 1972-1977.

[31] Pugh, K. R., Mencl, W. E., Jenner, A. R., Katz, L., Frost, S. J., Lee, J. R., Shaywitz, S.E. and Shaywitz, B.A., (2001). Neurobiological studies of reading and reading disability. *Journal of communication disorders*, *34*(6), 479-492.

[32] Stage, K. A. and Davis, A. S. (2005), Overcoming dyslexia: A new and complete science-based program for reading problems at any level. Psychol. Schs., 42: 117–118. doi: 10.1002/pits.20036

[33] Frackowiak, R. S., Friston, K. J., Frith, C. D., Dolan, R. J., and Mazziotta, J. C. (2004). Human brain function. *San Diego, CA.*

[34] Leinenger, Mallorie. "Phonological coding during reading." *Psychological bulletin* 140.6 (2014): 1534.

[35] Taroyan, N. A., and Nicolson, R. I. (2009). Reading words and pseudowords in dyslexia: ERP and behavioural tests in English-speaking adolescents.*International Journal of Psychophysiology*, *74*(3), 199-208.

[36] Rumsey, J. M., Horwitz, B., Donohue, B. C., Nace, K., Maisog, J. M., and Andreason, P. (1997). Phonological and orthographic components of word recognition. A PET-rCBF study. *Brain*, *120*(5), 739-759.

[37] Brunswick, N., McCrory, E., Price, C. J., Frith, C. D., and Frith, U. (1999). Explicit and implicit processing of words and pseudowords by adult developmental dyslexics. *Brain*, *122*(10), 1901-1917.

[38] Paulesu, E., Démonet, J. F., Fazio, F., McCrory, E., Chanoine, V., Brunswick,

N., Cappa, S.F., Cossu, G., Habib, M., Frith, C.D. and Frith, U. (2001). Dyslexia: cultural diversity and biological unity. *Science*, *291*(5511), 2165-2167.

[39] Shaywitz, S. E., Shaywitz, B. A., Pugh, K. R., Fulbright, R. K., Constable, R. T., Mencl, W. E., and Katz, L. (1998). Functional disruption in the organization of the brain for reading in dyslexia. *Proceedings of the National Academy of Sciences*, *95*(5), 2636-2641.

[40] Temple, E., Poldrack, R. A., Salidis, J., Deutsch, G. K., Tallal, P., Merzenich, M. M., and Gabrieli, J. D. (2001). Disrupted neural responses to phonological and orthographic processing in dyslexic children: an fMRI study. *Neuroreport*, *12*(2), 299-307.

[41] Rumsey, J. M., Andreason, P., Zametkin, A. J., Aquino, T., King, A. C., Hamburger, S. D., Pikus, A., Rapoport, J.L. and Cohen, R.M., (1992). Failure to activate the left temporoparietal cortex in dyslexia: An oxygen 15 positron emission tomographic study. *Archives of Neurology*, *49*(5), 527-534.

[42] Price, Cathy J., and Karl J. Friston. "Cognitive conjunction: a new approach to brain activation experiments." *Neuroimage* 5.4 (1997): 261-270.

[43] Usui, K., Ikeda, A., Takayama, M., Matsuhashi, M., Yamamoto, J. I., Satoh, T., Begum, T., Mikuni, N., Takahashi, J.B., Miyamoto, S. and Hashimoto, N., (2003). Conversion of semantic information into phonological representation: a function in left posterior basal temporal area.*Brain*, *126*(3), 632-641.

[44] Cohen, L., Dehaene, S., Naccache, L., Lehéricy, S., Dehaene-Lambertz, G., Hénaff, M. A., and Michel, F. (2000). The visual word form area. *Brain*, *123*(2), 291-307.

[45] Shaywitz, B. A., Shaywitz, S. E., Pugh, K. R., Mencl, W. E., Fulbright, R. K., Skudlarski, P., Constable, R.T., Marchione, K.E., Fletcher, J.M., Lyon, G.R. and Gore, J.C., (2002). Disruption of posterior brain systems for reading in children with developmental dyslexia. *Biological psychiatry*, *52*(2), 101-110.

[46] Vandenberghe, R., Price, C., Wise, R., Josephs, O., and Frackowiak, R. S. (1996). Functional anatomy of a common semantic system for words and pictures. *Nature*, *383*(6597), 254-6.

[47] Mummery, C. J., Patterson, K., Hodges, J. R., and Price, C. J. (1998). Functional neuroanatomy of the semantic system: divisible by what?.*Cognitive Neuroscience, Journal of*, *10*(6), 766-777.

[48] Binder, J. R., Frost, J. A., Hammeke, T. A., Cox, R. W., Rao, S. M., and Prieto, T. (1997). Human brain language areas identified by functional magnetic resonance imaging. *The Journal of Neuroscience*, *17*(1), 353-362.

[49] Richlan, F. (2012). Developmental dyslexia: dysfunction of a left hemisphere reading network. *Front Hum Neurosci*, *6*, 120.

[50] Nation, K., and Snowling, M. (1997). Assessing reading difficulties: The validity and utility of current measures of reading skill. *British Journal of Educational Psychology*, *67*(3), 359-370.

[51] Eden, G. F., VanMeter, J. W., Rumsey, J. M., and Zeffiro, T. A. (1996). The visual deficit theory of developmental dyslexia. *Neuroimage*, *4*(3), S108-S117.

[52] Demb, J. B., Boynton, G. M., and Heeger, D. J. (1998). Functional magnetic resonance imaging of early visual pathways in dyslexia. *The journal of neuroscience*, *18*(17), 6939-6951.

[53] McCrory, E., Frith, U., Brunswick, N., and Price, C. (2000). Abnormal functional activation during a simple word repetition task: A PET study of adult dyslexics. *Journal of Cognitive Neuroscience*, *12*(5), 753-762.

[54] Temple, E., Poldrack, R. A., Salidis, J., Deutsch, G. K., Tallal, P., Merzenich, M. M., and Gabrieli, J. D. (2001). Disrupted neural responses to phonological and orthographic processing in dyslexic children: an fMRI study. *Neuroreport*, *12*(2), 299-307.

[55] Boets, B., de Beeck, H. P. O., Vandermosten, M., Scott, S. K., Gillebert, C. R., Mantini, D., Bulthé, J., Sunaert, S., Wouters, J. and Ghesquière, P. (2013). Intact but less accessible phonetic representations in adults with dyslexia. *Science*, *342*(6163), 1251-1254.

[56] Eckert, M. (2004). Neuroanatomical markers for dyslexia: a review of dyslexia structural imaging studies. *The neuroscientist*, *10*(4), 362-371.

[57] Klingberg, T., Hedehus, M., Temple, E., Salz, T., Gabrieli, J. D., Moseley, M. E., and Poldrack, R. A. (2000). Microstructure of temporo-parietal white matter as a basis for reading ability: evidence from diffusion tensor magnetic resonance imaging. *Neuron*, *25*(2), 493-500.

[58] Vandermosten, M., Boets, B., Poelmans, H., Sunaert, S., Wouters, J., and Ghesquière, P. (2012). A tractography study in dyslexia: neuroanatomic correlates of orthographic, phonological and speech processing. *Brain*, *135*(3), 935-948.

[59] von Plessen, K., Lundervold, A., Duta, N., Heiervang, E., Klauschen, F., Smievoll, A. I., Ersland, L. and Hugdahl, K., (2002). Less developed corpus callosum in dyslexic subjects—a structural MRI study. *Neuropsychologia*, *40*(7), 1035-1044.

[60] Hampson, M., Peterson, B. S., Skudlarski, P., Gatenby, J. C., and Gore, J. C. (2002). Detection of functional connectivity using temporal correlations in MR images. *Human brain mapping*, *15*(4), 247-262.

[61] Koyama, M. S., Di Martino, A., Kelly, C., Jutagir, D. R., Sunshine, J., Schwartz, S. J., Castellanos, F.X. and Milham, M. P. (2013). Cortical signatures of

dyslexia and remediation: an intrinsic functional connectivity approach. *PloS one*,*8*(2), e55454.

[62] Schurz, M., Wimmer, H., Richlan, F., Ludersdorfer, P., Klackl, J., and Kronbichler, M. (2014). Resting-state and task-based functional brain connectivity in developmental dyslexia. *Cerebral Cortex*, bhu184.

[63] Zhou, W., Xia, Z., Bi, Y., and Shu, H. (2015). Altered connectivity of the dorsal and ventral visual regions in dyslexic children: a resting-state fMRI study.*Frontiers in human neuroscience*, *9*.

[64] Richards, T. L., and Berninger, V. W. (2008). Abnormal fMRI connectivity in children with dyslexia during a phoneme task: Before but not after treatment.*Journal of neurolinguistics*, *21*(4), 294-304.

[65] Quaglino, V., Bourdin, B., Czternasty, G., Vrignaud, P., Fall, S., Meyer, M. E., Berquin, P., Devauchelle, B. and de Marco, G. (2008). Differences in effective connectivity between dyslexic children and normal readers during a pseudoword reading task: an fMRI study. *Neurophysiologie Clinique/Clinical Neurophysiology*, *38*(2), 73-82.

[66] Cao, F., Bitan, T., and Booth, J. R. (2008). Effective brain connectivity in children with reading difficulties during phonological processing. *Brain and language*, *107*(2), 91-101.

[67] Ligges, C., Ungureanu, M., Ligges, M., Blanz, B., and Witte, H. (2010). Understanding the time variant connectivity of the language network in developmental dyslexia: new insights using Granger causality. *Journal of Neural Transmission*, *117*(4), 529-543.

[68] van der Mark, S., Klaver, P., Bucher, K., Maurer, U., Schulz, E., Brem, S., Martin, E. and Brandeis, D. (2011). The left occipitotemporal system in reading: disruption of focal fMRI connectivity to left inferior frontal and inferior parietal language areas in children with dyslexia. *Neuroimage*, *54*(3), 2426-2436.

[69] Finn, E. S., Shen, X., Holahan, J. M., Scheinost, D., Lacadie, C., Papademetris, X., Shaywitz, S.E., Shaywitz, B.A. and Constable, R. T. (2014). Disruption of functional networks in dyslexia: a whole-brain, data-driven analysis of connectivity.*Biological psychiatry*, *76*(5), 397-404.

[70] Duffy, F. H., Denckla, M. B., Bartels, P. H., Sandini, G., and Kiessling, L. S. (1980). Dyslexia: Automated diagnosis by computerized classification of brain electrical activity. *Annals of neurology*, *7*(5), 421-428.

[71] Karim, I., Abdul, W., and Kamaruddin, N. (2013, March). Classification of dyslexic and normal children during resting condition using KDE and MLP. In*Information and Communication Technology for the Muslim World (ICT4M), 2013 5th International Conference on* (pp. 1-5). IEEE.

[72] McIntosh, A. "Moving between functional and effective connectivity."*Analysis*

and Function of Large-Scale Brain Networks (2010): 15.

[73] Wang, C., Xu, J., Zhao, S., and Lou, W. (2016). Graph theoretical analysis of EEG effective connectivity in vascular dementia patients during a visual oddball task. *Clinical Neurophysiology*, *127*(1), 324-334.

[74] Park, H. J., and Friston, K. (2013). Structural and functional brain networks: from connections to cognition. *Science*, *342*(6158), 1238411.

[75] Greenblatt, R. E., Pflieger, M. E., and Ossadtchi, A. E. (2012). Connectivity measures applied to human brain electrophysiological data. *Journal of neuroscience methods*, *207*(1), 1-16.

[76] Wu, X., Li, J., and Yao, L. (2012, November). Determining effective connectivity from fMRI data using a gaussian dynamic Bayesian network. In *Neural Information Processing* (pp. 33-39). Springer Berlin Heidelberg.

[77] Lang, E. W., Tomé, A. M., Keck, I. R., Górriz-Sáez, J. M., and Puntonet, C. G. (2012). Brain connectivity analysis: a short survey. *Computational intelligence and neuroscience*, *2012*, 8.

[78] Friston, K. J. (2011). Functional and effective connectivity: a review. *Brain connectivity*, *1*(1), 13-36.

[79] Liu, Y., and Aviyente, S. (2012). Quantification of effective connectivity in the brain using a measure of directed information. *Computational and mathematical methods in medicine, 2012*.

[80] Xu, L., Fan, T., Wu, X., Chen, K., Guo, X., Zhang, J., and Yao, L. (2014). A pooling-LiNGAM algorithm for effective connectivity analysis of fMRI data.*Frontiers in computational neuroscience*, *8*.

[81] Signorelli. F. and Chirchiglia. D. (2013). Fucntional Brain Mapping and Endeavor to Understand the Working Brain. InTech.

[82] Lenz, M. (2010). Estimation of Effective Connectivity based on EEG and fMRI data. University of Applied Sciences Komblenz, RheinAhrCampus Remagen.

[83] Horwitz, B. (2003). The elusive concept of brain connectivity. *Neuroimage*, *19*(2), 466-470.

[84] Schreiber, T. (2000). Measuring information transfer. *Physical review letters*,*85*(2), 461.

[85] Sabesan, S., Good, L. B., Tsakalis, K. S., Spanias, A., Treiman, D. M., and Iasemidis, L. D. (2009). Information flow and application to epileptogenic focus localization from intracranial EEG. *Neural Systems and Rehabilitation Engineering, IEEE Transactions on*, *17*(3), 244-253.

[86] Harrison, L., Penny, W. D., and Friston, K. (2003). Multivariate autoregressive

modeling of fMRI time series. *NeuroImage*, *19*(4), 1477-1491.

[87] Haufea, S., and Nikulinc, V. V. (2012). Assessing brain effective connectivity from EEG – a simulation study. *Neuroimage*, pp. 1–62.

[88] Amblard, P. O., and Michel, O. J. (2011). On directed information theory and Granger causality graphs. *Journal of computational neuroscience*, *30*(1), 7-16.

[89] Hinrichs, H., Noesselt, T., and Heinze, H. J. (2008). Directed information flow—A model free measure to analyze causal interactions in event related EEG-MEG-experiments. *Human brain mapping*, *29*(2), 193-206.

[90] Hesse, W., Möller, E., Arnold, M., and Schack, B. (2003). The use of time-variant EEG Granger causality for inspecting directed interdependencies of neural assemblies. *Journal of neuroscience methods*, *124*(1), 27-44.

[91] Astolfi, L., Cincotti, F., Mattia, D., Salinari, S., Babiloni, C., Basilisco, A., Rossini, P.M., Ding, L., Ni, Y., He, B. and Marciani, M. G. (2004). Estimation of the effective and functional human cortical connectivity with structural equation modeling and directed transfer function applied to high-resolution EEG. *Magnetic resonance imaging*, *22*(10), 1457-1470.

[92] Babiloni, F., Cincotti, F., Babiloni, C., Carducci, F., Mattia, D., Astolfi, L., Basilisco, A., Rossini, P.M., Ding, L., Ni, Y. and Cheng, J. (2005). Estimation of the cortical functional connectivity with the multimodal integration of high-resolution EEG and fMRI data by directed transfer function. *Neuroimage*, *24*(1), 118-131.

[93] Baccalá, L. A., and Sameshima, K. (2001). Partial directed coherence: a new concept in neural structure determination. *Biological cybernetics*, *84*(6), 463-474.

[94] Schelter, B., Winterhalder, M., Eichler, M., Peifer, M., Hellwig, B., Guschlbauer, B., Lücking, C.H., Dahlhaus, R. and Timmer, J. (2006). Testing for directed influences among neural signals using partial directed coherence. *Journal of neuroscience methods*, *152*(1), 210-219.

[95] Astolfi, L., Cincotti, F., Babiloni, C., Carducci, F., Basilisco, A., Rossini, P. M. Salinari, S., Mattia, D., Cerutti, S., Dayan, D.B. and Ding, L., (2005). Estimation of the cortical connectivity by high-resolution EEG and structural equation modeling: simulations and application to finger tapping data. *Biomedical Engineering, IEEE Transactions on*, *52*(5), 757-768.

[96] Rajapakse, J. C., Wang, Y., Zheng, X., and Zhou, J. (2008). Probabilistic framework for brain connectivity from functional MR images. *Medical Imaging, IEEE Transactions on*, *27*(6), 825-833.

[97] Mutkule, S., Sonarkar, P., and Nagori, M. Establishing Effective Connectivity in Brain using Dynamic Bayesian Network.

[98] Bhattacharya, S., Ho, M. H. R., and Purkayastha, S. (2006). A Bayesian approach to modeling dynamic effective connectivity with fMRI data.*Neuroimage*, *30*(3), 794-812.

[99] Goldenberg, D., and Galván, A. (2015). The use of functional and effective connectivity techniques to understand the developing brain. *Developmental cognitive neuroscience*, *12*, 155-164.

[100] Koller, D., and Friedman, N. (2009) . Introduction. In Thomas Dietterich, (Ed.), *Probablistic Graphical models: principles and techniques* (pp. 1–14). Cambridge, Massachusetts: MIT press.

[101] Zheng, X., and Rajapakse, J. C. (2006). Learning functional structure from fMR images. *Neuroimage*, *31*(4), 1601-1613.

[102] Wu, X., Yu, X., Yao, L., and Li, R. (2014). Bayesian network analysis revealed the connectivity difference of the default mode network from the resting-state to task-state. *Frontiers in computational neuroscience*, *8*.

[103] Wanga, Z., and Wong, A. Using Dynamic Bayesian Networks to analyze genetic data. *Thursday May 20*, 85.

[104] Rajapakse, J. C., and Zhou, J. (2007). Learning effective brain connectivity with dynamic Bayesian networks. *NeuroImage*, *37*(3), 749-760.

[105] Carvalho, A. M. (2009). Scoring functions for learning Bayesian networks.*Inesc-id Tec. Rep*.

[106] Ben-Gal, I. (2008). Bayesian Networks. Encyclopedia of Statistics in Quality and Reliability.

[107] Tommi Jaakkola, course materials for 6.867 Machine Learning, Fall 2006. MIT OpenCourseWare (http://ocw.mit.edu/), Massachusetts Institute of Technology. Downloaded on [02, 02, 2016]

[108] Friedman, Nir, and Moises Goldszmidt. "Discretizing continuous attributes while learning Bayesian networks." *Icml*. 1996.

[109] Al-Akwaa, F. M., and Alkhawlani, M. M. (2012). Comparison of the Bayesian network structure learning algorithms. *International Journal of Advanced Research in Computer Science and Software Engineering*, *2*(3), 404-408.

[110] Koller, D., and Friedman, N. (2009) . Parameter Estimation. In Thomas Dietterich, (Ed.), *Probablistic Graphical models: principles and techniques* (pp. 717–782). Cambridge, Massachusetts: MIT press.

[111] Koller, D., and Friedman, N. (2009) .Structure Learning in Bayesian Network. In Thomas Dietterich, (Ed.), *Probablistic Graphical models: principles and techniques* (pp. 783–848). Cambridge, Massachusetts: MIT press.

[112] De Campos, L. M. (2006). A scoring function for learning Bayesian networks based on mutual information and conditional independence tests. *The Journal of Machine Learning Research*, *7*, 2149-2187.

[113] Wu, X., Wen, X., Li, J., and Yao, L. (2014). A new dynamic Bayesian network approach for determining effective connectivity from fMRI data. *Neural Computing and Applications*, *24*(1), 91-97.

[114] Li, J., Wang, Z. J., and McKeown, M. J. (2006, April). Dynamic Bayesian networks (DBNS) demonstrate impaired brain connectivity during performance of simultaneous movements in Parkinson's disease. In *Biomedical Imaging: Nano to Macro, 2006. 3rd IEEE International Symposium on* (pp. 964-967). IEEE.

[115] Mutlu, A. Y., and Aviyente, S. (2009, September). Inferring effective connectivity in the brain from EEG time series using dynamic bayesian networks. In *Engineering in Medicine and Biology Society, 2009. EMBC 2009. Annual International Conference of the IEEE* (pp. 4739-4742). IEEE.

[116] Burge, J., Lane, T., Link, H., Qiu, S., and Clark, V. P. (2009). Discrete dynamic Bayesian network analysis of fMRI data. *Human brain mapping*, *30*(1), 122-137.

[117] Li, J., Wang, Z. J., Palmer, S. J., and McKeown, M. J. (2008). Dynamic Bayesian network modeling of fMRI: a comparison of group-analysis methods. *Neuroimage*, *41*(2), 398-407.

[118] Smith, V. A., Yu, J., Smulders, T. V., Hartemink, A. J., and Jarvis, E. D. (2006). Computational inference of neural information flow networks. *PLoS Comput Biol*, *2*(11), e161.

[119] Bielza, C., and Larrañaga, P. (2014). Bayesian networks in neuroscience: a survey. *Frontiers in computational neuroscience*, *8*, 131.

[120] Haufe, S., Nikulin, V., and Nolte, G. (2011). Identifying brain effective connectivity patterns from EEG: performance of Granger Causality, DTF, PDC and PSI on simulated data. *BMC Neuroscience*, *12*(Suppl 1), P141.

[121] Friedman, N., Linial, M., Nachman, I., and Pe'er, D. (2000). Using Bayesian networks to analyze expression data. *Journal of computational biology*, *7*(3-4), 601-620.

[122] Hofmann, R., and Tresp, V. (1996). Discovering structure in continuous variables using Bayesian networks. *Advances in neural information processing systems*, 500-506.

[123] Fu, L. D., and Tsamardinos, I. (2005). A comparison of Bayesian network learning algorithms from continuous data. In *AMIA Annual Symposium*

Proceedings (Vol. 2005, p. 960). American Medical Informatics Association.

[124] Babiloni, C., Stella, G., Buffo, P., Vecchio, F., Onorati, P., Muratori, C., and Rossini, P. M. (2012). Cortical sources of resting state EEG rhythms are abnormal in dyslexic children. *Clinical Neurophysiology*, *123*(12), 2384-2391.

[125] Tong, S., and Koller, D. (2002). Support vector machine active learning with applications to text classification. *The Journal of Machine Learning Research*, *2*, 45-66.

[126] Peng, S., Xu, Q., Ling, X. B., Peng, X., Du, W., and Chen, L. (2003). Molecular classification of cancer types from microarray data using the combination of genetic algorithms and support vector machines. *FEBS letters*, *555*(2), 358-362.

[127] Guo, G., Li, S. Z., and Chan, K. L. (2001). Support vector machines for face recognition. *Image and Vision computing*, *19*(9), 631-638.

[128] Hsu, C. W., Chang, C. C., and Lin, C. J. (2003). A practical guide to support vector classification.

[129] Docs.opencv.org,. (2016). *Introduction to Support Vector Machines — OpenCV 2.4.12.0 documentation*. Retrieved 1 February 2016, from http://docs.opencv.org/2.4/doc/tutorials/ml/introduction_to_svm/introduction_to_svm.html.

[130] Elisseeff, A., and Pontil, M. (2003). Leave-one-out error and stability of learning algorithms with applications. *NATO science series sub series iii computer and systems sciences*, *190*, 111-130.

[131] Rajaraman, Anand, and Jeffrey D. Ullman. (1997). Dimensionality Reduction. Vol.1. *Mining of Massive Datasets* (pp. 405–437). Cambridge: Cambridge University Press.

[132] Ghodsi, A. (2006). Dimensionality reduction a short tutorial. *Department of Statistics and Actuarial Science, Univ. of Waterloo, Ontario, Canada*.

[133] Smith, L. I. (2002). A tutorial on principal components analysis. *Cornell University, USA*, *51*(52), 65.

[134] Schiavone, G., Linkenkaer-Hansen, K., Maurits, N. M., Plakas, A., Maassen, B. A., Mansvelder, H. D., van der Leij, A. and van Zuijen, T. L. (2014). Preliteracy signatures of poor-reading abilities in resting-state EEG. *Frontiers in human neuroscience*, *8*.

[135] Cedars-sinai.edu, "Diagnosing Epilepsy - Cedars-Sinai", 2016. [Online]. Available: http://www.cedars-sinai.edu/Patients/Programs-and-Services/Epilepsy-Program/Diagnosing-Epilepsy/. [Accessed: 26- Jan- 2016].

[136] Richlan, F., Kronbichler, M., and Wimmer, H. (2009). Functional abnormalities

in the dyslexic brain: A quantitative meta-analysis of neuroimaging studies.*Human brain mapping*, *30*(10), 3299-3308.

[137] Brainm.com, 2016. [Online]. Available: http://brainm.com/software/pubs/dg/BA_10 20_ROI_Talairach/nearesteeg.htm. [Accessed: 26- Jan- 2016].

[138] Breedlove, Breedlove, S. M. and Watson, N. V. (2013). Language and Hemispheric Assymetry. In 7th Ed. ,*Biological psychology: An introduction to behavioral, cognitive, and clinical neuroscience* (pp. 597-639). Sunderland, Massachusetts: Sinauer Associates, Inc.

[139] Song, L., Kolar, M., and Xing, E. P. (2009). Time-varying dynamic Bayesian networks. In *Advances in Neural Information Processing Systems* (pp. 1732-1740).

APPENDIX A

SUPPORT VECTOR MACHINE

The basic idea of a support vector machine is to introduce a hyper plane as the decision boundary between samples such that the margin between the samples of the classes is maximized [127]. Therefore, the goal is to find the hyper plane passing as far as possible from all sample points. So, the selected hyper plane by SVM algorithm gives the largest minimum distance to the samples used in training procedure. Twice this distance is called margin within SVM's theory. Figure A.1 illustrates the optimal separating hyper plane maximizes the margin of the training data with two features.

One might employ linear or non-linear SVM classifier to separate two groups in a dataset. Linear SVM classifiers separate data with a straight line (1 dimension), flat plane (2 dimensions) or an N-dimensional hyper plane, due to the number of feature dimension. However, in some cases a non-linear region classifies the data in a more efficient way. Non-linear SVM classifiers deal with these cases, by the so-called "kernel trick", where the data is transformed into a feature space with a higher dimension via a kernel function and then the best separating hyper plane is found to classify the data. In the datasets with large number of features, there is no need to transform the data into a higher dimension space. So, non-linear mapping does not improve our results and linear SVM classifiers are good enough to classify the two groups [128].

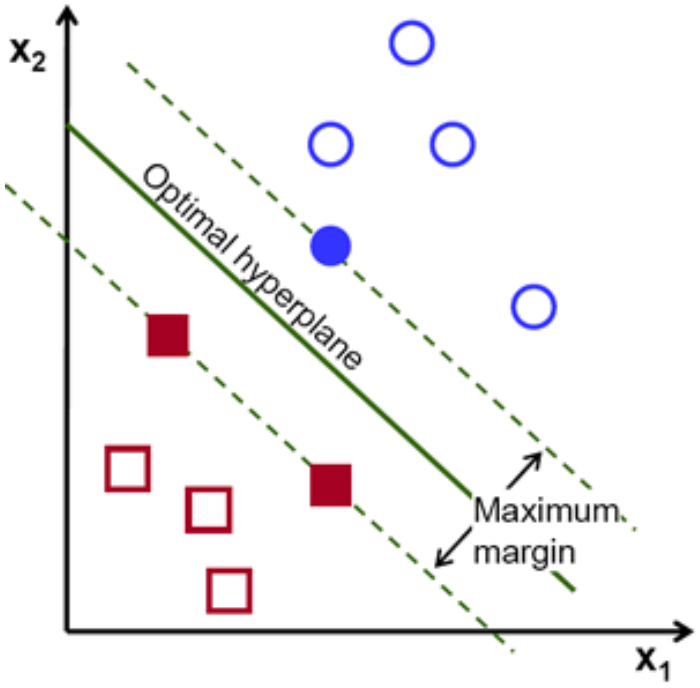

Figure A.1. SVM classification boundary and margin [129].

Like most of the other machine learning algorithms, scaling of the data is an important step before staring the classification algorithm. Scaling prevents the dominance of the features with greater numeric ranges on the influence of the other features. It involves mean centering and dividing by the standard deviation for all the features in the dataset [128].

APPENDIX B

FEATURE RECUTION ALGORITHMS

B.1 Principle Component Analysis

Many sources of data are demonstrated as large matrices. The data in many of these matrices may be summarized into smaller matrices which in some sense are close to the original matrix. These matrices have fewer number of columns or rows, which makes them more suitable for data processing algorithms. The process of detecting the smaller matrix from an original matrix is dimension reduction and Principle Component Analysis (PCA) is one of the popular techniques to reduce the dimension of the data under study. It was initially introduced by Pearson in 1901, and later in 1963, it was generalized by Loève [131].

Given a data set with n dimensions, PCA aims to detect a linear subspace with dimension d ($d < n$), that the data points lie mainly on. d orthogonal vectors characterizing the new subspace, are called the "principal components". The principal components are linear transformations of the original data points [132]. In practice, PCA combines related variables, and focus on uncorrelated or independent ones to reduce the number of variables in the data without losing important information.

To perform an efficient PCA, the mean is subtracted from each of the data dimensions. This process, called "mean subtraction" or "mean centering", makes certain that the calculated first principle component characterizes the direction of the maximum variation. After mean subtraction, covariance matrix and the associated eigenvalues and eigenvectors are derived from the data. The eigenvector with the highest eigenvalue is the principle component of the data, which is the linear combination of the variables in data that has maximum variance. Though, subsequent components clarify less variations among variables. Relative amount of the variation each

component accounts for is the ratio of the value of the corresponding eigenvalue to the total eigenvalues of the covariance matrix. To generate a new feature vector, the eigenvectors associated to the high eigenvalues are kept and the rest are ignored. The new feature vector contains most of the information in the data, since it involves the eigenvectors associated to the eigenvalues with high values. Finally, new data with reduced dimension is generated by multiplying the transpose of new feature vector by the transpose of mean-adjusted data matrix [133].

Each dynamic Bayesian network obtained for each subject, has 196 parameters. Since number of subjects is limited (58) in the data set, to perform an efficient classification task, it is required to reduce the dimension of the feature vector. For machine learning problems, the sample size should mostly be around six times the feature size. Here, we used the first ten principle component to generate the new data set. After applying PCA, each subject has ten parameters and dyslectics and controls are classified based on these parameters.

B.2 Statistical *t*-test

Other than PCA, which were applied to reduce the dimension of input features for the classification task, *t*-test was also applied to select significantly different variables (connections) between two groups, which were later employed to train the classifier. The *t*-test determines whether the means of two groups are statistically different from each other. Suppose there exists two distribution, *T* and *C*, which we aim to compare their group means. *t*-value is the quantity which is calculated in *t*-test analysis by the formula represented below, where $\bar{X}_T$ and $\bar{X}_C$ indicate the average, n_T and n_C are the number of samples and var_T and var_T are the variances of the two groups under investigation.

$$t = \frac{\bar{X}_T - \bar{X}_C}{\sqrt{\frac{var_T}{n_T} + \frac{var_C}{n_C}}}. \tag{12.1}$$

An essential part of any statistical test is the concept of "null hypothesis". Consider two sets of data with sample means μ_1 and μ_2. One of the datasets contains the weights of the DBNs for dyslectic and the other contains the same for control group. Here, the

null hypothesis indicates that the samples from both data sets are part of the same population such that their population means μ_1 and μ_2 are equal ($\mu_1 = \mu_2$).

In *t*-test analysis, p value is a measure of certainty that the obtained results represent a genuine effect present over the whole population. It actually is the probability that the observed result was obtained by chance or in other words, the null hypothesis is true. p-value can be determined based on the values of two parameters, t-value and the degree of freedom, from a standard table of significance. Degree of freedom (df) is equal to the sum of the number of samples in both group minus 2. After the *p*-value is identified, to test the significance level, a risk level of 0.05 is applied on the results. This means that if $p < 0.05$, then the null hypothesis is rejected and the distributions which the two groups were sampled from are significantly different from each other. Here, in this study, MATLAB built-in functions were used to apply *t*-test to detect the significantly different weights (obtained from DBN models) among two dyslectic and control groups.